

DEVELOPMENT AND EVALUATION
OF INGESTIBLE MICROBUBBLE-BASED CONTRAST AGENTS
FOR MEAL PRESSURE MRI WITHIN THE HUMAN STOMACH

EDWIN ABDURAKMAN

A thesis submitted in partial fulfillment of the requirements
of Nottingham Trent University for the degree of Doctor of Philosophy

December 2017

Declaration

This work is the intellectual property of the author. You may copy up to 5% of this work for private study, or personal, non-commercial research. Any re-use of the information contained within this document should be fully referenced, quoting the author, title, university, degree level and pagination. Queries or requests for any other use, or if a more substantial copy is required, should be directed in the owner(s) of the Intellectual Property Rights.

Abbreviations

This is a list of the abbreviations used throughout this thesis

B_0 : External magnetic field

BTfE: Balanced Turbo Field Echo sequence

CPMG: Carr-Purcell-Meiboom-Gill sequence

C₃F₈: Octafluoropropane gas

D: Proton diffusion coefficient

DEI: Diffraction Enhanced Imaging

DPPC: Dipalmitoyl Phosphatidylcholine

DSPC: Distearoyl Phosphatidylcholine

FDA: Food and Drugs Administration

FID: Free Induction Decay

GE: Gradient Echo

HASTE: Half-Fourier Acquisition Single-shot Turbo Spin Echo Imaging

LBG: Locust bean gum

MR: Magnetic Resonance

MRI: Magnetic Resonance Imaging

MSME: Multi Slice Multi Echo sequence

M_0 : Measurable net magnetisation

NaCl: Sodium chloride

N/A: Not available

NMR: Nuclear Magnetic Resonance

PEG: Polyethylene glycol

PET: Positron Emission Tomography

pH: A measure of acidity or alkalinity solution (pH stands for 'potential of Hydrogen')

RARE: Rapid Acquisition Relaxation Enhancement sequence

RF: Radiofrequency pulse

ROI: Region of interest

R_2 : Transverse relaxation decay rate

SE: Spin Echo

TSE: Turbo Spin Echo

T_1 : Longitudinal relaxation time

T_2 : Transverse relaxation time

T_2^* : Time constant for transverse relaxation in the absence of refocusing

T_2^{eff} : Effective transverse relaxation time

TE: Echo time

TE^{eff} : Effective echo time

TR: Repetition time

w/v: weight per volume ratio

χ : Magnetic susceptibility

2D: Two dimension

Abstract

Gas-filled microbubbles suspended in a liquid or suitable gel are useful as a pressure probe for MRI. These microbubbles create size-dependent magnetic perturbation in their immediate vicinity, which alters the measured MR signal. The flexibility of these biocompatible bubbles enables them to undergo a change in size due to a change in pressure, resulting in a measurable MR signal change. The novel work we present here focuses on demonstrating, by *in-vitro* and *in-vivo* investigations, that phospholipid microbubbles entrapped in alginate spheres can be used as a contrast agent to measure pressure variations in the human stomach.

The development of the pressure-sensitive contrast agent by entrapping microbubbles into alginate gel spheres is first presented. The T_2^{eff} relaxation time of the alginate spheres has been assessed using an MSME sequence and is found to decrease by a factor of 2 in the presence of microbubbles. Furthermore, by applying increasing pressure on to the alginate spheres containing microbubbles, the T_2^{eff} is seen to increase as the pressure increases, with a sensitivity of 43 % change per bar.

The pressure sensitivity of the contrast agent is further assessed, *in-vitro*, by performing rapid pressure cycle experiments with the use of the RARE sequence, which exhibited around 40 % signal change per bar, in both the 2.35T small animal Bruker and the 3T whole body Philips MRI scanners. Although this sensitivity is seen to decrease in the presence of a simulated gastric acid solution, the effect has been minimised by suspending the alginate spheres in a locust bean gum gel with a 2 % w/v concentration. The gel solution is also acting as an immobiliser tool preventing the spheres from rising due to the buoyancy of the microbubbles.

The capability of the contrast agent in sensing the dynamic pressure change in the stomach is then tested through *in-vivo* investigation. The study has been carried out on healthy human volunteers by preparing contrast agent as a meal for direct ingestion and

further imaged with the 3T whole body scanner. Initial results with the RARE sequence showed the signal change was dominated by the breathing movement, an artefact which was then dramatically reduced by the use of the BTfE sequence. However, the heterogeneity of the meal being captured in different images of the dynamic measurement was found to be another contributing artefact and we attempted to minimise this by locking the image acquisition to a specific volume of the meal with the use of respiratory triggering. As a result, the signal intensity change exhibited in the meal within the antrum region is between 5 to 10 %. This is slightly higher than expected signal variation which should be around 1.6 to 4.3 %, when considering the typical 40 % per bar sensitivity.

Nevertheless, a novel pressure-sensitive contrast agent has been produced and its capability in measuring pressure changes in simulated human gastric conditions has been demonstrated. Furthermore, the preliminary *in-vivo* study demonstrates that this contrast agent shows great potential in sensing the dynamic pressure change in the human stomach. As a medical diagnostic tool, this will be useful for the clinician as an alternative avenue from the current invasive methods in diagnosing the clinical conditions related to functional dyspepsia.

Acknowledgment

Firstly, I would like to express my gratitude to MARA (the Council of Trust for the Bumiputera), a Malaysian government agency, for funding my PhD research project.

My supervisor, Martin Bencsik, whom I sincerely grateful for his guide and encouragement from the beginning to the end. He tirelessly provided support that I needed while going through the process in completing this work. To my co-supervisors, Gareth Cave, I appreciate all the help especially when it came to the chemistry related works, and David Fairhurst, thank you for the advice and support.

Over the course of this project, I had the privilege to form a collaboration with one of the most prominent MRI research centers, the Sir Peter Mansfield Imaging Centre at the University of Nottingham. For that, I would like to thank Caroline Hoad, Richard Bowtell and Penny Gowland. Also, many thanks to Scott, for helping in the lab particularly in making the samples for the *in-vitro* and *in-vivo* experiments.

I would like to thank my lovely family, especially my parents, Abdurakman Hudini and Nurhanina Ladja, and my siblings for always believing and encouraging me to always follow my dreams. The physical distance (13 000 km from Malaysia to UK), obviously did not stop them from providing me the moral support and the comfort that I need.

Special thanks to Alexander Thieme who has always been there and tirelessly reminding me to keep believing in myself. Also many thanks to my friends whom I shared my experience with, inside and outside the university; Iro, Abeer, Maria P, Susan, Maria B and Giulia, without them the last 4 years would have not been so enjoyable. My very special friend in Malaysia, Noreen, words are not enough to express my gratitude to her for initiating all of this and for motivating me to apply for the MARA funding. I am in debts with her.

Finally, I would like to extend my thanks to everyone who has been involved, directly or indirectly, for making this work as successful as it has been. '*Terima kasih*' which is a Malay expression for 'Thank you'.

Preface

This thesis is divided into eight chapters detailing the works that have been undertaken in developing and testing a microbubble-based MRI contrast agent for pressure measurement in the human stomach. The research has been funded by MARA (Council of Trust for the Bumiputera), a Malaysian government agency, and the work has been carried out at the Nottingham Trent University and the University of Nottingham.

Chapter 1 provides an introduction that describes the practical motivation of the study and it further discusses the background information of the topics that are relevant to this work. Chapter 2 explains the detail of the components and the methods that have been used to design the microbubble-based contrast agents.

Chapters 3 to 6 discuss the experimental work involving *in-vitro* investigations to demonstrate the suitability and capability of the contrast agent in measuring pressure changes, including within the environment simulating the human gastric conditions. Each chapter is further divided into subsections explaining the experimental methods and results of the studies with the relevant discussions.

The remaining experimental chapter (Chapter 7) discusses the *in-vivo* investigations that were carried out on human volunteers demonstrating the functionality of the contrast agent, as a meal, in sensing the dynamic pressure change in the stomach. Finally, the summary of the works presented in this thesis is also provided in the final chapter of the document.

The appendix includes sections showing the scientific posters related to the study that have been presented by the author in various conferences, locally and internationally. It is in the author's professional opinion that there is at least one publishable manuscript that could potentially be produced from this study, where work towards achieving this has been initiated at the time of submitting this document.

CONTENTS

1.	INTRODUCTION	6
1.1	Practical Motivation	7
1.2	Aims and Objectives	8
1.3	The Principles of MRI.....	8
1.3.1	Magnetic Features of the Nucleus	8
1.3.2	Nuclear Magnetic Resonance	10
1.3.3	NMR Relaxation Time.....	11
1.3.4	Magnetic Field Gradients	12
1.3.5	Spatial Encoding	14
1.3.6	Generating Echoes	16
1.3.7	Basic MRI Pulse Sequences	18
1.3.8	Magnetic Susceptibility Effect.....	19
1.4	Microbubble-based Contrast Agents	23
1.4.1	Microbubble-based Contrast Agent Design.....	23
1.4.2	Production Methods	27
1.4.3	Commercial Products	31
1.5	Previous Works Relevant to the Field	32
1.5.1	Gas-filled Microbubble.....	33
1.5.2	Pressure Measurements in the Human Gastrointestinal System.....	40
1.5.3	Previous Studies of Alginate Spheres.....	42
2	DESIGN OF THE MICROBUBBLE-BASED CONTRAST AGENTS	52
2.1	Introduction.....	53
2.2	Components of the Contrast Agents.....	53
2.2.1	Materials	53

2.2.2	Gas-filled Microbubbles Preparations	54
2.2.3	Microbubble Suspending Medium.....	56
2.3	Entrapping Microbubbles in Alginate Spheres for MRI Pressure Measurements in the Human Stomach.....	58
2.3.1	Sphere Formation	59
2.3.2	Sphere Size	60
2.4	Suspending Medium for Microbubble-loaded Alginate Spheres.....	61
2.4.1	Simulated Gastric Acid Solution.....	61
2.4.2	Locust Bean Gum	62
2.5	Conclusions.....	63
3	MRI MEASUREMENTS OF THE CONTRAST AGENTS AT ATMOSPHERIC PRESSURE.	65
3.1	Introduction.....	66
3.2	MR Relaxation Assessment at 2.35T Using A Small Animal Scanner	66
3.2.1	Assessing the Effect of Curing Time	67
3.2.2	MRI Assessment of Alginate Spheres with and without Microbubbles ...	71
3.3	MR Relaxation Assessment at 3T using a Whole-Body Scanner	75
3.3.1	Methods	75
3.3.2	Results	77
3.4	Conclusions.....	78
4	T_2^{EFF} MAPPING OF MICROBUBBLE-LOADED ALGINATE SPHERES WITH PRESSURE	80
4.1	Introduction.....	81
4.2	Methods	81
4.2.1	Pressure Generation	81
4.2.2	Sample holder design.....	82
4.2.3	Contrast Agent preparations.....	82
4.2.4	Experimental set-up	83

4.3	Results	84
4.4	Conclusions.....	88
5	MRI SENSITIVITY OF MICROBUBBLE-LOADED ALGINATE SPHERES TO PRESSURE VARIATION	91
5.1	Introduction.....	92
5.2	In-Vitro Studies at 2.35 Tesla Using a Small Animal Scanner.....	92
5.2.1	NMR Signal Changes to Rapid Pressure Cycling in Water.....	92
5.2.2	MRI Sensitivity with Different Bubbles Densities, and Effect of an Acid Simulating Gastric Conditions	96
5.2.3	MRI Sensitivity at Body Temperature, 37 °C.....	100
5.3	In-Vitro Studies at 3 Tesla using Whole Body Scanner	102
5.3.1	Assessing the Sensitivity of Contrast Agent in Water Suspension at 37 °C	103
5.3.2	Assessing the Sensitivity of the Contrast Agent in Simulated Gastric Solution	108
5.3.3	MRI sensitivity in locust bean gum and acid solution simulating gastric conditions.....	112
5.4	Conclusions.....	115
6	DEMONSTRATING SPATIAL PRESSURE GRADIENT USING MICROBUBBLE-BASED MRI CONTRAST AGENTS.....	119
6.1	Practical Motivation	120
6.2	Microbubbles in Gellan Gel	121
6.2.1	Introduction	121
6.2.2	Sample holder design.....	121
6.2.3	Sample preparations	122
6.2.4	Pre-MRI experiment set-up.....	122
6.2.5	Experiment set-up.....	124

6.2.6	Results	125
6.3	Microbubbles Entrapped in Alginate Spheres.....	128
6.3.1	Introduction	128
6.3.2	Experimental Set-up.....	128
1.1.1	Results	129
6.4	Conclusions.....	131
7	MRI IN-VIVO STUDIES.....	135
7.1	Introduction.....	135
7.2	Study Design	135
7.2.1	Selection of Participants	135
7.2.2	The Contrast Agent Meal	137
7.2.3	Study Arrangement.....	137
7.3	Flavour Enhancement of the Contrast Agent.....	138
7.3.1	Experimental set-up.....	138
7.3.2	Results	139
7.4	In-Vivo Investigation using the RARE Sequence.....	140
7.4.1	Method.....	140
7.4.2	Results	141
7.5	Exploring HASTE and BTFE Sequences to Minimise the Effect of Movement Artefacts.....	142
7.5.1	Method.....	143
7.5.2	Results	143
7.6	Optimisation of the BTFE Sequence in Sensing Pressure Changes in the Human Stomach.....	148
7.6.1	In-Vivo Study: Varying the Image Resolution	148
7.6.2	In-Vitro Experiment: Varying the Slice Thickness of the BTFE Sequence.....	153

7.6.3	In-Vitro Experiment: Varying the T_2 prep Time of the BTFE Sequence ..	156
7.7	In-vivo Investigations of the Alginate Spheres Using the BTFE Sequence with Respiratory Triggering.....	158
7.7.1	In-Vivo Study on Alginate Spheres without Microbubbles	158
7.7.2	In-Vivo Study on Alginate Spheres with Microbubbles	162
7.8	Participants' Feedback	166
7.9	Conclusions.....	167
8	DISCUSSION	170
	APPENDIX	175

CHAPTER 1

INTRODUCTION

1. INTRODUCTION

1.1 Practical Motivation

Contrast agents are used widely in various medical applications providing a specific alteration and enhancement in the image contrast, useful to the clinical diagnostic. A notable combination between MRI and contrast agents has shown great impact in clinical applications, especially in helping to further distinguish between the healthy and unhealthy tissues or organs. Our work in this project is intended to explore the feasibility of using gas-filled microbubbles within a tailored MRI contrast agent and its suitability, for *in-vitro* and *in-vivo* applications, in measuring pressure changes in the human stomach.

It has been demonstrated in a previous MRI study (Alexander, McCreery et al. 1996) that microbubbles have great potential to be used within contrast agents in measuring pressure changes in the vascular system and other organs. Commonly, phospholipids molecules are used as a thin shell material encapsulating gas in the core creating micrometre-sized bubbles. The compressibility of these bubbles causes them to undergo size changes due to pressure, therefore altering the corresponding NMR signal. In ultrasound imaging, this type of bubble is commercially available in the form of an injectable fluid solution.

In some clinical conditions such as functional dyspepsia, the symptoms of the patient are greatly related to the disruptions of normal function of the stomach (Wilmer, Van Cutsem et al. 1998), and are thought to result in abnormal variations in the meal pressure exerted by the stomach. It should therefore be of great value to develop a pressure-sensitive MRI contrast agent. The solution we have explored in this study consists in entrapping microbubbles in alginate gel spheres and we further demonstrated its sensitivity in measuring the pressure changes in *in-vitro* and *in-vivo* applications.

In order to map pressure changes in different areas in the meal within the stomach, it would be challenging to use a fluid solution because the pressure would nearly equilibrate instantaneously throughout the meal's volume. However, using a soft-solid

material, such as a large collection of small alginate spheres as an artificial meal is expected to overcome this issue allowing measurement of pressure changes to local compression. In this way, the microbubbles are immobilised in an elastic gel network whilst maintaining its compressibility and flexibility.

1.2 Aims and Objectives

This work is focusing on the development of microbubble-based contrast agents for ingestion, for humans, with applications in diagnostic Magnetic Resonance Imaging of the gastrointestinal system, by means of non-invasive meal pressure measurement.

The aims of the works are

- to design a microbubble-based contrast agent for ingestion and *in-vivo* MR investigation of the pressure spatial distribution in the human stomach's meal.
- to rapidly map the NMR relaxation time changes within the contrast agent as the pressure change.
- to test and quantitate the performance of the contrast agent on *in-vitro* applications, including within the condition simulating the human stomach.
- to demonstrate a spatial pressure gradient on the microbubble-containing meal using MRI.
- to test, through *in-vivo* applications, the capability of the contrast agent in sensing pressure changes in the stomach of healthy human volunteers.

1.3 The Principles of MRI

In this section, we will discuss the basic theory related to Magnetic Resonance Imaging (MRI), to be able to have a fundamental understanding before we further discuss its application in our study.

1.3.1 Magnetic Features of the Nucleus

MRI works using the intrinsic magnetisation of some nuclei and also requires these to be placed in an external magnetic field. Nuclear spin is an intrinsic property of each atomic nucleus. It can be zero or non-zero for a given nucleus based on the combination

of protons and neutrons that constitute it. Nuclei with a non-zero spin exhibit magnetic moment and angular momentum characteristics. There are some biologically-relevant elements, in particular, hydrogen (^1H), carbon (^{13}C), oxygen (^{17}O) and sodium (^{23}Na) which are able to produce signals known as nuclear magnetic resonance (NMR). As the human body is composed of approximately 62 % of hydrogen atoms, the nucleus of this atom, the proton, is the principal element for generating NMR signals. The magnetic characteristics of the nucleus are described by the nuclear magnetic moment. It is a vectorial field quantity that can be represented by a collection of vectors indicating the magnitude and direction of the magnetic field distribution surrounding the nucleus. Basically, the spinning proton, or nuclear spin, generates its own small magnetic field.

A great abundance of spins aligned together will result in a measurable magnetic moment, called the macroscopic nuclear magnetisation. Naturally, the spins in a biological tissue for example, are distributed with random orientations due to the thermal energy being orders of magnitude larger than the magnetic energy interaction with the earth's magnetic field. As a result, the macroscopic magnetisation is approximately zero. However, if these spins are placed in a strong static external magnetic field, B_0 , they will tend to align with it in two possible orientations, either parallel or antiparallel to it. The orientation of each spin depends on how much energy it has, the anti-parallel requires higher energy than parallel spins. The energy difference between parallel and antiparallel states is directly proportional to the strength of B_0 . A slightly greater number of spins exist in a parallel direction resulting in a measurable net magnetisation, M_0 , in the direction of B_0 . This process is called nuclear spin polarisation. The ratio of the number of spins parallel (low energy) with spins antiparallel (high energy) is given by the Boltzmann distribution:

$$\frac{N_{high}}{N_{low}} = e^{-\frac{\gamma \hbar B_0}{kT}}$$

Equation 1.1

where N_{high} is the number of spins in the high energy, N_{low} is the number of spins in the low energy, γ is the gyromagnetic ratio of the nuclear species of interest, ($\hbar = h/2\pi$) is Planck's constant, B_0 is the strength of the external field, k is Boltzmann's constant and T is the temperature.

During the polarisation, the spin also experiences a torque which makes it precess around the direction of B_0 . The precession occurs at an angular frequency, known as the Larmor frequency, ω_0 , that is proportional to B_0 , as described by the Larmor equation,

$$\omega_0 = \gamma B_0$$

Equation 1.2

1.3.2 Nuclear Magnetic Resonance

To be able to measure M_0 , a brief radiofrequency (RF) excitation field, which is orthogonal to the direction of B_0 , is applied. This results in the tilting of M_0 , at an angle relative to the direction of B_0 , on to the plane which conventionally known as the transverse plane (x-y) (Figure 1.1). In order to have an effect, the frequency of the RF pulse, transmitted by a coil, is tuned to match the Larmor frequency. Furthermore, as the RF pulse is applied, all the spins are in phase coherence, which means that they point into the same direction.

As a result, a voltage is induced which is proportional to the angle of the M_0 relative to the direction of the B_0 . This voltage constitutes the NMR signal itself and can be monitored by using a receiver coil. In the absence of the external RF field, the net magnetisation will always attempt to return to the equilibrium state by precessing (at the Larmor frequency) about the direction of the static magnetic field. Therefore, when the RF pulse is turned off, M_0 is left to precess about the longitudinal axis and the amplitude of the magnetisation in the transverse plane decays exponentially to zero within a typical time called T_2 or transverse relaxation time.

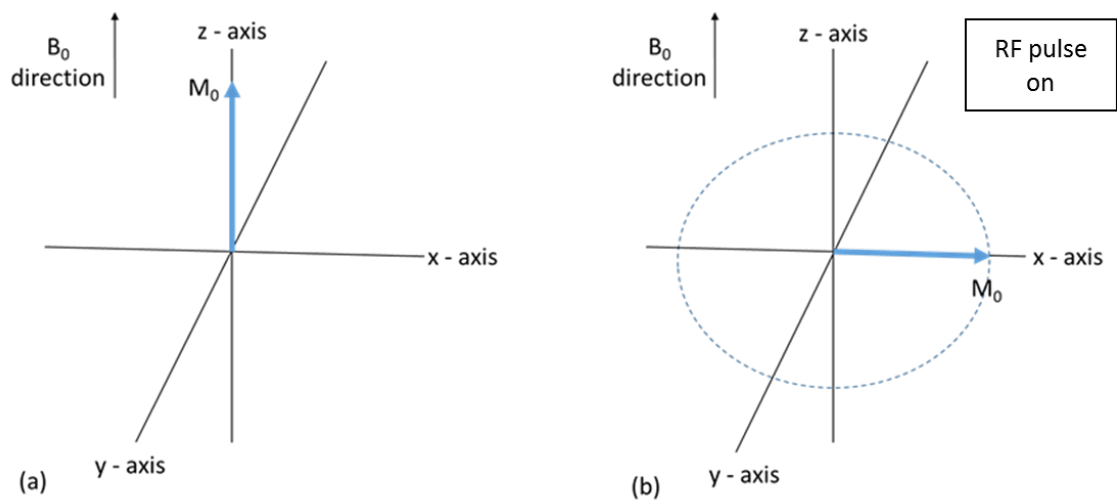


Figure 1.1 – (a) The net magnetisation (bolded arrow), M_0 , is parallel to the direction of B_0 on a z-axis called by convention the longitudinal axis. (b) After application of the RF pulse, M_0 resides in the transverse (x-y) plane. The dotted circle represents the trajectory of the magnetisation vector experiencing precession about the polarising field.

1.3.3 NMR Relaxation Time

Relaxation times describe how long the magnetisation takes to get back to equilibrium after an RF pulse. There are two types of relaxations involved, which are spin-spin and spin-lattice relaxation, also respectively known as T_2 and T_1 relaxations.

1.3.3.1 Spin-Spin Relaxation

Spin-spin relaxation is also called the T_2 relaxation. Whenever the spins come close to each other, an interaction takes place which affects their individual magnetic moment and relative phase angle, irreversibly. With time, phase scrambling increases, until it reaches the point where the spins are fully out of phase, resulting in a zero vector sum of nuclear magnetisation. Normally, the time taken for the magnetisation to reach zero is of the order of milliseconds (or longer), with an exponential time-course, as in:

$$M_{xy}(t) = M_0 e^{-t/T_2},$$

Equation 1.3

where $M_{xy}(t)$ is the transverse component of magnetisation at time, t , and M_0 is the transverse magnetisation at $t=0$. The relaxation time T_2 is therefore also the time taken by the transverse component of magnetisation to decay to approximately 37 % of its original amplitude after the excitation RF pulse.

Inhomogeneities in the polarising field will also further contribute to the spin phase scrambling. However, this effect is fully reversible in the absence of molecular diffusion, and partially reversible in the presence of molecular diffusion. After a single excitation pulse, the exponential decay time constant due to both spin-spin interaction and external field inhomogeneities is known as T_2^* , which is shorter than T_2 relaxation.

1.3.3.2 Spin-Lattice Relaxation

In parallel, after the RF pulse is switched off, the magnitude of longitudinal magnetisation begins to recover to equilibrium in an exponential time course, simultaneously with transverse magnetisation decay. However, the time taken for the longitudinal magnetisation to recover is usually longer (or equal) than for the transverse magnetisation. The term spin-lattice relaxation is describing the spins interacting with the lattice, e.g. the surrounding tissue. The time course of the magnetisation is as follows:

$$M_z(t) = M_z(0)e^{-t/T_1} + M_0(1 - e^{-t/T_1}),$$

Equation 1.4

where $M_z(t)$ is the longitudinal magnetisation at the time, t , and M_0 is the peak amplitude of the longitudinal magnetisation, in an equilibrium condition. When $t = T_1$, M_z is approximately $0.63M_0$, meaning that the T_1 relaxation time is the time taken by the longitudinal magnetisation to recover to 63 % of its peak amplitude.

1.3.4 Magnetic Field Gradients

In addition to the polarising field and RF coils, an MRI machine is normally equipped with a third coil assembly which enables the encoding of the NMR signal so as to reconstruct two or three-dimensional images. This coil is commonly known as the gradient coil. It is usually mounted in the core of the scanner generating a longitudinal magnetic field with

spatial variations in strength, enabling the information on the position where the NMR signal is emitted to be worked out from the frequency of the signal.

For example, one of the coil types that can be used for this purpose is the Maxwell pair, which uses a single pair of coils as shown in Figure 1.2 to generate a field gradient (G_z) in the z-axis, along the direction of the polarising field. The field generated by this coil has a linear spatial dependence towards the middle of it. At the centre of the gradient coils, and also the centre of the polarising coil, there is no additional magnetic field generated. The field resulting from the addition of the polarising field and that of the field gradient respectively increases or decreases linearly along the coordinate of the z-axis for positive and negative values of z.

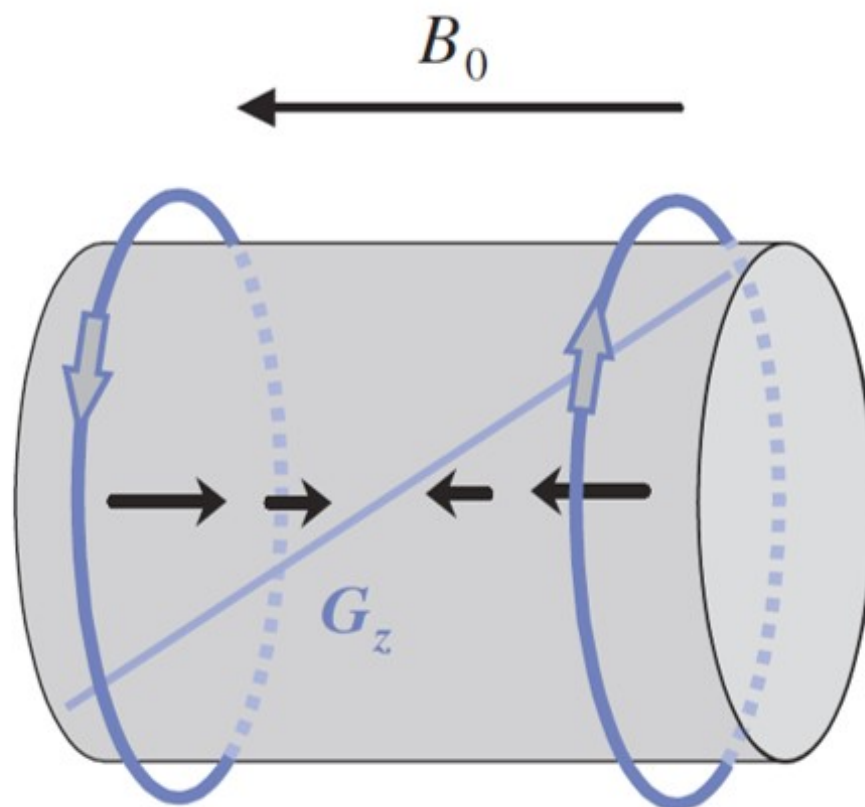


Figure 1.2 – A single pair of coils with counter-rotating currents (blue circles) known as the Maxwell pair is used to produce a field gradient (G_z), represented with the diagonal blue line, along the direction of the polarising field (z-axis), in the MRI scanner (McRobbie, Moore et al. 2006).

When both of the polarising and gradient fields are combined, the resulting externally applied field is now also spatially dependent, which consequently affects the

magnetisation precession frequency. This means that protons in the centre of the coil precess at the same frequency as those affected by the polarising field only, and increases or decreases respectively with distance from the centre. This spatially dependent Larmor frequency is represented by the equation below:

$$\omega(z) = \gamma(B_0 + G_z z)$$

Equation 1.5

The gradient field can be applied in different axis, G_x , G_y or G_z or combinations of these, which can be used for this purpose, allowing us to produce transverse, sagittal, coronal or oblique slices.

1.3.5 Spatial Encoding

The NMR signal is a rapidly changing electric voltage in the receiver coil, oscillating at high frequencies. This is converted to a digital signal which is stored temporarily in the computer before being reconstructed into the final image. It has been described in the previous section, by combining the polarising field and the RF excitation with a gradient, the MR interactions and information collections are focused to a two-dimensional plane, which also known as slice selection. In order to obtain a further localised information within this plane, the NMR signal is encoded in terms of the spatial frequencies of the object using phase encoding and frequency encoding gradients.

1.3.5.1 Phase Encoding

The phase-encoding is the process of locating an MR signal by altering the phase of spins in one dimension with a pulsed magnetic field gradient along that dimension prior to the acquisition of the signal. This allows the information to localise the signal to a particular row of the data matrix.

If the system starts with all the magnetic moments aligned, we can cause a spatially dependent de-phasing by applying this gradient. Then, when we switch off the gradient, all the nuclei will revert to their original frequency or speed, but will keep their different phase angles. This way, they are said to be phase encoded. The relative phase

differences between signals in different locations remain until either another gradient is applied or the phase become scrambled due to T_2^* .

1.3.5.2 Frequency Encoding

Frequency encoding uses the same gradients as in phase encoding but this time the magnetic resonance signal is collected during the application of the gradient. Using frequency encoding removes the need to wait for the repetition time between steps in the second dimension. In spin warp imaging, after the excitation RF pulse, a phase encoding step is performed at a given intensity before measuring the magnetic resonance signal during the application of a frequency encoding gradient. This is then repeated with different phase encoding gradient intensities.

If we applied frequency-encoding gradients in two directions at the same time we would have no way of knowing whether a particular frequency in the signal originated from one or the other (or both) of the applied gradients. By combining phase encoding and frequency encoding in two orthogonal directions we can collect all the spatial frequencies that we need to make the image unambiguous. The collected signal from both of these techniques is stored in k-space.

1.3.5.3 k-Space

k-Space is the raw data matrix, which is used to store the digitised MR signals during data acquisition. The signal information collected from the frequency and phase is encoded as rows and columns. During the collection of the information, the k-space is filled line by line. Once the matrix is full, the data in k-space is reconstructed using a mathematical operation called Fourier transform (a mathematical operation that relates the phase and encoding data) to produce the final image. Although the transformed data matrix size corresponds to the image matrix size, the pixels do not correspond directly with each other. For example, the information in the top right pixel in k-space does not contain the raw information for the top right pixel in the final image. Instead, in k-space, the central regions contain signal-to-noise and contrast information for the image, and data around the edges contain all the information about the image resolution.

1.3.6 Generating Echoes

There are two main types of echoes in MRI, the Spin Echo (SE) and the Gradient Echo (GE). Both techniques begin with an RF pulse excitation to flip the magnetisation into the transverse plane.

The spin echo phenomenon has been first discovered and explained by Hahn (Hahn 1950). A schematic representation of the spin echo generation is shown in Figure 1.3. In the SE technique, the RF pulse flips the longitudinal magnetisation to the transverse plane, leaving the spins to dephase naturally, as explained in section 1.3.2. Subsequently, an RF pulse with 180° flip angle, also called refocusing pulse, is applied to rephase the spins and to create an echo (Carr, Purcell 1954). Following the application of the refocusing 180° pulse, the phase angle of spins is inverted (Figure 1.3 (d) and (e)), resulting, after a specific time duration, in the partial cancellation of the dephasing effect caused by the polarising field inhomogeneities. After a delay of time equal to the time between 90° and 180° pulses ($TE/2$), the spins phase coherence is partially re-established, producing a spin echo. The time taken from the 90° RF pulse to the production of the spin echo is known as the echo time (TE).

The refocusing can be repeated several times to allow determination of the spin-spin relaxation exponential time constant. Because of molecular self-diffusion, the spins will not remain in the same magnetic field during this process, and in consequence the magnetisation will not return to its original value, instead returning to some percentage of it. The drop in peak magnetisation of each echo is another measure of the properties of the system and takes place exponentially with time constant known as the effective T_2 (T_2^{eff}). By choosing a suitable value for the echo time, the effect of the diffusive motion can be minimised or enhanced.

The main difference between SE and GE techniques is the absence of the refocusing RF pulse in GE. Gradient echo sequences use field gradients to dephase or refocus the magnetic moments. In the most basic GE sequence, after the application of the excitation RF pulse, a magnetic field gradient is applied which causes the spins to dephase rapidly. A field gradient with opposite polarity is further applied, after a period of time, $TE/2$, which change the direction of the induced precession. This causes the

spins to rephase and creating gradient echo. This means the spins are refocused by reversing the direction of the spins rather than flipping them over to the other side of the plane (the x-y plane) as occurs with the SE sequence. However, the effects of the polarising field inhomogeneities are not cancelled out in GE, which means the signal decays faster. The GE technique requires a relatively short time, hence, this method is widely used in fast MR imaging sequences.

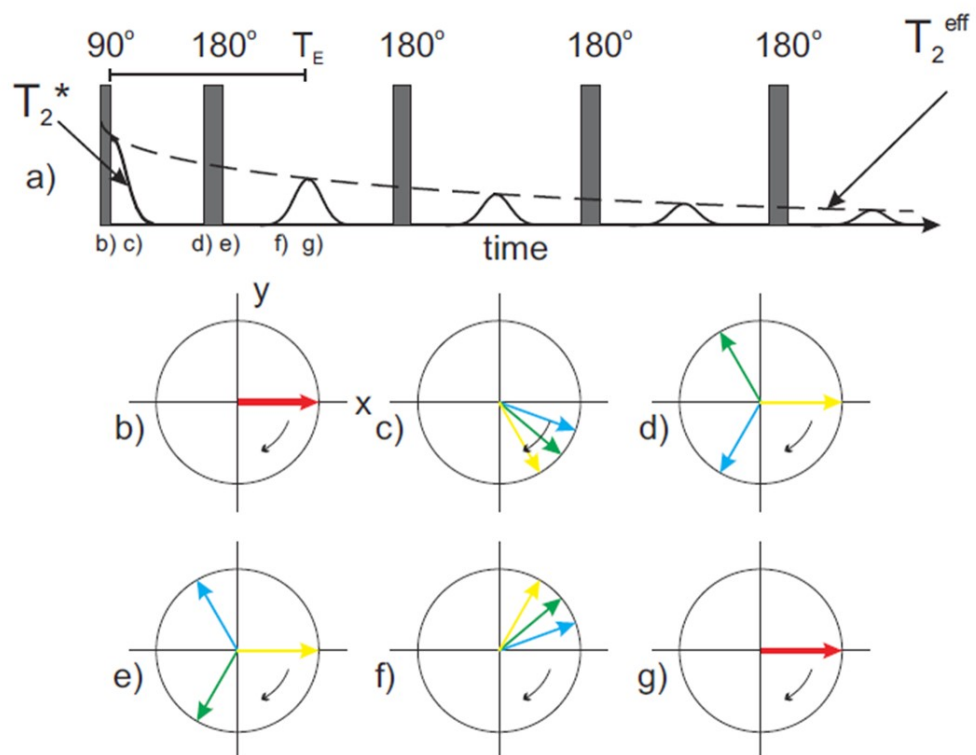


Figure 1.3 – Diagram showing the formation of a spin echo (SE). a) After the 90° RF pulse excitation, a subsequent 180° RF pulse is applied to refocus the spin and thus, the SE signal is formed after a delay of time, T_E . b) Magnetisation after tipping into transverse plane, c) Dephasing magnetisation, d) Dephased magnetisation, e) System after application of refocusing pulse along x, f) Magnetisation near beginning of echo envelope, g) Magnetisation at the echo time after the initial pulse. Red arrow is all magnetic moments in phase; yellow, green and blue arrows are, respectively, fast, medium and slowly dephasing magnetic moments. Diagram reproduced from Morris, 2009.

1.3.7 Basic MRI Pulse Sequences

A pulse sequence is a set of RF and gradients pulses which are usually repeated in a series, each separated by the repetition time, TR. Generally, a pulse sequence is created based on a spin echo or gradient echo. There is a great number of pulse sequences being used for MR image acquisition. In this study, three particular pulse sequences we used; Multi-Slice and Multi Echo (MSME), Rapid Acquisition with Relaxation Enhancement (RARE) and Balanced Turbo Field Echo (BTFE).

1.3.7.1 MSME Sequence

The MSME sequence works based on the SE technique (Carr, Purcell 1954). In this sequence, the excitation 90° RF pulse is applied to flip the longitudinal magnetisation into the transverse plane and then, followed by multiple refocusing 180° RF pulses to create an echo train. The amplitudes of the echoes are decreasing over time, in an exponential decay with decay constant called the effective transverse relaxation, T_2^{eff} . A train of echoes contribute to a single line in a raw data matrix, the k-space.

After a delay of time, TR, the same step is repeated, meaning another echo train is collected. This process is continuously repeated until the k-space is fully scanned. The imaging time is longer when compared to other sequences e.g. RARE, because each k-space line requires an excitation pulse. The advantage is a large amount of information is collected due to the multiple echoes. The MSME is effectively used as a method for measuring the T_2^{eff} value.

1.3.7.2 RARE Sequence

The RARE sequence is a fast imaging method with T_2 -weighting image quality (Hennig, Nauerth et al. 1986). The RARE sequence, which also known as Turbo Spin Echo (TSE), is a modification of the multi-echo sequence, thus involves RF excitation and echo train generation as seen before. Each echo in the echo train is individually phase encoded in an incremental order. In this sequence, each echo corresponds to a different line in the k-space. This means that a single echo train can be used to produce a full 2D image, if the T_2 value is long enough. One of the parameters to be determined for this sequence is the effective echo time, TE^{eff} , which is defined as the time between the application of

the excitation RF pulse and the echo acquired at the centre of k-space. In our application, the typical TE^{eff} explored is ranging between 300 to 600 ms.

1.3.7.3 BTFE Sequence

The Balanced Turbo Field Echo (BTFE) (Oppelt, Graumann et al. 1986), also commonly known as TrueFISP (True Fast Imaging with Steady-state Precession), is a gradient echo technique. This sequence is based on a gradient echo steady state magnetisation method, in which the magnetisation is kept constant with each repetition. This requires the same sequence of RF excitation pulse repeated with a very short TR, which is shorter than the T_2 value, until the magnitude of the magnetisation is constant from one repetition to the other. Once this equilibrium is reached, two types of signals are produced: the first signal is free induction decay (FID), which is formed after excitation with the most recent RF pulse. The second component is spin echo, which is formed when the residual echo from the previous RF excitation is refocused by the current RF pulse.

Due to the ultrashort acquisition time, the image quality of the BTFE images is not affected by motion, which make this sequence suitable for cardiac and abdomen imaging where breathing and organ involuntary movement could cause the image artefacts.

Additionally, it has been previously shown that it is possible to produce a T_2^{eff} -weighted MR image using single-shot BTFE with a spin echo (SE) preparation pulse, which is also known as the T_2 -preparation time, applied immediately before the BTFE pulse (Hoad, Cox et al. 2010). This method is particularly useful in our application as we need this time delay to leave some time for the T_2^* contrast to take place in the contrast agent.

1.3.8 Magnetic Susceptibility Effect

The application of an external magnetic field is able to induce a magnetisation in a material. The strength and polarity of the resulting magnetisation depend on the material under investigation, based on their electrons arrangement in the atomic and molecular structure. This is described macroscopically as the magnetic susceptibility effect.

The following equation defines the magnetic susceptibility of a material:

$$\mathbf{M} = \chi \mathbf{H}$$

Equation 1.6

where \mathbf{M} is the magnetisation of the material, χ is the magnetic susceptibility and \mathbf{H} is an externally applied magnetic field.

The magnetic susceptibility is classified into at least three categories: diamagnetic, paramagnetic and ferromagnetic. Diamagnetic materials induce an internal magnetisation effect, also known as negative susceptibility, which opposes to the external field direction, lowering the overall magnetisation within the material. Examples of diamagnetic materials are water and most organic compounds. In contrast, paramagnetic materials will slightly increase the resulting magnetic field, hence, it is defined as having a positive susceptibility. Gadolinium-based contrast agents, widely used in medical applications, exploit this effect. Similarly, ferromagnetic materials will also increase the local magnetic field, but to such an extent that it severely disturbs the magnetic field homogeneity, and consequently deteriorates the signal acquisition.

1.3.8.1 The Effect of Internal Magnetic Field Gradients

A gradual change of field strength, or magnetic field spatial gradient, is generated between two adjacent materials with different inherent magnetic susceptibilities. The susceptibility contrast created by these two materials causes a local field gradient commonly known as an internal magnetic field gradient. In some cases, this effect is regarded as a disadvantage because it can cause image artefacts for example in the brain, where the sinus spaces filled with air are in the immediate vicinity of bone and soft tissue generating strong internal gradients. However, this effect can be used to an advantage, such as in our work, where we exploited the magnetic susceptibility difference between gas and liquid in a gas-filled microbubble.

1.3.8.2 Magnetic Field Perturbation Around Compressible Sphere

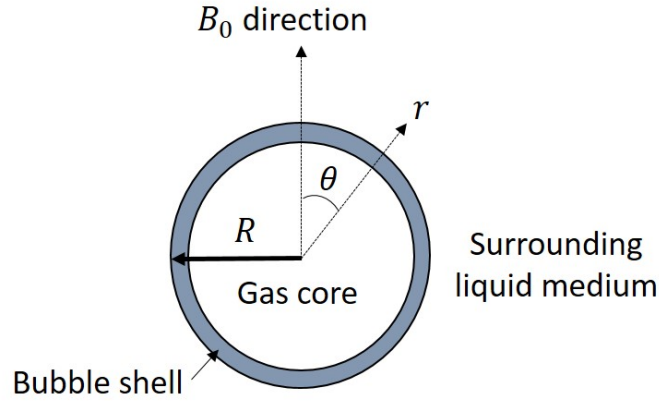


Figure 1.4 – Schematic representation of the gas-filled microbubble with radius R showing the local magnetic perturbation at the coordinates (r, θ) in an external field B_0 as explained in Equation 1.7.

The effect of a gas-filled microbubble residing in a liquid and further placed in a static magnetic field has been explored in previous work. A magnetic susceptibility step change takes place at the microbubble periphery due to the gas-liquid interface at the microbubble shell. This is defined by the following (spherical coordinate system) equation (Dharmakumar, Plewes et al. 2002)

$$\frac{\Delta B(r, \theta)}{B_0} = \frac{1}{3} \Delta \chi \left(\frac{R}{r} \right)^3 (3 \cos^2 \theta - 1),$$

Equation 1.7

where ΔB is the local magnetic perturbation at the coordinates (r, θ) , r is the radial distance from the centre of the microbubble at angle θ from the direction of the static polarising magnetic field, B_0 , and $\Delta \chi$ is the magnitude of magnetic susceptibility difference between the bubble gas with the surrounding medium, and R is the radius of the microbubble (Figure 1.4).

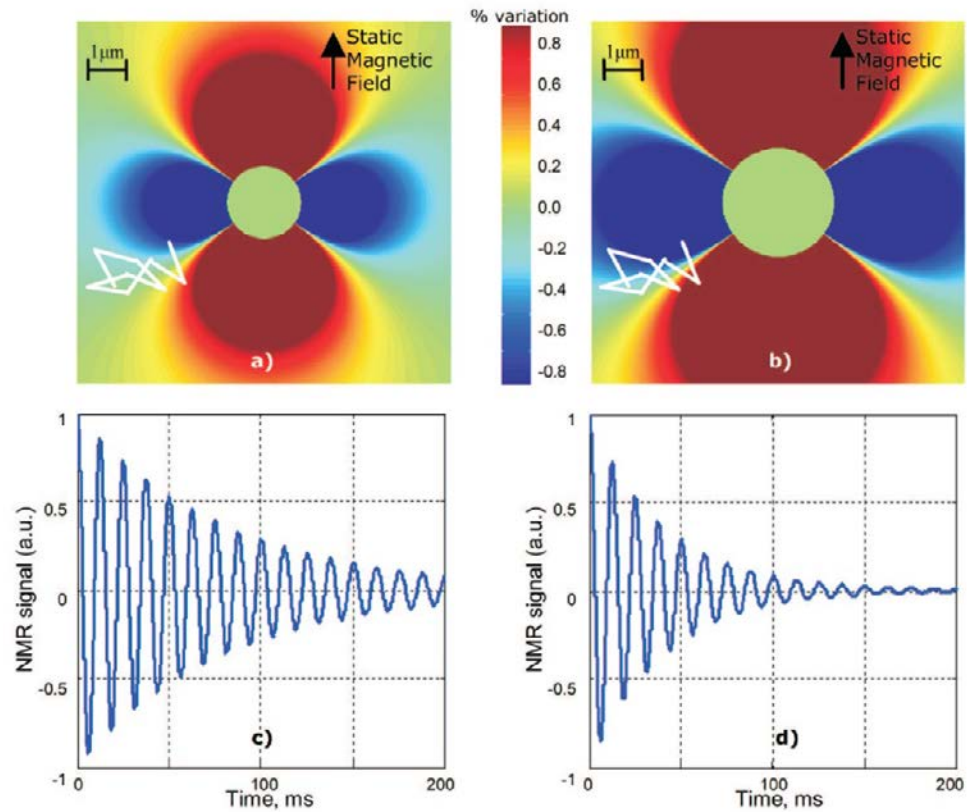


Figure 1.5 – Schematic plot showing the magnetic field perturbation of two different sizes of bubbles (central disc), (a) 2 μm and (b) 3 μm , with the proton undergoing the same diffusion random path (white lines). Their measured FID is shown respectively in (c) and (d) (Morris 2009).

As the proton-carrying molecules in the suspending fluid diffuse around a microbubble, they sample different magnetic field strengths as a result of the perturbations, with the molecules closer to the vicinity of the microbubble experiencing faster dephasing compared to those farther away. In addition to this, the compressibility of these bubbles enables them to undergo a radius change when an external pressure is applied, which consequently changes the spatial distribution of the local magnetic field perturbation and thus the T_2^* NMR relaxation time (Alexander, McCreery et al. 1996). This effect is demonstrated in Figure 1.5. The greater the field perturbations sampled by the proton, the greater the extent to which the signal will decay due to dephasing, which yields image contrast to fluid pressure. There is a number of works that have been published, theoretical and experimental, regarding the application of this system, and these are exhaustively discussed in section 1.5.

1.4 Microbubble-based Contrast Agents

As we have seen, gas-filled microbubbles create a magnetic susceptibility effect due to the air to liquid interface. Various works have demonstrated that microbubbles with this unique susceptibility effect offer the design of promising contrast agents for a direct pressure measurement in fluid. The potential application of the microbubble in MRI was initially described by Unger et al., suggesting this can be used as a contrast agent to improve visualisation of blood circulation in the brain (Unger, Ugurbil et al. 1994). Soon after, the application of these bubbles in an MRI pressure measurement was experimentally explored and proposed as a non-invasive technique to evaluate a cardiovascular function (Alexander, McCreery et al. 1996).

1.4.1 Microbubble-based Contrast Agent Design

1.4.1.1 Components

Microbubbles are typically formulated from biocompatible materials, such as phospholipids and biopolymers, as a shell and a gas filling in the core (Chow, Chan et al. 2010). Concomitantly, the main components of our contrast agent consist of the shell material of the microbubbles, the gas filling and the medium in which they are suspended. The properties of each of these components are discussed in this section.

1.4.1.1.1 Shell Materials

The shell material is used to encapsulate the gas in forming the microbubble. The selection of its material is important to obtain a stable microbubble preparation. In medical imaging applications, the microbubble shell consists of biocompatible materials to enable this type of contrast agent suitable to be used in the human body. There are two types of microbubble shell currently available, the stiff type which is typically made from polymers (Glynos, Koutsos et al. 2009) and the flexible shell normally composed of phospholipids (Santos, Morris et al. 2012). In our works, we used phospholipid as the bubble shell material of our contrast agent, due to its compressibility, in response to an external pressure. The characteristics of both shell types will be explained in this section.

1.4.1.1.1.1 Phospholipids

For MRI pressure measurement, phospholipids such as Dipalmitoyl Phosphatidylcholine (DPPC) and Distearoyl Phosphatidylcholine (DSPC) are preferable for a flexible shell to maximise the compressibility effect (Kaur, Morris et al. 2009).

A phospholipid is an amphiphilic molecule, with a hydrophilic head group and a hydrophobic tail, which works as an air-water interface layer between the gas bubble and its surrounding medium. As suggested in Figure 1.6, the hydrophilic polar head orients itself spontaneously facing outwards to the aqueous region, whilst the hydrophobic tail consisting of hydrocarbon chains tends to face inwards to the air or gas phase (Tanford 1980).

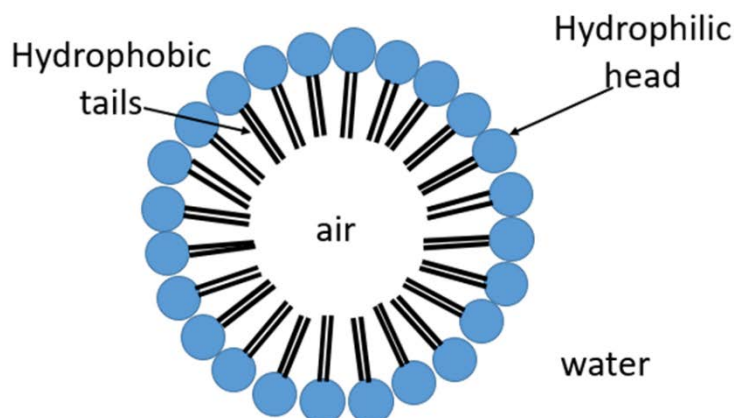


Figure 1.6 – The hydrophilic polar head orients itself spontaneously facing outwards to the aqueous region, while the hydrophobic tail tends to face inwards to the air or gas phase.

In addition, it has been shown by adding cholesterol to the components of phospholipid formulations that the stability of microbubbles can be significantly increased without affecting its size (Kaur, Morris et al. 2009). This component acts as an additional hydrophilic coating to the microbubble shell and prevents them from coalescing, which increases their longevity in the surrounding medium.

1.4.1.1.1.2 Polymer

Another type of gas-filled microbubble that is currently used is the polymeric microbubble (Bloch, Wan et al. 2004), but not in the pressure measurement context. Its shell component is made from polymer materials such as polymer polylactide. Compared to the phospholipid microbubble, the shell properties of polymeric microbubble are generally stiffer (Glynos, Koutsos et al. 2009). Nevertheless, this type of microbubbles is extensively used as an ultrasound contrast agent, particularly in monitoring blood flow through the circulatory system, and has shown a great success as a drug delivery carrier in biomedical applications (Hernot, Klibanov 2008).

1.4.1.1.2 Gas Filling

The properties of the gas filling in the core of microbubbles have an influential effect on its stability. In the early design of microbubbles, the air was used as a gas filling. They were made commercially available for ultrasound imaging applications, requiring an injection into blood vessels (Keller, Glasheen et al. 1989). The challenge when using this contrast agent is that the microbubbles disappear from the bloodstream within seconds after administration because of the high solubility of air in the blood (Schutt, Klein et al. 2003). Schutt et al. explained the reason for this is that the gas pressure within the bubbles is the sum of the equilibrium pressure (Henry's law); the Laplace pressure, and the blood pressure, which together exceed the gas pressure in the blood.

Hence, inert gases with high molecular weight and low solubilities such as perfluorocarbons and sulphur hexafluoride have been used in more recent microbubble contrast agents (Sboros 2008). This increases their stability and has effectively prolonged their lifespan in the medium compared to the air (Kogan, Gessner et al. 2010). For this particular reason, in our study, perfluorocarbon gas, octafluoropropane, was used in all of our preparations to make stabilised microbubbles and the methods of production will be fully discussed in chapter 2 of this thesis. A list of commercially available microbubbles and their gas filling is shown in Table 1.1.

1.4.1.2 Suspending Medium

The suspending medium is the viscous solution surrounding the microbubbles and constituting a full part of the contrast agent. It serves as an immobilising tool, and also

enables the MR measurements to be taken. Normally, the microbubbles are produced in an aqueous solution which gives these bubbles a natural buoyancy. It is essential that the suspending medium fulfils certain requirements, not just to prevent the bubbles from rising but also to keep them functional. It should furthermore contain free water molecules which are able to diffuse around the microbubble with a self-diffusion coefficient as close to that of bulk water as possible. In addition, the suspending medium must be made from materials which are harmless to the human body allowing us to use the contrast agents for medical purposes.

Within the past MRI investigations, the earliest work was using methylcellulose as a microbubble suspending medium, as reported in 1996 (Alexander, McCreery et al. 1996), where the bubbles were seen to rise within the preparation. Over the past years, several other types of suspending media have been used relating to microbubble-based contrast agents and mostly containing polysaccharide molecules, for example, gellan gum and xanthan gum (Morris, Bencsik et al. 2008). The long chain properties of polysaccharide molecules (Figure 1.7), enables them to form a polymer network to entangle the microbubbles, making this molecule one of the most common materials used as a suspending medium for microbubbles. Morris has demonstrated the gellan gel at 2 % (w/v) concentration was able to immobilise the bubble with minimal reduction in the diffusion coefficient. Furthermore, another useful property of many polysaccharides is that their viscosity can be further increased by cross-linking their structure with a salt.

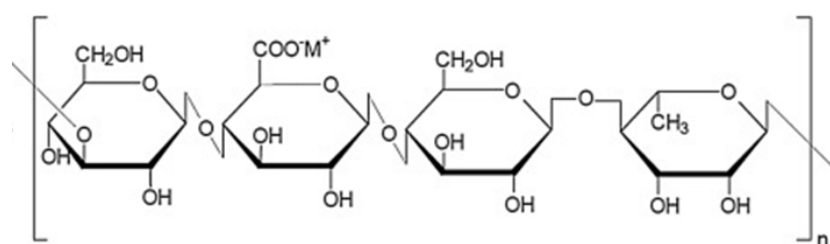


Figure 1.7 – The Chemical structure of the gellan gum (Cassanelli, Norton et al. 2017).

For the purpose of our study, we used gellan gel (2 % w/v) to immobilise the bubbles in the initial part of our experiments, and then we further moved on to using alginate as it is able to entrap microbubbles and form a soft solid gel while maintaining flexibility to compression. This owes to their special ability to form a sphere mainly in the presence

of calcium ions (Draget, SkjakBraek et al. 1997). When these ions are added, the molecular chains in the alginate solution bound to each other in a process known as cross-linking (Figure 1.8). In general, alginate is a natural polysaccharide commonly extracted from brown algae, which is part of the cell wall and intracellular material (Rinaudo 2014). It has been widely used in the food industry (Lee, Rogers 2012) as a food additive, stabiliser and thickening agent. In addition, this substance is available at food grade standard which allows us to use this semi-solid sphere with microbubbles entrapped as a meal and contrast agent for pressure measurements in the stomach using MRI.

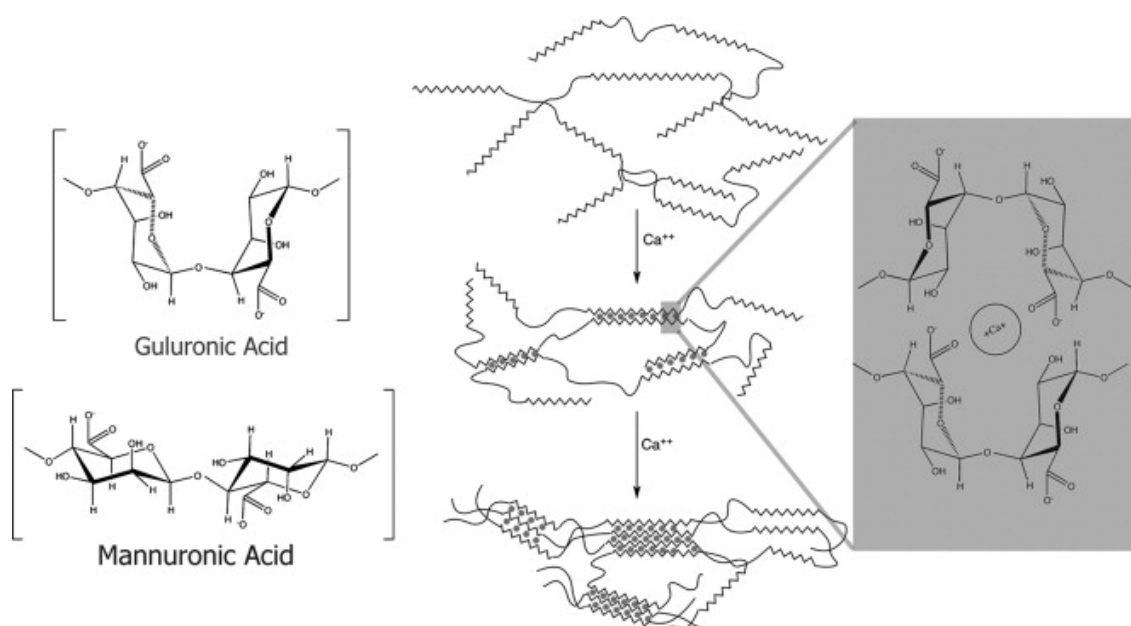


Figure 1.8 – Diagram showing the structures of molecules in the alginate (far left) and the chains of these molecules bound to each other in the presence of calcium ion (right). Source: (Lee, Rogers 2012).

1.4.2 Production Methods

Advancement in the production techniques of gas-filled microbubbles has primarily enhanced the stability, concentration and monodispersity of these bubbles, which are the key points in most of their applications. Over the years, there have been various techniques developed to create these microbubbles. In this section, we discussed three main methods of gas-filled microbubbles production: shear mixing, flow focusing and sonication.

1.4.2.1 Shear Mixing

Shear mixing is one of the conventional techniques in manufacturing microbubbles. It uses mechanical agitation to produce sufficient force to introduce gas from the ambient environment into the aqueous lipid mixture, resulting in the formation of stabilised microbubbles. Commonly, a vial is filled with lipid suspension with a gas head space and then shaken rapidly to yield the microbubbles. The rate of this alternating motion is important in determining the amount and size of the microbubbles formed, with higher rate making a smaller size bubble. There are several variants of the equipment in making microbubble using this method, a popular mechanical shaker (VIALMIX®) used in clinical applications to create a leading ultrasound contrast agent has a shaking frequency of approximately 4500 oscillations per minute (Sboros, Moran et al. 2001). In our work, we used this technique to fabricate our microbubbles because the equipment is comparatively inexpensive and produces microbubbles rapidly and in large enough density and overall quantity. The method of production will be further explained in chapter 2 (section 2.2.2) of this document. Figure 1.9 shows the microscopic image of microbubbles produced using this technique.

The size of the microbubbles is controllable up to a point by varying the speed of the shearing motion, with faster shearing giving smaller bubbles. At too slow speed, neither cavitation nor vortexing occurs whilst at too high speed, the membrane is just disrupted with no formation of bubbles.

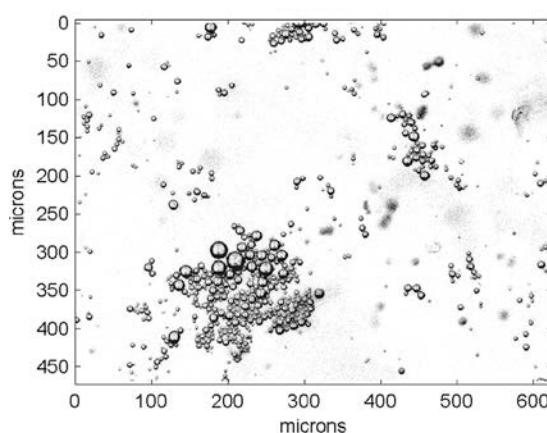


Figure 1.9 – Microscopic image reproduced from Bencsik et al. (2012), showing the gas-filled microbubbles with the mean size of $2.3\ \mu\text{m}$ (standard deviation $1.7\ \mu\text{m}$) produced by using the same mechanical shaker (CapMix™) we used for our microbubbles preparation.

1.4.2.2 Flow Focusing

The flow focusing technique offers an alternative route for microbubble production with high reproducibility and improved control over the size distribution. The microbubbles are generated by utilising the flow focusing technique, using a microfluidic device, to force a central stream of gas and two opposing inlets of aqueous lipid solution through a narrow orifice, forming microbubbles with a well-defined constant size (Figure 1.10). Previously, Talu et al. (2007) has demonstrated the size distribution of microbubbles produced from flow focusing technique is more monodisperse with diameter $3.7\ \mu\text{m}$ (standard deviation $0.2\ \mu\text{m}$) compared to the commercially available microbubbles Definity®, which are made from shear mixing, with diameter $2.7\ \mu\text{m}$ (standard deviation $2.0\ \mu\text{m}$) (Figure 1.11). In microfluidic flow focusing systems, the selection of parameters such as liquid pressure and gas flow rate are primarily determining the microbubble size (Talu, Hettiarachchi et al. 2007).

Regardless of how advanced this technique is in the ability to produce highly monodisperse microbubbles, it suffers from disadvantages as it is usually time consuming and suffers from low microbubble concentrations, for example it takes approximately 10 min to produce 1 ml of microbubbles solution using this technique (Peyman, Abou-Saleh et al. 2012), whilst it only takes 45 s to achieve twice of the amount using shear mixing method (Bencsik, Al-Rwaili et al. 2013). This drawback is the major reason we have not used this technique in making our microbubbles preparation.

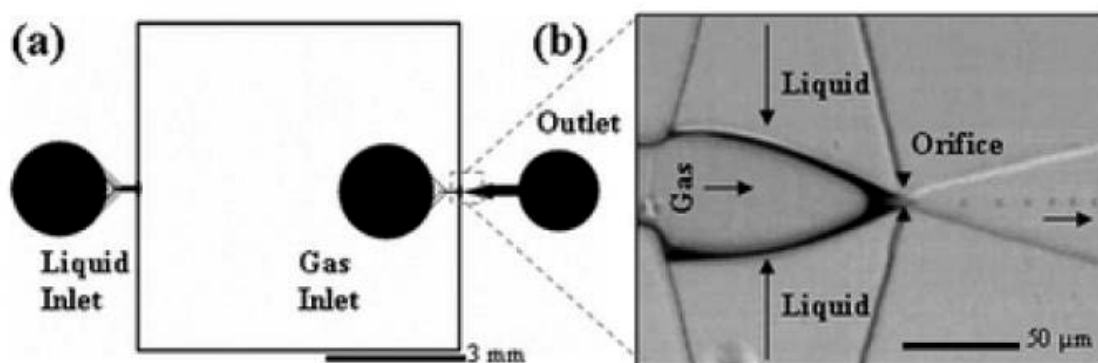


Figure 1.10 – Illustration reproduced from Hettiarachchi et al. (2007) showing a typical design of a flow focusing system. (a) The device consists of liquid inlet and gas inlet. (b) By controlling the liquid (phospholipid solution) and gas flow rate, the microbubbles are produced out from the small orifice into the collection reservoir.

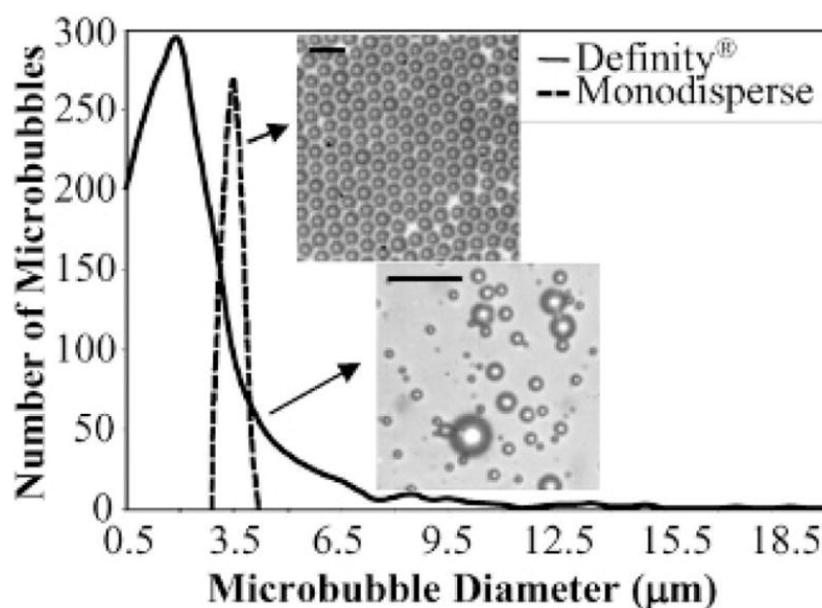


Figure 1.11 – Comparison of the size distribution between microbubbles produced from shear mixing (Definity®) and flow focusing techniques. The microbubbles manufactured by flow focusing technique (Talu, Hettiarachchi et al. 2007) is highly monodisperse with diameter 3.7 μm (standard deviation 0.2 μm) compared to the commercially available contrast agent Definity®, diameter 2.7 μm (standard deviation 2.0 μm). Reproduced from Talu et al. (2007).

1.4.2.3 Sonication

Another technique that was previously used in generating gas-filled microbubbles is sonication. This method is very similar to the shear mixing technique, with the main difference being that it involves the application of a sonication probe (with ultrasonic frequency around 20 kHz), instead of the mechanical agitation, to the suspending fluid (commonly lipids solution) resulting in the microbubbles formation (Otto 2007). It has been demonstrated that the bubbles size distribution produced from sonication is found to be twice bigger than the bubbles from mechanical agitation (Daeichin, van Rooij et al. 2017). One of the first generation of commercially available microbubbles (Albunex®) had been produced using this technique, with the bubble size around 4 μm (Keller, Glasheen et al. 1989).

1.4.3 Commercial Products

There are multiple variants of microbubble contrast agents that are commercially available. They are used widely in ultrasound imaging (Klibanov 2009), hence, most of these products have been tailored for their utilisation in this particular field. Nevertheless, their application is not only limited to this, their potential has attracted interest from various fields particularly in MRI, diffraction-enhanced imaging (DEI) and positron emission tomography (PET), and has been exploited over the years (Kogan, Gessner et al. 2010).

Among the first generations of microbubble contrast agents that became commercially available was Echovist® which was first approved in France and Italy, then followed by Germany, in 1991 (UBM Medica Network 2017). This contrast agent marketed by Schering (Berlin, Germany) in Europe for the ultrasound imaging examination of the heart and venous system (Baert 2008). It contains galactose, which is a type of sugar, and air as gas filling but unfortunately is not stable enough to survive in the blood system after injection for any time duration greater than 5 minutes. Soon, its formulation was improved and then replaced by Levovist® in 1995. In the meanwhile, Albunex® received its clearance from the FDA in the U.S.A. in 1994 for use in echocardiography. Its ingredients consist of human albumin as shell material and air as gas filling (Keller, Glasheen et al. 1989). However, due to its instability and rapid dissolution in the blood, it is also no longer available in the market and has been replaced by its enhanced version, Optison® (GE Healthcare, New Jersey, U.S.A.) (Podell, Burrascano et al. 1999).

The second generations of commercial microbubble contrast agents are usually filled with a perfluorocarbon gas. As we have discussed in the section 1.4.1.1.2, this plays an important role in enhancing the stability of microbubbles due to its low solubility. Optison® is one of the first commercial products using a perfluorocarbon gas, octafluoropropane, as a microbubble core filling. It obtained its first approval in 1998 in the U.S.A. and later in most European countries.

In 2001, Definity® was approved in the U.S.A. for clinical use, as well as in Canada. It also uses octafluoropropane as a gas filling with phospholipid as its shell property (Lantheus Medical Imaging 2017). In the same year, SonoVue® (Bracco Imaging, Milan, Italy), which

consists of phospholipid as a shell material encapsulating sulphur hexafluoride in the core, has also received its approval for clinical use in Europe. Table 1.1 shows some other commercially available products of microbubbles with different shell properties, gas filling and their size distributions.

Name	Shell material	Gas filling	Size (μm)
Echovist[®]	Galactose	Air	N/A
Albunex[®]	Albumin	Air	4.3
Optison [™]	Albumin	Octafluoropropane	N/A
Quantison [™]	Albumin	Air	4.5
Pesda [™]	Albumin	Decafluorobutane	4.7
Definity [®]	Phospholipid	Octafluoropropane	1.1-3.3
Imagent [®]	Phospholipid	Perfluorohexane	6
Sonovue [®]	Phospholipid	Sulfur hexafluoride	2
Levovist [®]	Phospholipid	Air	2-4
BiSphere[™]	Polylactide/Albumin	Nitrogen	3
Imagify [™]	Polylactide	Perfluoropropane	N/A
Sonazoid [™]	Lipid	Perfluorobutane	2.2
Sonavist	Cyanoacrylate	Air	N/A

Table 1.1 – Commercial products of microbubbles with different shell properties, gas filling and size distributions (Sboros 2008, Stride, Saffari 2003). Some of these products (**bold**) are no longer available in the market.

1.5 Previous Works Relevant to the Field

This section covers the important points of previous works that are relevant to the field of our study. The first part explains the developmental work regarding microbubbles and

their current applications, and the second part discusses the importance of pressure measurement for the human gastrointestinal system and the currently available methods.

1.5.1 Gas-filled Microbubble

1.5.1.1 Application in Ultrasound

In a medical application, ultrasound imaging works by using of a transducer to send ultrasound waves, ranging from 2 to 10 MHz (Bushberg, Seibert 2011), which propagate through the tissues and become partially reflected, or scattered, from acoustic heterogeneities, usually interfaces between different tissue types. This heterogeneity occurs due to the differences in acoustic impedance of each type of the tissue. Then, the reflected waves are detected at the outer surface of the body under investigation, usually by the same transducer that sent them in, and recorded and processed.

Gas-filled microbubbles have been used as an effective contrast agent in medical ultrasound imaging to enhance the image contrast, which helps to further differentiate between tissue types, both normal and pathological (Ophir, Parker 1989). Their application has been extensively explored as an intravascular contrast agent in ultrasonography (Keller, Segal et al. 1989). The appearance of these microbubbles in the blood circulation system creates an acoustic impedance difference between the bubbles and the surrounding tissue, offering a unique avenue in manipulating the signal and image contrast. This is made possible due to the unique ability of these bubbles to intimately interact with the ultrasound beam; they either oscillate, coalesce or fragment (Figure 1.12), which then emit variable spectral and energy of the reflected waves. Furthermore, the magnitude of the scattered wave is extensively enhanced by up to ten fold more than that of red blood cells due to the ability of the microbubble to oscillate in response to the ultrasound wave (Ophir, Parker 1989), enabling the detection of a single microbubble.

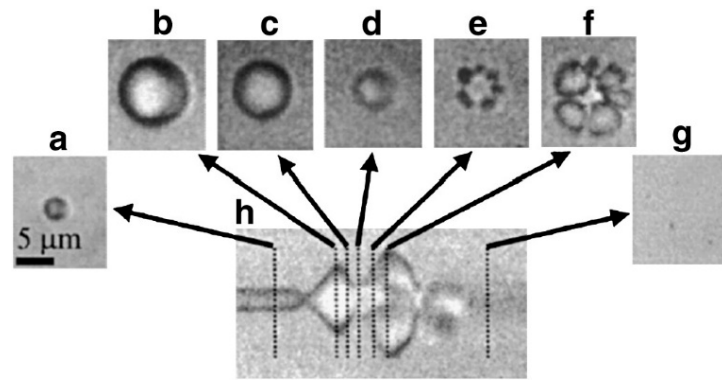


Figure 1.12 – Optical frame images corresponding to the oscillation (a - d) and fragmentation (f) of microbubble in response to the ultrasound wave. The bubble has an initial diameter of 3 μm , shown in (a). The streak image in (h) shows the diameter of the bubble as a function of time, and dashed lines represent the times at which the two-dimensional frame images in (a) – (g) were acquired relative to the streak image. (Chomas, Dayton et al. 2000).

This phenomenon can be explained by Equation 1.8 below (Schutt, Klein et al. 2003), describing the intensity of ultrasound scattered by small spherical particles, which is smaller than the wavelength of the ultrasound beam. It is seen to be proportional to the square of the difference in compressibility and the difference in density of the scatterer and the medium.

$$I/I_0 \sim 1/9nV [k^4 r^6 (\gamma_c + \gamma_d \cos \theta)^2 / d^2]$$

Equation 1.8

Where I is the scattered intensity, I_0 is incident intensity, n is the number density of the scattering particles, V is the scattering volume, k is the wave number, r is the radius of the particle, γ_c is the compressibility term, γ_d is the density term, θ is the scattering angle and d is the distance from the scatterer.

Following the intravenous injection of microbubbles, this technique enables the visualisation of the real-time images of blood flowing through the heart chambers, vessels, and capillaries.

1.5.1.2 MR Experimental Work

1.5.1.2.1 MR Pressure Probing

The first experimental work exploring the potential of microbubbles as MRI contrast agent was published by Alexander and colleagues (Alexander, McCreery et al. 1996). In this study, the authors used phospholipid for the microbubbles shell and investigated a variety of gases as a core filling for their effect on the MR signal, including nitrogen, argon, air, oxygen, xenon, neon, perfluoropentane, perfluorobutane, and sulphur hexafluoride. The average sizes of the microbubbles produced were between 4 and 9 μm . Additionally, a 2 % methylcellulose solution was used as a suspending medium to immobilise the microbubbles during the MRI measurements. Spin-echo and gradient echo pulse sequences were used to measure signal intensity coming from the microbubbles.

It was demonstrated that the nature of the gas in the microbubbles has an influence on the susceptibility effect, which consequently further affects the transverse relaxation time of the preparations, with a higher gas concentration exhibiting lower relaxation times. They discovered that the microbubbles with oxygen, perfluorocarbon and air filling demonstrated the greatest effect on the T_2^{eff} with the increase in gas concentration. Then, the authors applied pressure between 0 and 300 mmHg to the microbubbles in a contained fluid system and demonstrated that microbubbles with an air filling exhibited an increase in relaxation rate, $1/T_2^{\text{eff}}$, with an increase in pressure, compared to the neon-filled microbubbles.

In addition, they also investigated the (T_2^* -weighted) signal intensity change on the air-filled microbubbles by cycling the pressure between 0 and 300 mmHg. They showed the MR signal intensities consistently increased with increasing pressure on gas-filled microbubbles. However, they discovered that the signal intensity had only partially returned to its original when the applied pressure was released. They suggested that this could be due the rise of the microbubbles within the phantom and microbubbles deterioration over the course of the MR measurements.

This endeavour has disclosed a substantial potential for microbubbles and opened up the route for their use as contrast agents in MR imaging, which further lead to various

experimental and numerical works undertaken by many researchers exploring its susceptibility effect.

In 2012, Bencsik and colleagues published work demonstrating phospholipid microbubbles exhibiting MR sensitivity up to 23 % signal change per bar (Bencsik, Al-Rwaili et al. 2013). It was demonstrated that this high sensitivity was solely due to the bubble radius change as the applied pressure was changed. In this occasion, the microbubbles with a mean radius of $1.2 \pm 0.8 \mu\text{m}$ were produced from a mechanical agitation method. Phospholipids were used as shell material and octafluorocarbon (C_3F_8) gas was used in the core. In addition, a 2 % (w/v) gellan gel was used as a suspending medium to further immobilise the bubbles. In this paper, the authors presented their experimental data and corroborated them with numerical simulation to further validate the results.

1.5.1.2.2 MR Tracking

There are several other MRI investigations demonstrating the susceptibility effect of gas-filled microbubbles (Wong, Huang et al. 2004, Cheung, Chow et al. 2009), but not in the context of fluid pressure mapping. Cheung and colleagues carried out an *in-vivo* investigation demonstrating the susceptibility effect of microbubbles in the brain blood vessels (Cheung, Chow et al. 2009). In their work, the microbubble suspensions were injected into rats intravenously following which they demonstrated a linear correlation between T_2^* with the microbubble volume fractions, using MRI at 7T. They suggested that microbubbles have the potential use as a real-time MRI guidance in various applications such as vascular drug delivery for diagnostic and therapeutic purposes.

However, inadequate sensitivity is the main limitation for the clinical application because the microbubble induced susceptibility effect is relatively weak compared with other MR susceptibility contrast agent. This means that this contrast agent requires a dosage of microbubbles too high to allow a useful effect in clinical applications.

1.5.1.3 MR Numerical Simulation Studies

1.5.1.3.1 Sensitivity

The NMR relaxation change due to bubble size change at atmospheric pressure has been modelled by Dharmakumar in terms of external magnetic field strength, bubble concentration and susceptibility difference between encapsulated gas and surrounding fluid, both for gradient echo and spin echo sequences (Dharmakumar, Plewes et al. 2005, Dharmakumar, Plewes et al. 2002). As a result from their numerical simulations, Dharmakumar and co-workers have shown the extent to which the sensitivity of the microbubbles related to pressure change was affected by these variables. However, the effects of these variables have not been experimentally fully explored yet.

In this simulation work, the authors modelled the microbubble by placing a single sphere in the centre of the 'universe' which was made of a cubic space of length L discretised into series of smaller cubes of length $\sqrt{2D\Delta t}$, where D is the proton diffusion coefficient and $\Delta t = 10 \mu s$ is the duration of time spent by a water proton at a given point. The ratio of the sphere volume to the universe volume simulates the bubble gas volume fraction. Then, 10^4 protons were randomly disseminated around the sphere with a uniform distribution within this universe. Each proton was able to move in different directions at every time interval of Δt , but not allowed to enter the sphere. From this estimation, they determined the NMR free induction decay (FID) rate ($1/T_2^*$ or R_2^*) and the CPMG signal decay rate ($1/T_2^{eff}$ or R_2^{eff}) due to the presence of the microbubbles. The procedure was repeated with different pressure conditions, investigating the dependence of these parameters.

Following the results, it was found that the relation between relaxation rates and the pressure sensitivity to the bubble size are different for the FID and CPMG signals (Figure 1.13). The sensitivity of R_2^* increased with the increase in bubble radius up to a critical value, which is identified as R_{crit} on the plot. Beyond this point, the sensitivity remained constant. However, the sensitivity of R_2^{eff} rose with an increase in bubble size and peaked at R_{crit} and then decreased thereafter. The simulation result is in agreement with the theory.

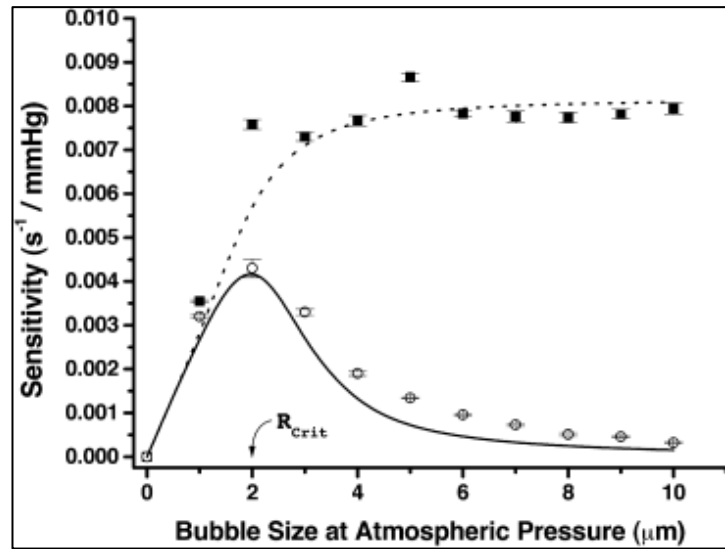


Figure 1.13 – Plot of the relation of the bubble size with the pressure sensitivity of both R_2^* and R_2^{eff} . The black square and the open circle, respectively, indicate R_2^* and R_2^{eff} simulations, while the dotted line and the solid line, respectively, represent R_2^* and R_2^{eff} theory (Dharmakumar, Plewes et al. 2002).

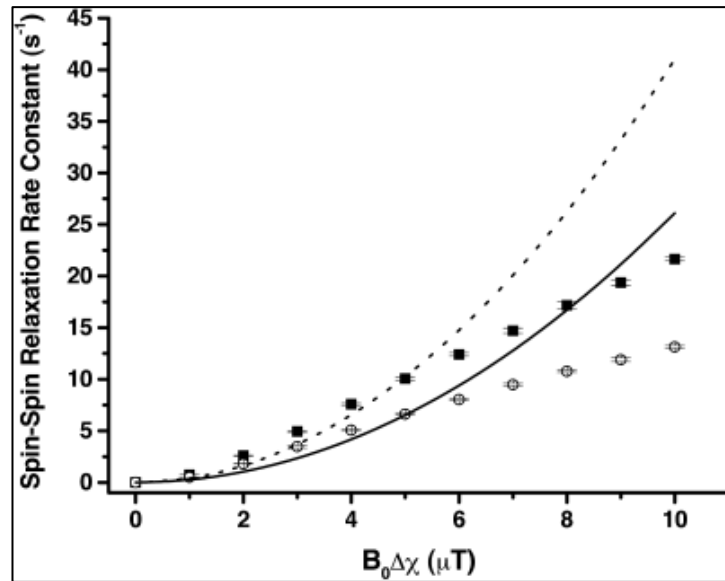


Figure 1.14 – Plot of the relation of field strength and susceptibility difference with FID and CPMG spin-spin relaxation rate constants (Dharmakumar, Plewes et al. 2002). The symbols are the same as in Figure 1.13.

However, the dependence of the external field strength, B_0 , and susceptibility difference, $\Delta\chi$, on R_2^* and R_2^{eff} was different between the theory and the simulation result, which was respectively seen in linear and quadratic relations (Figure 1.14). Soon after, Bencsik et al. (2013) improved this result, also through a numerical simulation, where he successfully demonstrated the simulation result synced with the theory, in quadratic correlation (Bencsik, Al-Rwaili et al. 2013). This was achieved by optimising the Δt value, specifically changing this parameter on different bubble size.

1.5.1.3.2 Enhancing susceptibility Effect

The microbubble inadequate sensitivity to a small pressure change is severely limiting its potential for *in-vivo* applications. By increasing the magnetic susceptibility of the microbubbles, it should be possible to open up a range of imaging techniques to allow the monitoring of blood pressure in the body with a much lower density of microbubbles. Dharmakumar and co-workers have published another paper exploring the possibility to increase the efficiency of the microbubbles by exploiting the susceptibility effect using numerical simulations (Dharmakumar, Plewes et al. 2005).

In this work, the authors suggested enhancing the susceptibility by incorporating magnetic nanoparticles of high dipole moment, such as iron, magnetite and hematite, on the lipid shell of the microbubbles, thereby extensively increasing the susceptibility difference between the bubble gas and the medium. In theory, as the bubble changes in size, for a given change in pressure, the differential changes in the dipole moment is larger relative to the uncoated microbubbles, imposing greater field variations sampled by the spins. They investigated this effect through numerical estimations, by comparing the R_2 changes on the air-filled microbubbles coated with magnetite with the ones without coating. It was found that even with a much lower volume fraction, the pressure sensitivity of microbubbles with magnetite coating is significantly higher compared to the microbubbles without coating (Figure 1.15).

Soon after, it was demonstrated that the susceptibility effect of gas-filled polymeric microbubbles can substantially increase by entrapping iron oxide nanoparticles into the microbubble shell, a method suggested to be applicable to lipid-shell microbubbles too (Chow, Chan et al. 2010). Thus, it was shown that microbubbles with a unique

susceptibility effect offer a promising and viable contrast agent for a direct pressure measurement in tissue and fluid.

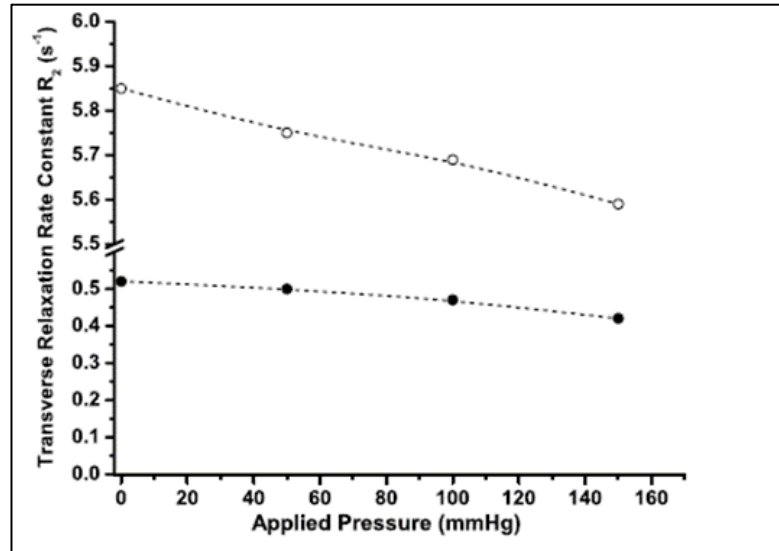


Figure 1.15 – Plot comparing the effect of pressure changes on R_2^{eff} of microbubbles with (open circle) and without (solid circle) magnetite coating, with the air volume fractions 0.0344 % and 0.1527 %, respectively (Dharmakumar, Plewes et al. 2005).

1.5.2 Pressure Measurements in the Human Gastrointestinal System

1.5.2.1 Practical Motivation

Great efforts have been taken to understand the behaviour of clinical conditions related to functional gastrointestinal disorders (Wilmer, Van Cutsem et al. 1998) and MRI has been known as a non-invasive method to study these diseases (Marciani 2011, Parker, Tucker et al. 2016). They are generally associated with the disturbance on the normal activities of muscle movement, known as the motility of the gastrointestinal, or of the sensitivity of the nerves of these organs.

One of the conditions which is known as functional dyspepsia, is associated with hypersensitivity to gastric distention (Tack, Caenepeel et al. 2001). Commonly, there are multiple symptoms present in the patient with this syndrome, including a pain in the epigastric area (located in the upper central region of the abdomen), bloating, nausea, belching and vomiting. In the past, it has been shown that there are abnormal patterns

of the gastric motility (Wilmer, Van Cutsem et al. 1998), especially at the distal part of the stomach, the antrum. The pattern of the digestive muscle contractions of the stomach wall has been observed by inserting a catheter with a probe into the stomach. This customary probe is fully equipped with multiple pressure sensors enabling the detection of pressure waves propagated from the muscle tensions. Using this technique, it was found in a previous study that the pressure exerted in the antrum during digestive period is ranging between 30 and 82 mmHg (Bortolotti, Annese et al. 2000).

However, even with the help of advanced computer analysis, this technique still lacks the ability to identify a specific motility pattern, allowing the differentiation of the healthy individuals with the patients with functional dyspepsia. Additionally, this existing method of diagnosis can cause discomfort to the patient due to its invasive procedure. The catheter can also occasionally be moved from the intended area, which can impede the accuracy of the measurement (Wilmer, Van Cutsem et al. 1998). We further discuss this procedure in the following subsection 1.5.2.2.

In a more recent study, the symptoms of the patients suffering from this disease have also been shown to be intensified after having a meal (Farre, Vanheel et al. 2013). Having this in mind, in order to help the clinicians to further understand the disease, it would be tremendously useful to have a tool for diagnosis which is able to simulate a meal and simultaneously measure the dynamic meal pressure variation supplied by the stomach, by using a much less intrusive technique. No such method is currently available, hence, the exploration of such an edible contrast agent combined with MR imaging is the point of this study. Fundamentally, developing the right diagnostic tool, particularly being able to measure the dynamic pressure changes within the meal in the stomach, can produce a great impact on the clinical understanding of this disease which can lead to better decision making and ultimately to the treatment option.

1.5.2.2 Current available methods

In the study of the function of the gastrointestinal tract, currently available methods, manometry (Herbella, Aprile et al. 2014) and barostat (Farre, Vanheel et al. 2013), have shown promise in assessing the pressure exerted by the human stomach. Both

techniques involve the insertion of a catheter or tube into the stomach through the oesophagus, from the nose or mouth.

The manometry technique works by introducing pressure-sensitive sensors and locating them in various areas in the stomach. Then, this probe is connected to a recording apparatus and computer to quantify the pressure changes in the stomach. There are two types of procedures performed using this method: ambulatory or stationary. The first one (Bortolotti, Annese et al. 2000) requires a prolonged measurement, which usually takes about 24 hours of observation. During this period, the participants are supplied with portable devices for the measurement and encouraged to carry on with their normal daily routine. On the other hand, stationary manometry (Stanghellini, Ghidini et al. 1992) is usually performed in a short term, up to 5 hours. For this procedure, after the insertion of the probe, the participants are being monitored in a controlled area and normally being asked to lie on a hospital bed for the period of observation.

The barostat study involves the introduction of a tube with a deflated balloon at the tip through the mouth and into the stomach (Farre, Vanheel et al. 2013). A fluoroscopy scanning is usually performed during the insertion of the tube to assist the positioning of the balloon in the stomach. This tube is then further connected to the barostat device enabling a volume of air to be driven to inflate or deflate the balloon. The volume and pressure measurements are taken as the balloon inflates and deflates in the stomach.

Both of these conventional techniques are invasive, which can perturb the true physiology of the stomach (de Zwart, Haans et al. 2007) and are less comfortable to the patient, compared with the one we have explored in our study.

1.5.3 Previous Studies of Alginate Spheres

Alginates are polysaccharide compounds, extracted from brown seaweeds (Rioux, Turgeon et al. 2007), where their main role is to provide a structural matrix to support a cell. In food industry, alginates are commonly reacted with calcium ions to create a more elastic and stable gel (Duez, Mestdagh et al. 2000), which is widely used as a thickening and stabilising agent (Draget, SkjakBraek et al. 1997).

There have been studies investigating the behaviour of alginate spheres in gastrointestinal conditions (Hoad, Rayment et al. 2009, Rayment, Wright et al. 2009),

but not in the context of MRI pressure probing, and no involvement of microbubbles. In the initial *in-vitro* investigations undertaken by Reyman and co-workers (Rayment, Wright et al. 2009), they suggested that the alginate spheres have a great potential to be utilised as a non-invasive monitoring technique for gastrointestinal studies, as an alternative method to the existing invasive approaches. Soon after, the same group of investigators published the second part of their work, *in-vivo* investigations, demonstrating the characteristics of these spheres in the human gastrointestinal system using MR imaging (Hoad, Rayment et al. 2009).

In these studies, they have shown that there is a significant decrease in the T_2^{eff} values of the alginate spheres when they were placed in the acidic (pH 2) human gastric solution. They suggested that this phenomenon should be attributed to the distinctive character of the alginate, in that it forms a tighter gel network in a lower pH environment, which further caused them to shrink resulting in the expulsion of the 'free' water molecules from the sphere.

Hence, by taking this valuable information, we initially anticipated that these alginate spheres could be used as a carrier to our microbubbles in measuring the pressure exerted by the human stomach. Therefore, we loaded them with gas-filled microbubbles and explored their functionality *in-vitro* and *in-vivo*, and this constitutes the main body of the present study.

References

1. ALEXANDER, A.L., McCREERY, T.T., BARRETTE, T.R., GMITRO, A.F. and UNGER, E.C., 1996. Microbubbles as novel pressure-sensitive MR contrast agents. *Magnetic Resonance in Medicine*, **35**(6), pp. 801-806.
2. WILMER, A., VAN CUTSEM, E., ANDRIOLI, A., TACK, J., COREMANS, G. and JANSSENS, J., 1998. Ambulatory gastrojejunal manometry in severe motility-like dyspepsia: lack of correlation between dysmotility, symptoms, and gastric emptying. *Gut*, **42**(2), pp. 235-242.
3. McROBBIE, D., MOORE, E., GRAVES, M. and PRINCE, M., 2006. *MRI from picture to proton*. 2 edn. Cambridge: Cambridge University Press.
4. HAHN, E.L., 1950. Spin Echoes. *Physical Review*, **80**(4), pp. 580-594.
5. CARR, H.Y. and PURCELL, E.M., 1954. Effects of diffusion on free precession in Nuclear Magnetic Resonance experiments. *Physical Review*, **94**(3), pp. 630-638.
6. HENNIG, J., NAUERTH, A. and FRIEDBURG, H., 1986. RARE imaging - a fast imaging method for clinical MR. *Magnetic Resonance in Medicine*, **3**(6), pp. 823-833.
7. OPPELT, A., GRAUMANN, R., BARFUSS, H., FISCHER, H., HARTL, W. and SCHAJOR, W., 1986. FISP—a new fast MRI sequence. *Electromedica*, **54**(1), pp. 15-18.
8. HOAD, C.L., COX, E.F. and GOWLAND, P.A., 2010. Quantification of T2 in the abdomen at 3.0 T using a T2-prepared balanced turbo field echo sequence. *Magnetic Resonance in Medicine*, **63**(2), pp. 356-364.
9. DHARMAKUMAR, R., PLEWES, D.B. and WRIGHT, G.A., 2002. On the parameters affecting the sensitivity of MR measures of pressure with microbubbles. *Magnetic Resonance in Medicine*, **47**(2), pp. 264-273.
10. MORRIS, R.H., 2009. *Advanced design and experimental validation of MRI contrast agents for fluid pressure mapping using microbubbles*, Nottingham Trent University.

11. UNGER, E.C., UGURBIL, K. and LATCHAW, R.E., 1994. Contrast agents for cerebral perfusion MR-Imaging. *Journal of Magnetic Resonance Imaging*, **4**(3), pp. 235-242.
12. CHOW, A.M., CHAN, K.W.Y., CHEUNG, J.S. and WU, E.X., 2010. Enhancement of gas-filled microbubble R(2)* by Iron Oxide nanoparticles for MRI. *Magnetic Resonance in Medicine*, **63**(1), pp. 224-229.
13. GLYNOS, E., KOUTSOS, V., MCDICKEN, W.N., MORAN, C.M., PYE, S.D., ROSS, J.A. and SBOROS, V., 2009. Nanomechanics of biocompatible hollow thin-shell polymer microspheres. *Langmuir*, **25**(13), pp. 7514-7522.
14. SANTOS, E.B., MORRIS, J.K., GLYNOS, E., SBOROS, V. and KOUTSOS, V., 2012. Nanomechanical Properties of Phospholipid Microbubbles. *Langmuir*, **28**(13), pp. 5753-5760.
15. KAUR, R., MORRIS, R., BENCSIK, M., VANGALA, A., RADES, T. and PERRIE, Y., 2009. Development of a novel Magnetic Resonance Imaging contrast agent for pressure measurements using lipid-coated microbubbles. *Journal of Biomedical Nanotechnology*, **5**(6), pp. 707-715.
16. TANFORD, C., 1980. *The hydrophobic effect: formation of micelles and biological membranes*. 2nd edn. New York: John Wiley & Sons Inc.
17. BLOCH, S., WAN, M., DAYTON, P. and FERRARA, K., 2004. Optical observation of lipid- and polymer-shelled ultrasound microbubble contrast agents. *Applied Physics Letters*, **84**(4), pp. 631-633.
18. HERNOT, S. and KLIBANOV, A.L., 2008. Microbubbles in ultrasound-triggered drug and gene delivery. *Advanced Drug Delivery Reviews*, **60**(10), pp. 1153-1166.
19. KELLER, M.W., GLASHEEN, W. and KAUL, S., 1989. Albunex: A safe and effective commercially produced agent for myocardial contrast echocardiography. *Journal of the American Society of Echocardiography*, **2**(1), pp. 48-52.

20. SCHUTT, E., KLEIN, D., MATTREY, R. and RIESS, J., 2003. Injectable microbubbles as contrast agents for diagnostic ultrasound imaging: The key role of perfluorochemicals. *Angewandte Chemie-International Edition*, **42**(28), pp. 3218-3235.
21. SBOROS, V., 2008. Response of contrast agents to ultrasound. *Advanced Drug Delivery Reviews*, **60**(10), pp. 1117-1136.
22. KOGAN, P., GESSNER, R.C. and DAYTON, P.A., 2010. Microbubbles in Imaging: applications beyond ultrasound. *Bubble Science Engineering and Technology*, **2**(1), pp. 3-8.
23. MORRIS, R.H., BENCSIK, M., NESTLE, N., GALVOSAS, P., FAIRHURST, D., VANGALA, A., PERRIE, Y. and MCHALE, G., 2008. Robust spatially resolved pressure measurements using MRI with novel buoyant advection-free preparations of stable microbubbles in polysaccharide gels. *Journal of Magnetic Resonance*, **193**(2), pp. 159-167.
24. CASSANELLI, M., NORTON, I. and MILLS, T., 2017. *Effect of alcohols on gellan gum gel structure: Bridging the molecular level and the three-dimensional network*.
25. DRAGET, K., SKJAKBRAEK, G. and SMIDSRØD, O., 1997. Alginate based new materials. *International Journal of Biological Macromolecules*, **21**(1-2), pp. 47-55.
26. RINAUDO, M., 2014. Biomaterials based on a natural polysaccharide: alginate. *TIP*, **17**(1), pp. 92-96.
27. LEE, P. and ROGERS, M.A., 2012. Effect of calcium source and exposure-time on basic caviar spherification using sodium alginate. *International Journal of Gastronomy and Food Science*, **1**(2), pp. 96-100.
28. SBOROS, V., MORAN, C.M., PYE, S.D. and MCDICKEN, W.N., 2001. Contrast agent stability: a continuous B-mode imaging approach. *Ultrasound in Medicine & Biology*, **27**(10), pp. 1367-1377.
29. TALU, E., HETTIARACHCHI, K., ZHAO, S., POWELL, R.L., LEE, A.P., LONGO, M.L. and DAYTON, P.A., 2007. Tailoring the size distribution of ultrasound contrast agents:

Possible method for improving sensitivity in molecular imaging. *Molecular Imaging*, **6**(6), pp. 384-392.

30. PEYMAN, S.A., ABOU-SALEH, R.H., McLAUGHLAN, J.R., INGRAM, N., JOHNSON, B.R.G., CRITCHLEY, K., FREEAR, S., EVANS, J.A., MARKHAM, A.F., COLETTA, P.L. and EVANS, S.D., 2012. Expanding 3D geometry for enhanced on-chip microbubble production and single step formation of liposome modified microbubbles. *Lab on a Chip*, **12**(21), pp. 4544-4552.

31. BENCSIK, M., AL-RWAILI, A., MORRIS, R., FAIRHURST, D.J., MUNDELL, V., CAVE, G., McKENDRY, J. and EVANS, S., 2013. Quantitation of MRI Sensitivity to quasi-monodisperse microbubble contrast agents for spatially resolved manometry. *Magnetic Resonance in Medicine*, **70**(5), pp. 1409-1418.

32. OTTO, C.M., 2007. Ultrasonographic contrast agent. *The practice of clinical echocardiography*. Philadelphia, PA: Saunders/Elsevier, pp. 895.

33. DAEICHIN, V., VAN ROOIJ, T., SKACHKOV, I., ERGIN, B., SPECHT, P.A.C., LIMA, A., INCE, C., BOSCH, J.G., VAN DER STEEN, A.F.W., DE JONG, N. and KOOIMAN, K., 2017. Microbubble composition and preparation for high-frequency contrast-enhanced ultrasound imaging: In vitro and in vivo evaluation. *IEEE Transactions on Ultrasonics Ferroelectrics and Frequency Control*, **64**(3), pp. 555-567.

34. KLIBANOV, A.L., 2009. Preparation of targeted microbubbles: ultrasound contrast agents for molecular imaging. *Medical & Biological Engineering & Computing*, **47**(8), pp. 875-882.

35. UBM MEDICA NETWORK, 2nd June 2017, 2017-last update, Diagnostic Imaging [Homepage of UBM Medica Network], [Online]. Available: <http://www.diagnosticimaging.com/articles/schering-sells-ultrasound-contrast-agent-europe> [06/03, 2017].

36. BAERT, A.L., 2008. *Encyclopedia of Diagnostic Imaging*. 1st edn. Berlin: Springer-Verlag Berlin Heidelberg.

37. PODELL, S., BURRASCANO, C., GAAL, M., GOLEC, B., MANIQUIS, J. and MEHLHAFF, P., 1999. Physical and biochemical stability of Optison®, an injectable ultrasound contrast agent. *Biotechnology and Applied Biochemistry*, **30**(3), pp. 213-223.
38. LANTHEUS MEDICAL IMAGING, 2017-last update, Definity [Homepage of Lantheus Medical Imaging, Inc.], [Online]. Available: <http://www.lantheus.com/products/overview/definity/> [Jan/24, 2017].
39. STRIDE, E. and SAFFARI, N., 2003. Microbubble ultrasound contrast agents: a review. *Proceedings of the Institution of Mechanical Engineers Part H-Journal of Engineering in Medicine*, **217**(H6), pp. 429-447.
40. BUSHBERG, J.T. and SEIBERT, J.A., 2011. *Essential physics of medical imaging*. Philadelphia: Wolters Kluwer Health.
41. OPHIR, J. and PARKER, K., 1989. Contrast Agents in Diagnostic Ultrasound. *Ultrasound in Medicine and Biology*, **15**(4), pp. 319-333.
42. KELLER, M., SEGAL, S., KAUL, S. and DULING, B., 1989. The behavior of sonicated albumin microbubbles within the microcirculation - a basis for their use during myocardial contrast echocardiography. *Circulation Research*, **65**(2), pp. 458-467.
43. CHOMAS, J., DAYTON, P., MAY, D., ALLEN, J., KLIBANOV, A. and FERRARA, K., 2000. Optical observation of contrast agent destruction. *Applied Physics Letters*, **77**(7), pp. 1056-1058.
44. WONG, K.K., HUANG, I., KIM, Y.R., TANG, H.Y., YANG, E.S., KWONG, K.K. and WU, E.X., 2004. In vivo study of microbubbles as an MR susceptibility contrast agent. *Magnetic Resonance in Medicine*, **52**(3), pp. 445-452.
45. CHEUNG, J.S., CHOW, A.M., GUO, H. and WU, E.X., 2009. Microbubbles as a novel contrast agent for brain MRI. *NeuroImage*, **46**(3), pp. 658-664.

46. DHARMAKUMAR, R., PLEWES, D.B. and WRIGHT, G.A., 2005. A novel microbubble construct for intracardiac or intravascular MR manometry: a theoretical study. *Physics in Medicine and Biology*, **50**(20), pp. 4745-4762.
47. MARCIANI, L., 2011. Assessment of gastrointestinal motor functions by MRI: a comprehensive review. *Neurogastroenterology and Motility*, **23**(5), pp. 399-407.
48. PARKER, L., TUCKER, E., HOAD, C.L., PAL, A., COSTIGAN, C., HUDDERS, N., PERKINS, A., BLACKSHAW, E., GOWLAND, P., MARCIANI, L. and FOX, M.R., 2016. Development and validation of a large, modular test meal with liquid and solid components for assessment of gastric motor and sensory function by non-invasive imaging. *Neurogastroenterology and Motility*, **28**(4), pp. 554-568.
49. TACK, J., CAENEPEEL, P., FISCHLER, B., PIESSEVAUX, H. and JANSSENS, J., 2001. Symptoms associated with hypersensitivity to gastric distention in functional dyspepsia. *Gastroenterology*, **121**(3), pp. 526-535.
50. BORTOLOTTI, ANNESE, COCCIA and BORTOLOTTI, M., 2000. Twenty-four hour ambulatory antroduodenal manometry in normal subjects (co-operative study). *Neurogastroenterology & Motility*, **12**(3), pp. 231-238.
51. FARRE, R., VANHEEL, H., VANUYTSEL, T., MASAOKA, T., TORNBLUM, H., SIMREN, M., VAN OUDENHOVE, L. and TACK, J.F., 2013. In functional dyspepsia, hypersensitivity to postprandial distention correlates with meal-related symptom severity. *Gastroenterology*, **145**(3), pp. 566-573.
52. HERBELLA, F.A.M., APRILE, L.R.O. and PATTI, M.G., 2014. High-resolution manometry for the evaluation of gastric motility. *Updates in Surgery*, **66**(3), pp. 177-181.
53. STANGHELLINI, V., GHIDINI, C., MACCARINI, M., PAPARO, G., CORINALDESI, R. and BARBARA, L., 1992. Fasting and postprandial gastrointestinal motility in ulcer and nonulcer dyspepsia. *GUT*, **33**(2), pp. 184-190.
54. DE ZWART, I.M., HAANS, J.J.L., VERBEEK, P., EILERS, P.H.C., DE ROOS, A. and MASCLÉE, A.A.M., 2007. Gastric accommodation and motility are influenced by the barostat device:

assessment with magnetic resonance imaging. *American Journal of Physiology-Gastrointestinal and Liver Physiology*, **292**(1), pp. G208-G214.

55. RIOUX, L.E., TURGEON, S.L. and BEAULIEU, M., 2007. Characterization of polysaccharides extracted from brown seaweeds. *Carbohydrate Polymers*, **69**(3), pp. 530-537.

56. DUEZ, J., MESTDAGH, M., DEMEURE, R., GOUEMANT, J., HILLS, B. and GODWARD, J., 2000. NMR studies of calcium-induced alginate gelation. Part I - MRI tests of gelation models. *Magnetic Resonance in Chemistry*, **38**(5), pp. 324-330.

57. HOAD, C., RAYMENT, P., COX, E., WRIGHT, P., BUTLER, M., SPILLER, R. and GOWLAND, P., 2009. Investigation of alginate beads for gastro-intestinal functionality, Part 2: In vivo characterisation. *Food Hydrocolloids*, **23**(3), pp. 833-839.

58. RAYMENT, P., WRIGHT, P., HOAD, C., CIAMPI, E., HAYDOCK, D., GOWLAND, P. and BUTLER, M.F., 2009. Investigation of alginate beads for gastro-intestinal functionality, Part 1: In vitro characterisation. *Food Hydrocolloids*, **23**(3), pp. 816-822.

59. LOZANO, M.M. and LONGO, M.L., 2009. Microbubbles coated with disaturated lipids and DSPE-PEG2000: phase behavior, collapse transitions, and permeability. *Langmuir*, **25**(6), pp. 3705-3712.

60. NEEDHAM, D. and KIM, D.H., 2000. *PEG-covered lipid surfaces: bilayers and monolayers*. US Patent 6210611.

61. AVANTI POLAR LIPIDS, 2017-last update, 16:0 PC (DPPC) [Homepage of Avanti Polar Lipid, Inc.], [Online]. Available: <https://avantilipids.com/product/850355/> [04/01, 2017].

62. VENTURA, M.G., PANINHO, A.I., NUNES, A.V.M., FONSECA, I.M. and BRANCO, L.C., 2015. Biocompatible locust bean gum mesoporous matrices prepared by ionic liquids and a scCO₂ sustainable system. *RSC Advances*, **5**(130), pp. 107700-107706.

63. CHAN, L.W., LEE, H.Y. and HENG, P.W.S., 2006. Mechanisms of external and internal gelation and their impact on the functions of alginate as a coat and delivery system. *Carbohydrate Polymers*, **63**(2), pp. 176-187.
64. DEGRASSI, A., TOFFANIN, R., PAOLETTI, S. and HALL, L., 1998. A better understanding of the properties of alginate solutions and gels by quantitative magnetic resonance imaging (MRI). *Carbohydrate Research*, **306**(1-2), pp. 19-26.
65. ABLETT, S., LILLFORD, P., BAGHDADI, S. and DERBYSHIRE, W., 1976. NMR relaxation in polysaccharide gels and films. *ACS Symposium Series*, (34), pp. 344-359.
66. PRESS, W.H., TEUKOLSKY, S.A., VETTERLING, W.T. and FLANNERY, B.P., 1992. *Numerical recipes in C : the art of scientific computing*. 2nd edn. Cambridge University Press.
67. ZUO, Y.Y., CHEN, R., WANG, X., YANG, J., POLICOVA, Z. and NEUMANN, A.W., 2016. Phase transitions in Dipalmitoylphosphatidylcholine monolayers. *Langmuir*, **32**(33), pp. 8501-8506.
68. BORDEN, M.A. and LONGO, M.L., 2002. Dissolution behavior of lipid monolayer-coated, air-filled microbubbles: effect of lipid hydrophobic chain length. *Langmuir*, **18**(24), pp. 9225-9233.
69. VESANEN, P.T., ZEVENHOVEN, K.C.J., NIEMINEN, J.O., DABEK, J., PARKKONEN, L.T. and ILMONIEMI, R.J., 2013. Temperature dependence of relaxation times and temperature mapping in ultra-low-field MRI. *Journal of Magnetic Resonance*, **235**, pp. 50-57.
70. BENCSIK, M. and RAMANATHAN, C., 2001. Direct measurement of porous media local hydrodynamical permeability using gas MRI. *Magnetic Resonance Imaging*, **19**(3-4), pp. 379-383.
71. MORRIS, R.H., BENCSIK, M., VANGALA, A.K. and PERRIE, Y., 2007. Three-dimensional fluid pressure mapping in porous media using Magnetic Resonance Imaging with gas-filled liposomes. *Magnetic Resonance Imaging*, **25**(4), pp. 509-512.

CHAPTER 2

DESIGN OF THE MICROBUBBLE-BASED CONTRAST AGENTS

2 DESIGN OF THE MICROBUBBLE-BASED CONTRAST AGENTS

2.1 Introduction

This chapter covers the methods that have been used to generate microbubble-based contrast agents for the purpose of our study. Concerning the contrast agent preparations, we can divide this into two stages, which are *in-vitro* and *in-vivo* experiments. Most of the contrast agent preparations for *in-vitro* works were carried out in a standard chemistry laboratory. In order to produce a contrast agent that is suitable for human consumption, the methods that have been used for the *in-vitro* study were reproduced in a food-safe laboratory with food-grade ingredients.

2.2 Components of the Contrast Agents

The microbubbles were prepared following the method described in a previous study (Bencsik, Al-Rwaili et al. 2013). Generally, the components of microbubble contrast agents consist of a gas, a thin lipid shell and a suspending medium.

2.2.1 Materials

The following is a list of the materials that have been used to produce the microbubble contrast agents for our study.

- a) The phospholipids used as the microbubble shell materials were DPPC (1,2-dihexadecanoyl-sn-glycero-phosphocoline) and DSPE-PEG2000-PE (1,2-distearoyl-sn-glycero-3-phosphoethanolamine-N-[methoxy (polyethylene glycol) – 2000]) (Figure 2.1). A long-chain lipid from the DPPC provides a stable bubble shell which has low surface tension and reduced gas permeability (Lozano, Longo 2009). The additional PEG components on the phospholipids (DSPE-PEG2000-PE) formulations can significantly increase the stability of microbubbles by acting as an additional coating to the microbubble shell and prevents them from coalescing (Needham, Kim 2000). Both of these substances were purchased from the Avanti Polar Lipid, Alabama, USA (Avanti Polar Lipids 2017).

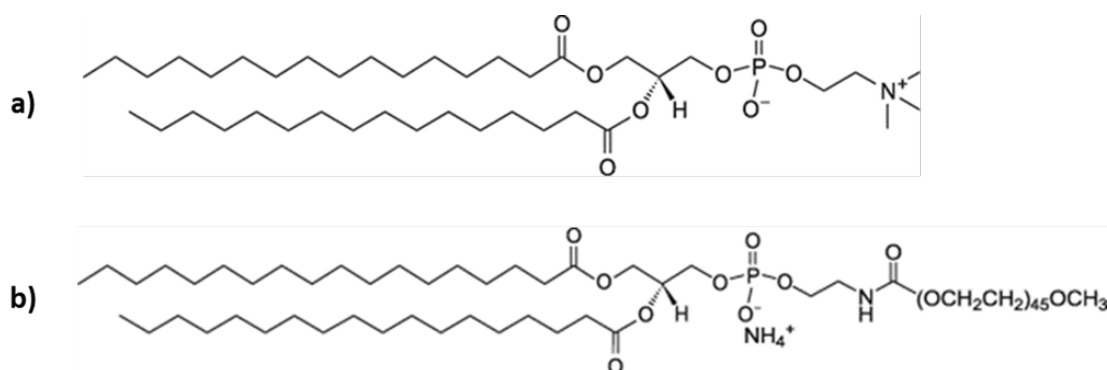


Figure 2.1 – The chemical structures of the phospholipids used as microbubbles shell materials; a) DPPC and b) DSPE-PEG2000-PE (Avanti Polar Lipids, 2017).

- b) A perfluorocarbon gas, octafluoropropane (C_3F_8), was used as the core-filling gas of our microbubbles. This particular gas is innocuous (non-toxic gas) and it has a lower solubility in water compared to other gases, e.g. nitrogen and air (Podell, Burrascano et al. 1999), which increases the stability of the bubbles in the medium. Besides, the resulting microbubbles from using C_3F_8 gas exhibit a high monodispersity in term of size distribution.
- c) Gellan gum in a powder form obtained from CP Kelco, UK.
- d) Sodium alginate powder purchased from Special Ingredients, UK.
- e) Calcium lactate powder purchased from Special Ingredients, UK.
- f) Locust bean gum powder purchased from Special Ingredients, UK.

2.2.2 Gas-filled Microbubbles Preparations

The microbubbles were prepared following the method described in a previous study (Bencsik, Al-Rwaili et al. 2013). The preparation involved two distinct consecutive parts in creating the bubbles. The first part of the preparation involved the formulation of a phospholipids solution in a standard chemistry laboratory:

- a) Firstly, 500 mg of DPPC powder was dissolved into 200 ml of chloroform.

- b) Separately, 25 mg of DSPE-PEG2000 was dissolved in a mixture of chloroform (9 ml) and methanol (1 ml).
- c) Both solutions were mixed in a round bottom flask to a v/v ratio of 1.6/1.36 and then evaporated at 60°C to eliminate the chloroform solvent.
- d) The resulting thin film layer of lipids at the bottom of the flask was hydrated with a premixed solution of water (99 ml), glycerol (1 ml) and NaCl (396 mg) and further sonicated for 1 hour.
- e) Finally, the phospholipid solution was transferred into a vial and ready to be used for microbubbles production in the second part of the preparation.

The second part of the process involved the introduction of the gas into the phospholipids solution to create the microbubbles:

- a) A volume of 1 ml of the phospholipids solution was transferred into a 2ml vial with a rubber septum cap. Two needles with different lengths were inserted into the vial through the cap as shown in Figure 2.2. Using the longer needle, 10 ml of C_3F_8 gas was bubbled through the solution via a gas-tight syringe within 30s. The second needle provided an exhaust for the gas to escape.

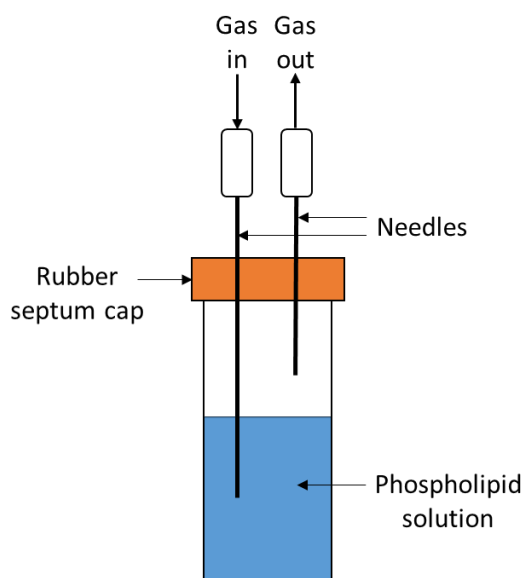


Figure 2.2 – Two needles were inserted into a 2-ml vial to bubble through the phospholipids solution with perfluorocarbon, C_3F_8 , gas.

- b) Both needles were then removed simultaneously as soon as the syringe was empty.
- c) The vial was then shaken (4300 oscillations per minute) for 45s using a capsule mixing device (CapMix™; 3M, Bracknell, UK) (Figure 2.3).
- d) Fairly monodisperse gas-filled microbubbles were made by mechanical agitation with a mean size distribution $2.4 \pm 1.7 \mu\text{m}$ (Bencsik, Al-Rwaili et al. 2013) (Figure 1.9Figure 1.9 – Microscopic image reproduced from Bencsik et al. (2012), showing the gas-filled microbubbles with the mean size of $2.3 \mu\text{m}$ (standard deviation $1.7 \mu\text{m}$) produced by using the same mechanical shaker (CapMix™) we used for our microbubbles preparation.).



Figure 2.3 – Left: A capsule mixing device (CapMix™) with a 2 ml vial containing the phospholipids solution and the C_3F_8 gas, placed on the lever and ready to be shaken. Right: A shaken phospholipids solution vial, with microbubbles giving it a milky appearance, in a 2 ml vial.

2.2.3 Microbubble Suspending Medium

A polysaccharide gel was used as a suspending medium for the microbubbles preparation to further immobilise them. It prevented buoyant advection and assisted the distribution of microbubbles homogeneously throughout the medium whilst allowing a very high self-diffusion of water molecules. Morris et al. demonstrated the diffusion coefficient of water molecules in a polysaccharide gel (gellan gum) is within 93 % similar to that of bulk water, in a temperature between 298 and 338 K (Morris, Bencsik et al.

2008). We used two types of the polysaccharide gel in our study, they are gellan and alginate gels.

2.2.3.1 Gellan Gel Preparation

For our study, 2 % (w/v) concentration of gellan gel was used as a suspending medium for the microbubbles. The preparations of the gel are described as follows:

- a) An appropriate quantity of gellan powder was weighed (typically 5 g to produce a final quantity of 250 ml of gel with 2 % w/v concentration).
- b) 250 ml of distilled water was placed in a flask and a few drops of antibacterial solution were added to prevent the solution from quickly deteriorating due to bacterial contamination.
- c) The Gellan powder was added slowly into the distilled water at room temperature and stirred constantly. (Adding all the powder at the same time would cause powder coagulation, in our case 1 g of gel powder was added every half hour).
- d) The powder was given time to fully dissolve, usually requiring continuous stirring for about 2-3 hours.
- e) The gel was left at room temperature and stirred occasionally for eight hours to release any trapped gas (air).
- f) Finally, the gel was further thoroughly degassed, using a high vacuum pump to prevent inclusion of gas bubbles within the gel, which could lead to spurious measurements in the later experiments.

This fully prepared gellan gel, as a suspension medium, should be stored for no more than five weeks before use otherwise it becomes susceptible to deterioration due to contamination by microorganisms e.g. bacteria.

2.2.3.2 Alginate Gel Preparation

The alginate gel with 2 % (w/v) concentration was prepared following the procedure as previously described in section 2.2.3.1. Typically, 5 g of sodium alginate powder was

dissolved in 250 ml of distilled water. In the case for *in-vivo* study, the freshly prepared gel was used to make the contrast agent meal for each volunteer.

2.3 Entrapping Microbubbles in Alginate Spheres for MRI Pressure Measurements in the Human Stomach

In our initial attempt to entrap the microbubbles within the alginate spheres, we firstly tried a relatively low concentration (1 % w/v) of sodium alginate preparation, but this solution was found to not be viscous enough to immobilise the microbubbles as they were seen to rise within the spheres (Figure 2.4). Therefore, a higher concentration of sodium alginate gel (2 % w/v), which appeared viscous enough to immobilise the microbubbles, was used to make the microbubble-loaded alginate spheres for our study. In the following sub-section, the procedure to entrap the microbubbles into the alginate spheres is further explained. To the best of our knowledge, this method has never been explored before.

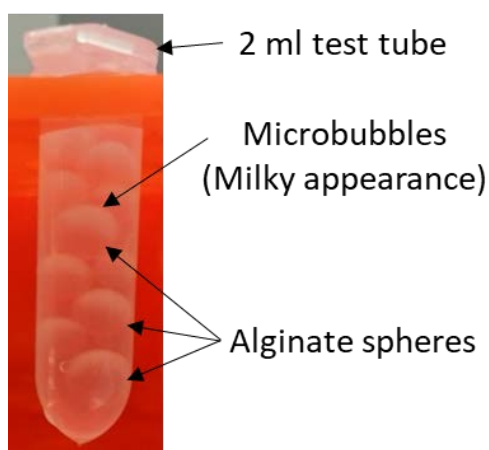


Figure 2.4 – Image showing the alginate spheres with entrapped microbubbles in a 2-ml test tube. These alginate spheres were prepared using sodium alginate gel at 1 % w/v concentration and the microbubbles appeared to rise within the spheres (milky appearance in the spheres), indicating that this concentration was not viscous enough in immobilising the microbubbles, hence, we used a 2 % concentration in the other preparations instead.

2.3.1 Sphere Formation

Alginates are commonly reacted with calcium ions to create a more elastic and stable gel (Duez, Mestdagh et al. 2000). Soft-solid spheres were formed spontaneously when sodium alginate gel was dripped into a calcium lactate solution due to cross-linking between polymer chains of the alginate molecules. We further exploited this material to our advantage by using it as a medium to entrap the microbubbles. Following is the description of the preparation of the alginate spheres with microbubbles:

- a) The previously prepared gas-filled microbubbles (Section 2.2.2) were gently introduced into the sodium alginate solution (2 % w/v) in a 50 ml test tube. The solution was mixed gently, by horizontally rotating the test tube slowly until the initially clear alginate gel appeared milky, to ensure that the microbubbles were distributed evenly throughout the sodium alginate gel.
- b) The mixture was then transferred into a syringe and added dropwise into a calcium lactate aqueous solution (0.5 % w/v), then left in the solution for a time duration which is known as curing time. In order to reduce the variations in curing times between the individual spheres, three different containers of calcium lactate solution were used, so that the error due to curing time was minimised (no more than one minute) whilst the average curing time we ended up was 10 minutes. The investigation on the selection of the 10 minutes as an optimum curing time is further detailed in the next chapter (section 3.2.1).
- c) The resulting alginate spheres with entrapped microbubbles were then sieved from the calcium lactate solution (Figure 2.5).
- d) The spheres were further dabbed with a paper towel to dry and eliminate any excessive calcium solution before being placed into distilled water for storage.



Figure 2.5 – The alginate spheres with entrapped microbubbles were sieved out from the calcium lactate aqueous solution after being left to cure for 10 mins.

2.3.2 Sphere Size

The consistency of dripping the mixture of sodium alginate and microbubbles into the calcium lactate solution will affect the size distribution and the shape of the spheres. When it comes to *in-vivo* studies, which require the human volunteer to swallow the contrast agent as a meal, it is important to keep the spheres in optimum size so that we can have homogeneous spheres to ease the quantitation of the meal's pressure from the region of interest (ROI) where numerous pixels are averaged. During preparations, this optimum size is achieved by keeping the distance between sodium alginate and calcium lactate solution constant while dripping (about 1 m apart), as well as the volume of the sodium alginate being dripped overtime. In order to measure their size, 20 spheres were selected randomly immediately after preparation and their diameters were measured using a calliper. Then, the mean and the standard deviation of the diameter of these spheres were calculated and was found as 4.98 ± 0.30 mm. Figure 2.6 shows three randomly selected alginate spheres with microbubbles and their corresponding sizes.

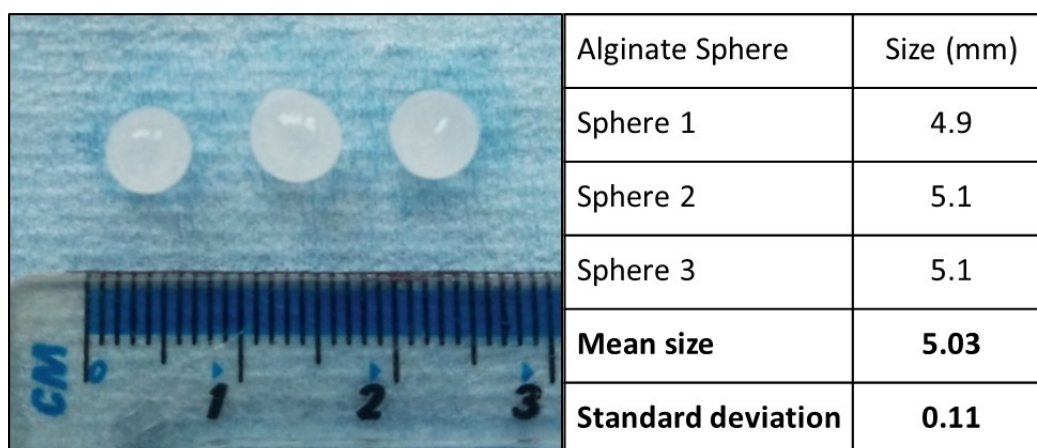


Figure 2.6 – The image is showing three randomly selected alginate spheres with entrapped microbubbles accompanied with their measured size in millimetres. The mean diameter of these spheres is 5.03 ± 0.11 mm.

2.4 Suspending Medium for Microbubble-loaded Alginate Spheres

2.4.1 Simulated Gastric Acid Solution

In order to simulate human gastric conditions for *in-vitro* studies, an acid solution mimicking the acid secretion from the stomach was used to investigate the effect on the microbubble contrast agent. This solution has been prepared following the formulation previously used in investigating the alginate spheres functionality (Hoad, Rayment et al. 2009). The details of the formulation of this solution are explained in the subsections below.

2.4.1.1 Materials

The following is the list of the ingredients (obtained from Sigma-Aldrich, UK) that were used to formulate the simulated gastric acid solution. The preparation of this solution is further described in the next subsection (2.4.1.2).

- a) Sodium chloride
- b) Potassium chloride
- c) Calcium chloride
- d) Hydrochloric acid

2.4.1.2 Preparations

- a) The ingredients were weighed as follows: 2.86 g of sodium chloride, 0.865 g of potassium chloride, and 0.4 g of calcium chloride.
- b) These were mixed and diluted into 1 L of distilled water.
- c) Then, while constantly stirring using a magnetic stirrer, hydrochloric acid was added gradually into the solution. A pH monitoring meter was used to observe the pH of the solution reduced to 2.0.
- d) The resulting solution was then used for the contrast agent experiments simulating a human gastric acid solution.

2.4.2 Locust Bean Gum

Naturally, the alginate spheres with incorporated microbubbles float in water, which is a disadvantage to our study. Therefore, it is important to have a suspending medium which enables these spheres to be immobilised while keeping their functionality. For this purpose, we used a 2 % (w/v) solution of locust bean gum to set the spheres in place and preventing them from floating. Essentially, it is only the alginate spheres with microbubbles within the contrast agent meal that provide the MR sensitivity to pressure, therefore, these spheres need to be homogeneously distributed in the stomach to enable the mapping of the spatially varying pressure changes.

The locust bean gum is a polysaccharide (Figure 2.7) vegetable gum, which is commonly extracted from the seeds of the carob tree, and it is widely used in the food industry as a thickening agent. The preparation of this gum is fully described below.

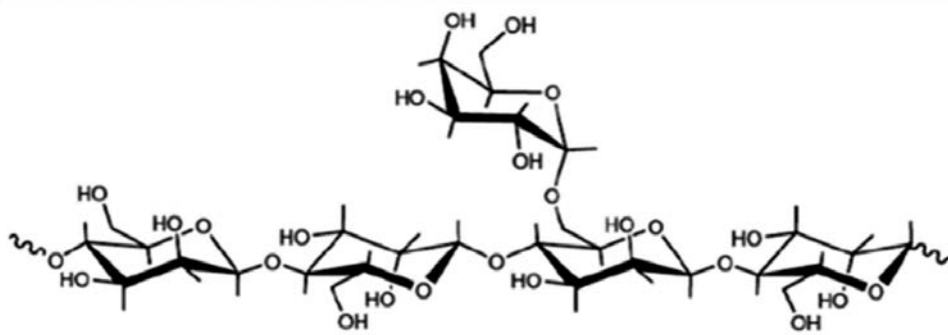


Figure 2.7 – The chemical structure of the locust bean gum (Ventura, Paninho et al. 2015).

2.4.2.1 Preparations

- a) An appropriate amount of locust bean gum powder was weighed (typically 5 g in order to reach a final volume of 250 ml of solution with 2 % w/v concentration).
- b) 250 ml of distilled water was placed in a beaker and heated up to 60°C.
- c) The locust bean gum powder was further added slowly into the distilled water while being stirred.
- d) The powder was given time to dissolve by constantly stirring the mixture using a magnetic stirrer for about 1 hour.
- e) The resulting solution was then used as a suspending medium for the alginate spheres with microbubbles.

2.5 Conclusions

The microbubble-based contrast agents that have been described in this chapter are further used for the studies in the other following chapters. The studies involve *in-vitro* experiments and *in-vivo* applications of the contrast agent in investigating the pressure exerted by the human stomach. The next chapter discusses the effect of the curing time on the T_2^{eff} of the alginate spheres, which leads us to the selection of the optimum curing time for our preparation. The effect of the presence of microbubbles in the alginate spheres on the T_2^{eff} value is also explored.

References

1. BENCSIK, M., AL-RWAILI, A., MORRIS, R., FAIRHURST, D.J., MUNDELL, V., CAVE, G., McKENDRY, J. and EVANS, S., 2013. Quantitation of MRI Sensitivity to quasi-monodisperse microbubble contrast agents for spatially resolved manometry. *Magnetic Resonance in Medicine*, **70**(5), pp. 1409-1418.
2. LOZANO, M.M. and LONGO, M.L., 2009. Microbubbles coated with disaturated lipids and DSPE-PEG2000: phase behavior, collapse transitions, and permeability. *Langmuir*, **25**(6), pp. 3705-3712.
3. NEEDHAM, D. and KIM, D.H., 2000. PEG-covered lipid surfaces: bilayers and monolayers. *US Patent 6210611*.
4. AVANTI POLAR LIPIDS, 2017-last update, 16:0 PC (DPPC) [Homepage of Avanti Polar Lipid, Inc.], [Online]. Available: <https://avantilipids.com/product/850355/> [04/01, 2017].
5. PODELL, S., BURRASCANO, C., GAAL, M., GOLEC, B., MANIQUIS, J. and MEHLHAFF, P., 1999. Physical and biochemical stability of Optison®, an injectable ultrasound contrast agent. *Biotechnology and Applied Biochemistry*, **30**(3), pp. 213-223.
6. MORRIS, R.H., BENCSIK, M., NESTLE, N., GALVOSAS, P., FAIRHURST, D., VANGALA, A., PERRIE, Y. and McHALE, G., 2008. Robust spatially resolved pressure measurements using MRI with novel buoyant advection-free preparations of stable microbubbles in polysaccharide gels. *Journal of Magnetic Resonance*, **193**(2), pp. 159-167.
7. DUEZ, J., MESTDAGH, M., DEMEURE, R., GOUEMANT, J., HILLS, B. and GODWARD, J., 2000. NMR studies of calcium-induced alginate gelation. Part I - MRI tests of gelation models. *Magnetic Resonance in Chemistry*, **38**(5), pp. 324-330.
8. HOAD, C., RAYMENT, P., COX, E., WRIGHT, P., BUTLER, M., SPILLER, R. and GOWLAND, P., 2009. Investigation of alginate beads for gastro-intestinal functionality, Part 2: In vivo characterisation. *Food Hydrocolloids*, **23**(3), pp. 833-839.

CHAPTER 3

MRI MEASUREMENTS OF THE CONTRAST AGENTS AT ATMOSPHERIC PRESSURE

3 MRI MEASUREMENTS OF THE CONTRAST AGENTS AT ATMOSPHERIC PRESSURE

3.1 Introduction

Viscous sodium alginate gel can be produced by dissolving a specific amount of sodium alginate powder in water. However, a stronger gel can be produced in the presence of salts, such as calcium ions, in the solution. When these ions are added to the alginate gel solution, the molecular chains become bound to each other in a process known as cross-linking, forming a rigid matrix at concentrations as low as 1 % w/v (Lee, Rogers 2012). In manufacturing a pressure-sensitive contrast agent for gastrointestinal study, we use this strong gel to entrap the microbubbles and create a soft-solid sphere. The time duration of residence of the mixture of sodium alginate gel and microbubbles in the calcium lactate solution, also known as the curing time, will affect the resulting signal intensity on MR images. This chapter covers the MRI measurements investigating the effect of the curing time in term of relaxation time decay.

Following that, the MRI measurements demonstrating the effect of the presence of microbubbles are undertaken by comparing the T_2^{eff} of the alginate spheres with and without microbubbles. The experimental set-up and the equipment required to perform the MRI experiments are also discussed.

In the early development of our contrast agents, the MR experiments were initially carried out on a 2.35T BIOSPEC Bruker scanner, which can only accommodate small specimen for *in-vitro* testing of our contrast agent. In later stages of our study, *in-vitro* experiments were also carried out using a 3T Philips whole body MR scanner, to optimise the MRI sequences for the *in-vivo* experiments on the human volunteers. The results of the *in-vitro* experiments from both scanners are presented in this chapter as well as in later chapters.

3.2 MR Relaxation Assessment at 2.35T Using A Small Animal Scanner

The image acquisitions performed for this section were carried out using a 2.35T Biospec Bruker MR scanner (Figure 3.1) within the Physics Department of the Nottingham Trent University.



Figure 3.1 – The small animal MR scanner BIOSPEC 2.35T Bruker at the Nottingham Trent University. The scanner is equipped with a proton-imaging RF coil (inner diameter 72 mm) and an imaging software Paravision 4.0.

3.2.1 Assessing the Effect of Curing Time

For the first part of the experiment, we aimed to investigate the effect of the curing time on the resulting MR images. To demonstrate this effect, we acquired MR images using a Multi-Slice Multi Echo, MSME sequence, assessing the T_2^{eff} of the microbubble-entrapped alginate spheres with different curing time.

3.2.1.1 Sample Preparations

The alginate spheres with microbubbles were prepared following the procedure fully described in section 2.3. In this experiment, the microbubbles were loaded into 2 % w/v sodium alginate gel and then divided into five batches; each of them was loaded into different syringes. Then, the sodium alginate gel was dripped into a 0.5 % w/v calcium

lactate aqueous solution in five different containers and left to cure respectively for 5, 10, 20, 30 and 60 minutes. Following curing, each batch of the spheres was sieved out of the calcium solution and placed in distilled water in a 2-ml plastic test tube for MRI assessments.

3.2.1.2 MR Measurements

The five test tubes containing microbubble-loaded alginate spheres with differing curing times were assessed in terms of T_2^{eff} . They were placed in a homemade acrylic holder at the centre of the scanner prior to acquiring the MR images.

The multi-slice T_2^{eff} -weighted images were acquired using an MSME sequence with a short echo time available, $TE = 10$ ms and a long repetition time, $TR = 14000$ ms, to ensure that all the magnetisation has returned to rest. The slice thickness was set to a 0.4 mm, and 8 averages were taken for this measurement which lasted for 6 hours.

3.2.1.3 Data Processing

Home written Matlab® code was used to analyse the resulting images, by fitting a monoexponential decay curve to every pixel acquired at different echo times, producing the pixel effective relaxation time, T_2^{eff} , within the alginate spheres with the microbubbles. The thermal noise was also measured by quantitating the pixel intensity outside the sample. Then, it was subtracted from the signal intensity prior to the exponential function fitting.

3.2.1.4 Results

The results of this experiment are demonstrated in Figure 3.2 and Figure 3.3. The curing process is clearly affecting the MR images, resulting in a decrease of the pixel intensity in the alginate spheres with increasing curing time. This indicates that the longer the curing time of the alginate spheres, the lower the T_2^{eff} value (Figure 3.3). In addition, the change in the T_2^{eff} is seen to be much rapid in a lower curing time and then it slows down as the curing time progresses from 30 to 60 min. This is perhaps caused by the decline in the concentration of 'free' calcium ions within the solution after a period of time of the crosslinking process. The results show that the 10-min curing time provides spheres

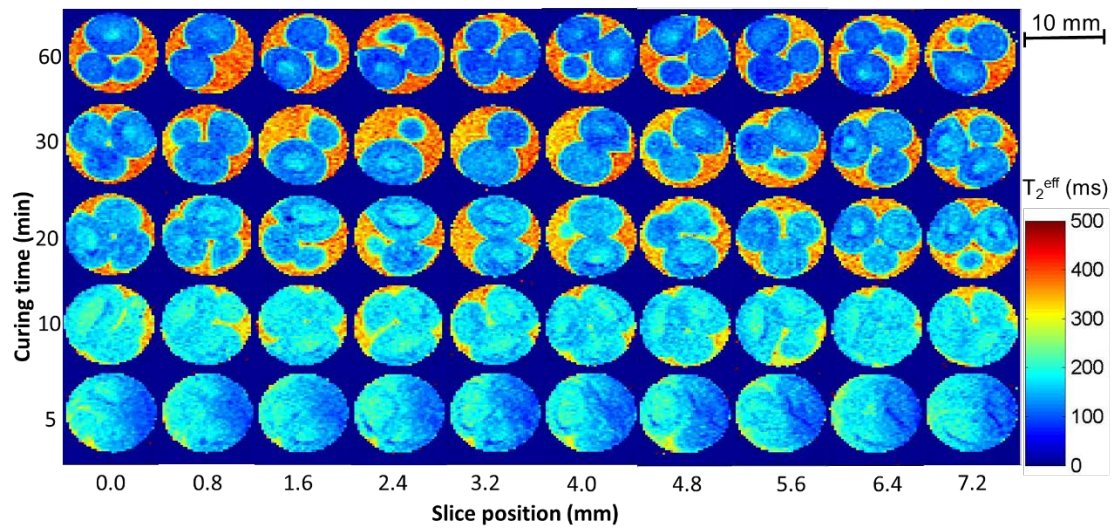


Figure 3.2 – Multi-slice T_2^{eff} images (obtained with the MSME sequence) showing the effect of different curing times on the alginate spheres with microbubbles. The signal intensity in the spheres decreases as the curing time increases. Unfortunately, imaging artefacts causing a signal deterioration in some parts of the 5 min curing time images can be seen.

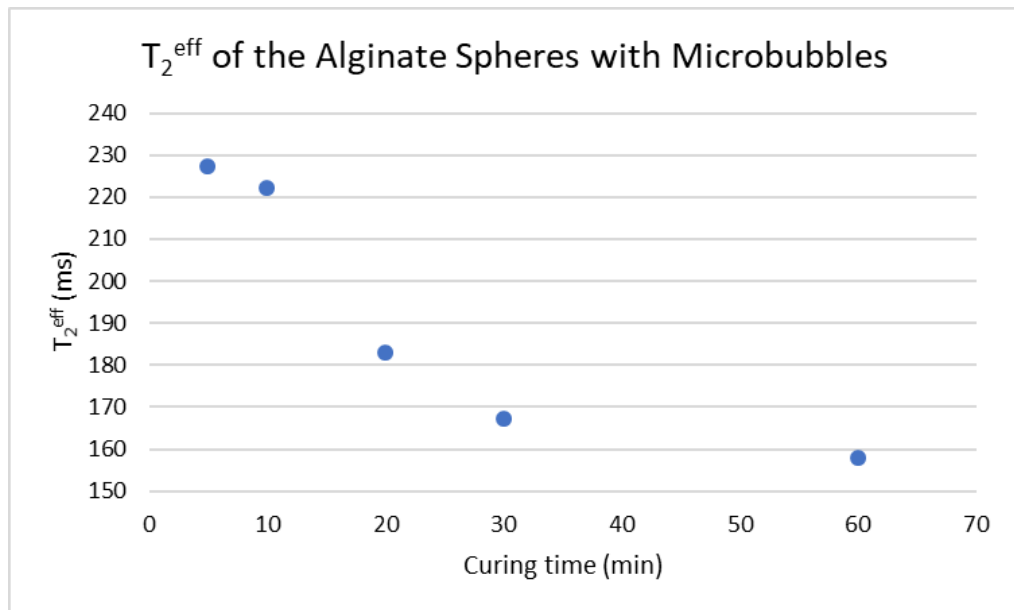


Figure 3.3 – Plot showing the mean of the T_2^{eff} of alginate spheres with microbubbles, taken from one of the image slice in Figure 3.2 (slice position at 0.0 mm), differing in curing times. The T_2^{eff} value decreases as the curing time increases. The change in the T_2^{eff} is seen to be much rapid in the lower curing time and then this effect slows down as the time progresses from 30 to 60 min.

that are stable with a comparatively homogeneous signal intensity across the spheres, with less appearance for spatially varying T_2^{eff} .

Although the 5-min curing time spheres appear homogenous on the MR image, unfortunately, they easily disintegrate in water which makes them less favourable for our preparations because the stability and the flexibility of the spheres are crucial to enable the contrast agent to withstand the pressure variations involved during ingestion. For curing time greater than 10 minutes, the pixel intensity of the entire sphere decreases, and radially decreasing T_2^{eff} can be gradually seen. This effect can be ascribed to the declivity of the gelation process of the spheres which takes place from the surface to the centre. When the sodium alginate is dipped into calcium solution, the calcium ions cross-linking starts at the surface of the sphere pulling the polymer chain of alginate closer together and creating a less permeable surface, which consequently slows down the calcium ions diffusion and crosslinking process as it goes further to the centre of the sphere (Chan, Lee et al. 2006). Hence, we decided to move forward with subsequent experiments in the current study with the 10 min-long curing preparations, which has a less spatially resolved effect yet adequate structural strengths in keeping the microbubbles inside the spheres.

Another finding we have obtained from this experiment is that the pixel intensity coming from the surrounding water is higher, at least twice, to that coming from the alginate spheres indicating that the T_2^{eff} of these gel spheres is significantly lower than the bulk water. For polysaccharide solutions, such as alginate gel, the NMR signal is regulated by the exchange between water and polysaccharide chain protons (Degrassi, Toffanin et al. 1998). This results in a considerable decrease in the transverse relaxation time of the gel, due to the reduction of the mobility of the proton in polysaccharide chain compared to bulk water (Ablett, Lillford et al. 1976).

In the future, there are several experiments that we could venture into to further explore the preparation of the contrast agent. Firstly, the curing effect can be further investigated in forming a stable alginate sphere by manipulating the concentration of the calcium lactate solution. Secondly, exploring a different method of manufacturing the alginate spheres could result in the creation of homogeneous spheres, in particular,

internal gelation mechanism has been previously demonstrated as an alternative method with such a potential (Chan, Lee et al. 2006).

3.2.2 MRI Assessment of Alginate Spheres with and without Microbubbles

3.2.2.1 Sample Holder Design

A two-compartment cell was manufactured from transparent acrylic tubing. The design of this homemade sample holder is shown in Figure 3.4. Firstly, a tube with 3 mm wall thickness, 15 mm length and 37 mm diameter, was cut along a longitudinal section to create identical halves which are labelled C1 and C2 on the diagram. Then, a rectangular piece of acrylic was cut by using a laser cutter, with dimensions of 15x30 mm² and thickness of 3 mm, labelled as B on the diagram. Another piece of acrylic was cut to form two disks with 37 mm diameters, labelled as A and D, and then, two circular apertures with diameters of 9 mm were cut on disk D.

Afterwards, all parts were glued together as shown in Figure 3.4 by using an acrylic adhesive. Before it was further used for the experiment, the integrity of the sample holder was tested by filling it with water and pressurising it up to 2 bars to check for any leakage. The photo of the finished product is shown in Figure 3.5, containing two preparations of the alginate spheres.

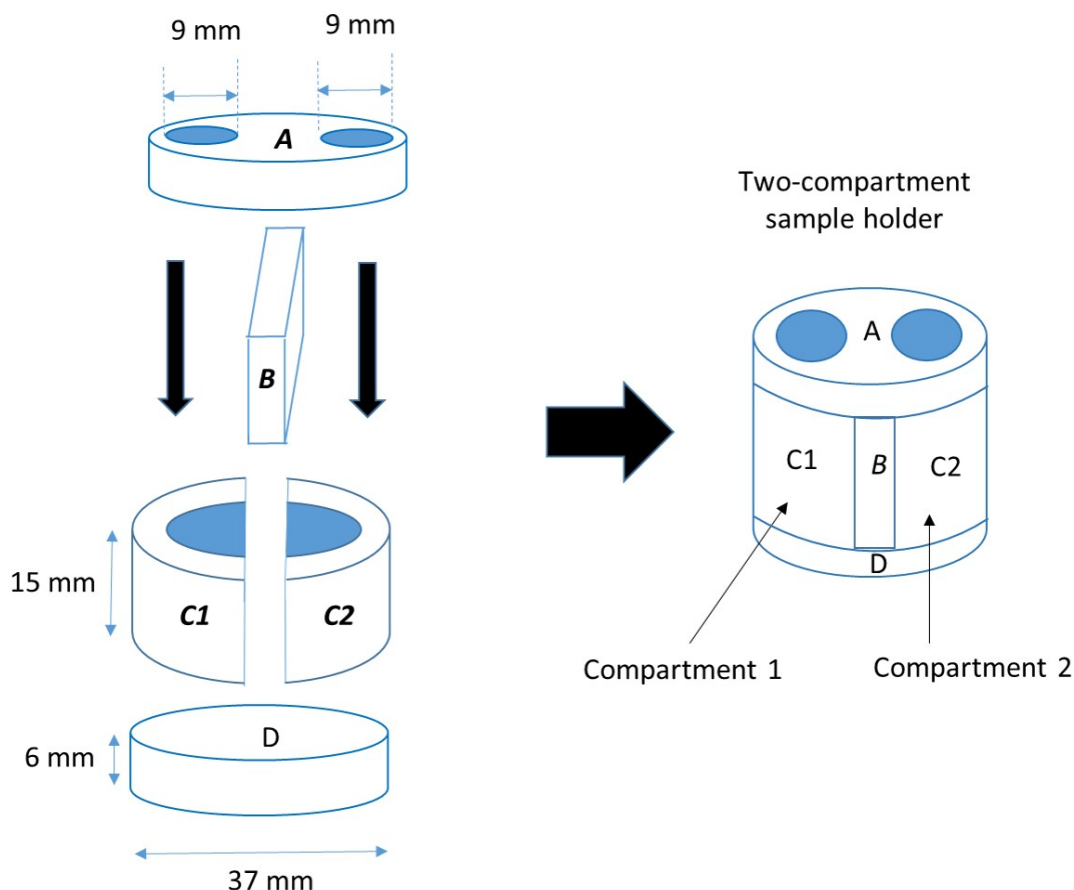


Figure 3.4 – Diagram showing the design of a sample holder, manufactured from transparent acrylic tubing, which was cut by a laser cutter into five pieces, A, B, C1, C2 and D. Then, all the pieces were glued together forming a two-compartment cell with one hole providing an inlet for each compartment.

3.2.2.2 Sample Preparations

In assessing the effect of the presence of microbubbles within the alginate sphere on the T_2^{eff} value, two preparations of alginate spheres were made following the method described in Chapter 2 (section 2.3). The two preparations were made identical except for the presence of microbubbles; one preparation was without microbubbles and the other one was with microbubbles entrapped. The spheres were transferred into the previously described two-compartment sample holder (Figure 3.5), to facilitate simultaneous assessment of both preparations, and then further placed in the 2.35T Bruker MR scanner for image acquisition.



Figure 3.5 – Twin-compartment sample holder containing both preparations of alginate spheres, with (left hand side) and without (right hand side) microbubbles, in water suspension. The milky appearance of the left hand side specimen indicates the presence of the microbubbles in the alginate spheres. The sample holder is also equipped with Swagelok connectors and tubing, enabling pressure to be applied to the system to be changed, which is particularly useful for the pressurised experiment and this will be further discussed in Chapter 5.

3.2.2.3 MR Measurements

The MSME sequence at TE = 10 ms and a relatively shorter repetition time, TR = 2500 ms, to further reduce the acquisition time, was used to acquire the multi-slice MR images with 2 mm slice thickness to demonstrate the T_2^{eff} value of both preparations. This also allows further optimisation of the next MRI sequence, used for the rapid image acquisition for pressure cycling experiments in Chapter 5 and provides evidence on the spatial distribution of the bubbles within the spheres.

3.2.2.4 Results

The results of this experiment are shown in Figure 3.6 and Figure 3.7. The T_2^{eff} image in Figure 3.6 shows two clearly differentiated compartments containing alginate spheres with different T_2^{eff} pixel intensities, demonstrating that the T_2^{eff} value is reduced by a typical factor of 2 in the presence of microbubbles within the spheres (compartment on the left-hand side). By plotting the T_2^{eff} pixel intensities distributions for both sphere preparations (Figure 3.7), their significant differences are further highlighted and quantitated. The T_2^{eff} values are ranging between 200 and 300 ms for the spheres without microbubbles and between 100 and 200 ms for the spheres with microbubbles. This result agrees with the principle of the gas-filled microbubble acting as a magnetic field perturber, creating a magnetic field gradient at the gas-liquid interface, which consequently affects the MR signal (Alexander, McCreery et al. 1996). The average T_2^{eff}

value (180 ms) from this experiment is then used to optimise the imaging parameter of the RARE sequence in measuring the rapid pressure changes in the later chapter.

An interesting additional outcome of this experiment is the demonstration of a spatial gradient of T_2^{eff} value seen between the centre and the periphery of alginate spheres with microbubbles. The microbubbles' density and the curing process may both contribute to the mechanisms causing this radial spatial gradient. This effect will be further explored, also in Chapter 5, by measuring the sensitivity of the two areas to pressure changes.

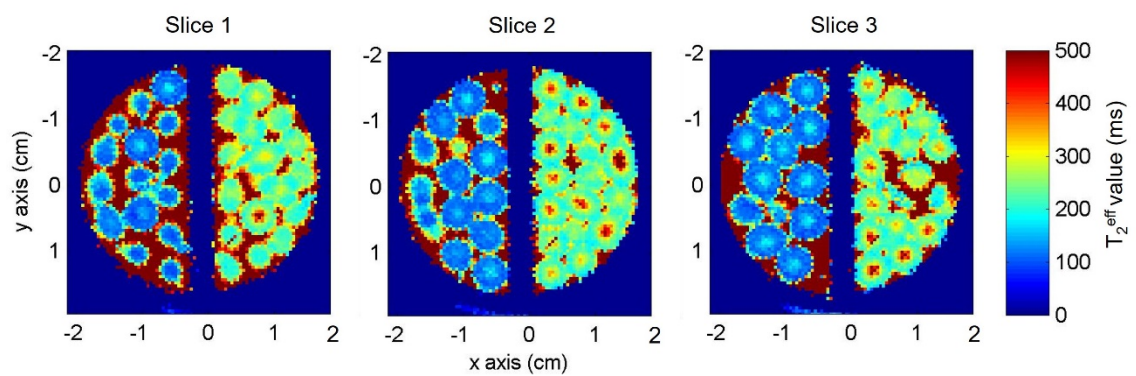


Figure 3.6 – Three consecutive slices of the T_2^{eff} images showing alginate spheres with (left compartments) and without microbubbles (right compartments). The T_2^{eff} is lower, typically by a factor of 2, in alginate sphere with microbubbles.

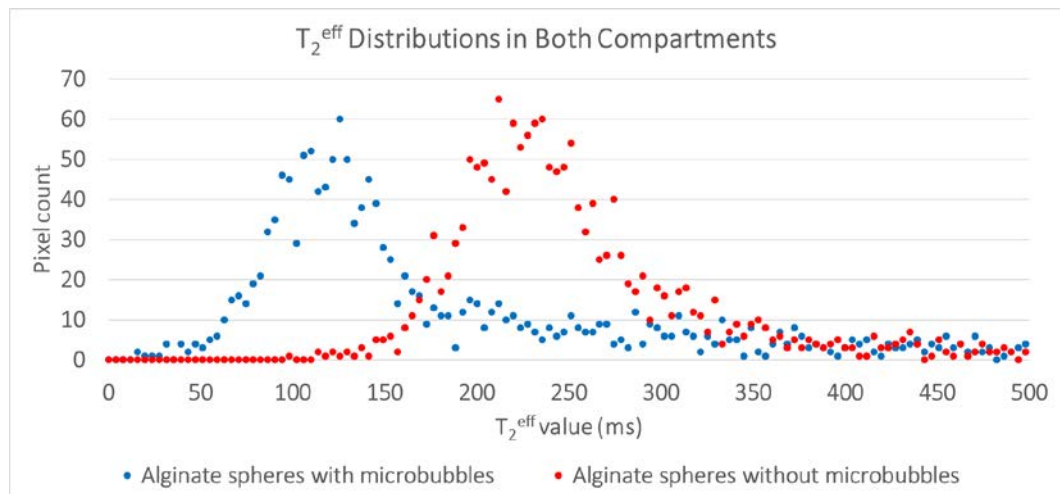


Figure 3.7 – The plot showing the T_2^{eff} distribution of the MR image of slice 1 in Figure 3.6, demonstrating the clear difference between both preparations, alginate spheres with and without microbubbles. The T_2^{eff} distribution of the alginate spheres with microbubbles is significantly lower than the spheres without microbubbles.

3.3 MR Relaxation Assessment at 3T using a Whole-Body Scanner

The image acquisitions in this section were performed using a 3T Philips Achieva whole body MR scanner (Philips, Best, Netherland) in the Sir Peter Mansfield Imaging Centre at the University of Nottingham. The experiments were carried out to optimise the MRI sequences for the preparation for *in-vivo* experiments and further validating the results obtained in our previous experiments using a 2.35T small animal scanner.

3.3.1 Methods

3.3.1.1 Sample Preparation

The contrast agent comprising alginate spheres with microbubbles was prepared following the method which previously described in section 2.3, with 10 minutes curing time. The spheres were suspended in a distilled water at room temperature. An hour before the MRI experiment, the spheres were loaded into a single-compartment sample holder (Figure 3.9) and then placed in a water bath at 37 °C, simulating the human body inner temperature. Later, the sample was wrapped in foam before being placed in the centre of the MR scanner.



Figure 3.8 – The 3.0 Tesla Philips Achieva whole body MR scanner at the Sir Peter Mansfield Imaging Centre, University of Nottingham.



Figure 3.9 – A homemade single-compartment sample holder containing the alginate spheres with microbubbles, in water suspension.

3.3.1.2 MRI Sequence

The MR acquisition was carried out using a Balanced Turbo Field Echo sequence, BTFE, to measure the T_2^{eff} of the alginate spheres with microbubbles on the 3T whole body scanner. Eight sets of a single slice at 3 mm thickness were acquired by varying the echo time of the T_2 preparation pulses, T_2 -prep time, before running a standard BTFE readout. The values of the T_2 -prep echo times were 20, 50, 80, 120, 180, 300, 500 and 800 ms.

After the MRI acquisition, the BTFE data were fitted by Dr Caroline Hoad from the University of Nottingham for the T_2^{eff} using a model to generate the decay curve spanning the evolution of the magnetisation after each radiofrequency pulse used in the sequence (Hoad, Cox et al. 2010). The difference between the modelled and acquired data was further minimised using a Powell fitting algorithm (Press, Teukolsky et al. 1992).

3.3.2 Results

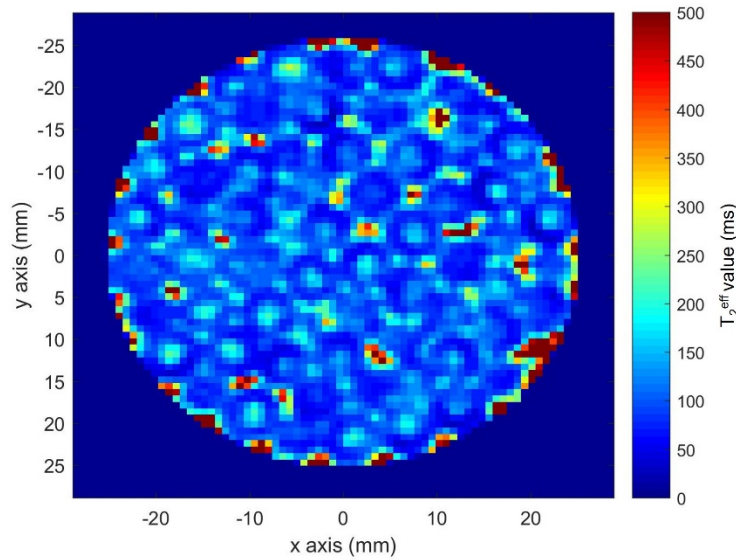


Figure 3.10 – MR image (acquired with the BTFE sequence) showing the T_2^{eff} value of the alginate spheres with microbubbles on the 3T Philips Achieva MRI scanner.

The BTFE MR image in Figure 3.10 shows the T_2^{eff} -weighted of the sample containing alginate spheres with microbubbles. As a result, the T_2^{eff} differences can be seen between the centre and periphery, a similar effect to the one we have discovered in the previous experiment when using the 2.35T small animal MRI scanner. The T_2^{eff} value of the centre of the spheres is ranging between 150 and 240 ms and the periphery between 55 and 100 ms. The average value ($T_2^{\text{eff}} = 135$ ms) is then used to optimise the next MRI sequence in measuring the sensitivity of the alginate spheres with microbubbles under pressure cycling in chapter 5.

From this result, we can see that the overall T_2^{eff} value of the alginate spheres with microbubbles is approximately 33 % lower, as expected, than observed on the 2.35T scanner in section 3.2.2, which agrees with the theory in Equation 1.7 described in section 1.3.7.2 and in the numerical simulations demonstrated by previous researchers (Dharmakumar, Plewes et al. 2002, Bencsik, Al-Rwaili et al. 2013). This described that, in a higher external magnetic field, the magnetic susceptibility difference between the bubble and its surrounding is increased, which then cause the increase of the magnetic field perturbation on the microbubble surrounding. Consequently, the water molecule experiencing greater dephasing, hence the decrease in the T_2^{eff} .

3.4 Conclusions

In this work, monodisperse gas-filled microbubbles were loaded into alginate spheres forming an MRI susceptibility contrast agent with a great potential for measuring pressure changes in the human stomach. The MRI measurements were performed on the contrast agent by assessing the T_2^{eff} and compared to that of the alginate spheres without microbubble. We have successfully demonstrated and quantified that the T_2^{eff} relaxation time substantial decreases in the presence of gas-filled microbubbles in the alginate sphere, at two different field strengths.

Beforehand, the effect of curing time was also quantitatively assessed in terms of T_2^{eff} . As a consequent of curing, changes in the T_2^{eff} is seen over time and this may result from structural changes in the spheres' characteristics, more specifically creating a more rigid matrix, which then influenced the interaction between the 'free' and 'bound' water molecules. In addition to that, the spatially variation of the T_2^{eff} is clearly revealed, showing gradual curing from the periphery towards the centre of the spheres. The T_2^{eff} of the periphery of the sphere is much lower to that of the core, typically by a factor of 2.1, suggesting that there are more bubbles trapped in the periphery. This phenomenon will be further explored in chapter 5 revealing the sensitivity difference to the pressure changes of the two areas in alginate spheres.

References

1. ABLETT, S., LILLFORD, P., BAGHDADI, S. and DERBYSHIRE, W., 1976. NMR relaxation in polysaccharide gels and films. *ACS Symposium Series*, (34), pp. 344-359.
2. ALEXANDER, A.L., McCREERY, T.T., BARRETTE, T.R., GMITRO, A.F. and UNGER, E.C., 1996. Microbubbles as novel pressure-sensitive MR contrast agents. *Magnetic Resonance in Medicine*, **35**(6), pp. 801-806.
3. BENCSIK, M., AL-RWAILI, A., MORRIS, R., FAIRHURST, D.J., MUNDELL, V., CAVE, G., MCKENDRY, J. and EVANS, S., 2013. Quantitation of MRI sensitivity to quasi-monodisperse Microbubble Contrast Agents for spatially resolved manometry. *Magnetic Resonance in Medicine*, **70**(5), pp. 1409-1418.
4. CHAN, L.W., LEE, H.Y. and HENG, P.W.S., 2006. Mechanisms of external and internal gelation and their impact on the functions of alginate as a coat and delivery system. *Carbohydrate Polymers*, **63**(2), pp. 176-187.
5. DEGRASSI, A., TOFFANIN, R., PAOLETTI, S. and HALL, L., 1998. A better understanding of the properties of alginate solutions and gels by quantitative magnetic resonance imaging (MRI). *Carbohydrate research*, **306**(1-2), pp. 19-26.
6. DHARMAKUMAR, R., PLEWES, D.B. and WRIGHT, G.A., 2002. On the parameters affecting the sensitivity of MR measures of pressure with microbubbles. *Magnetic Resonance in Medicine*, **47**(2), pp. 264-273.
7. HOAD, C.L., COX, E.F. and GOWLAND, P.A., 2010. Quantification of T2 in the abdomen at 3.0 T using a T2-prepared balanced turbo field echo sequence. *Magnetic Resonance in Medicine*, **63**(2), pp. 356-364.
8. LEE, P. and ROGERS, M.A., 2012. Effect of calcium source and exposure-time on basic caviar spherification using sodium alginate. *International Journal of Gastronomy and Food Science*, **1**(2), pp. 96-100.
9. PRESS, W.H., TEUKOLSKY, S.A., VETTERLING, W.T. and FLANNERY, B.P., 1992. *Numerical recipes in C : the art of scientific computing*. 2nd edn. Cambridge University Press.

CHAPTER 4

T_2^{EFF} MAPPING OF MICROBUBBLE-LOADED ALGINATE SPHERES WITH PRESSURE

4 T_2^{EFF} MAPPING OF MICROBUBBLE-LOADED ALGINATE SPHERES WITH PRESSURE

4.1 Introduction

In this chapter, we measure the MR signal intensity changes when varying pressure is being applied to the alginate spheres with microbubbles. The MRI measurement is carried out by acquiring a series of MSME images whilst the pressure is simultaneously increased and independently measured. The experimental set-up and the equipment required performing the MRI experiment are also explained.

When the pressure is applied, it is known that the microbubbles component in the contrast agent undergoes a change in size due to its flexibility and compressibility, which consequently alter the NMR signal, hence the change on its relaxation time (Dharmakumar, Plewes et al. 2002). In this chapter, we quantitatively explore this effect with a specific focus on the newly designed contrast agent, the alginate spheres with microbubbles.

4.2 Methods

4.2.1 Pressure Generation

In order to apply a pressure to the microbubbles contrast agent, a pump is needed to drive a volume of excess fluid into a closed system where the contrast agent reside. In our experiments, a Gilson® pump Model 303 (Gilson Inc., Wisconsin, U.S.A.) (Figure 4.1) was used to deliver this task because it provided an adjustable and a constant flow rate allowing a good control of the resulting pressure.



Figure 4.1 – The Gilson® pump Model 303 used to drive a volume of fluid into a closed system in order to apply a pressure to the microbubble-based contrast agent.

4.2.2 Sample holder design

A single-compartment cell was manufactured from transparent acrylic tubing. The design of this homemade sample holder is shown in Figure 4.2. The part of the cell labelled as B on the diagram was built from a round tube, with 3 mm wall thickness, 15 mm length and 37 mm diameter. Next, a piece of acrylic was cut by using a laser cutter to form two disks, each with a diameter of 37 mm and 6 mm thickness, labelled as A and C. Then, 9 mm circular apertures were formed on both pieces, one at the centre for disk A and one off-centred for disk C. Afterwards, all parts were glued together as shown in Figure 4.2 using an acrylic adhesive. Before it was used for the experiment, the integrity of the sample holder was tested by filling it with water and pressurising it up to 4 bars to check for any leakage.

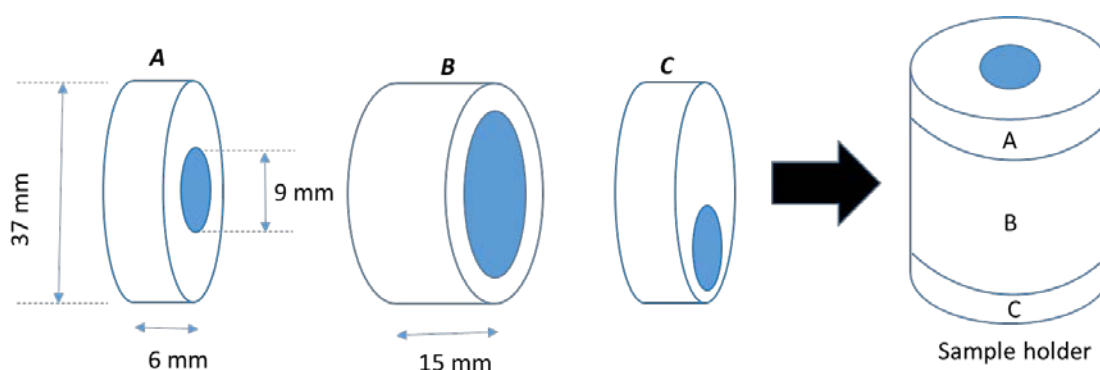


Figure 4.2 – Diagram showing the design of a sample holder, manufactured from transparent acrylic tubing. The second circular aperture, which is on disk C, was created to assist the filling process of the contrast agent into the sample holder, and it placed off-centred to ease the removal of any trapped air pocket by simply tipping the container to the side.

4.2.3 Contrast Agent preparations

Alginate spheres with microbubbles were prepared following the preparation as previously described in Chapter 2 (section 2.3). These spheres were suspended in distilled water before being transferred into the described sample holder with approximately 5 ml capacity (Figure 4.3) and then connected to a pump and a pressure gauge. While loading the contrast agent into the sample holder, an active measure was

taken to avoid any air pocket being trapped in the system, which can affect the effectiveness of the measurement if they were left in the sample.



Figure 4.3 – Picture showing the sample holder containing microbubble-entrapped alginate spheres suspended in distilled water. The sample holder is equipped with inlet and outlet, which can be connected to the Swagelok tubing, enabling the fluid being driven into the system in order to apply pressure to the contrast agent.

4.2.4 Experimental set-up

The experiment was set up as shown in Figure 4.4. The sample holder containing alginate spheres with microbubbles was connected to the pump and then placed in the Bruker Biospec 2.35T MR scanner. The pump was further set to flow at a very low rate, 2 ml/hr, to supply a slowly increasing pressure to the system. Immediately after the pump was switched on, MR images were acquired simultaneously using the MSME sequence at $TE = 10$ ms and $TR = 3000$ ms (for a significant time saving), acquiring a dynamic measurement of the effective transverse relaxation time, T_2^{eff} , of the contrast agent. The experiment lasted for 2.5 hours allowing 15 separate sets of three-slice T_2^{eff} images to be taken every 9 minutes as the pressure in the system was very slowly increased, from 0 bar to 1 bar.

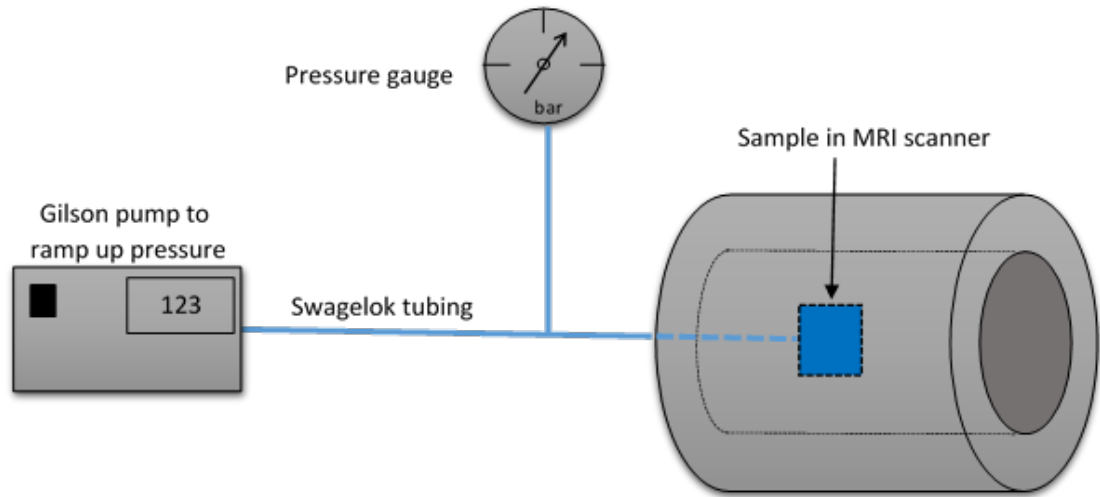


Figure 4.4 – Illustration showing the equipment set-up for the experiment allowing the measurement of the T_2^{eff} increase to pressure increase. A sample holder containing alginate spheres with microbubbles was connected to a pump and pressure gauge by Swagelok tubing

4.3 Results

The resulting MSME images were processed using a home built Matlab® code, as previously described in section 3.2.1.3. Figure 4.5 shows two sets of the multi-slice T_2^{eff} images of the sample with different intensities demonstrating the T_2^{eff} change within the alginate spheres with microbubbles. These two sets of the three-slice images were taken at two different pressure values, 0.15 and 0.89 bar respectively. An increase of the signal intensity is clearly seen all over the spheres on a higher pressure value.

In order to calculate the sensitivity of the spheres to pressure changes, for each repetition of the MSME sequence, we estimated the mean T_2^{eff} of the contrast agent by selecting the pixels corresponding to alginate spheres with microbubbles for each measured pressure. From the graph, the sensitivity of this contrast agent to the pressure change appears to be as high as 43 % T_2^{eff} change per bar. A linear correlation is demonstrated with a clear increase of T_2^{eff} with increasing measured pressure seen all over the spheres as shown in Figure 4.6. This is directly linked to the change of the microbubble radius size in the alginate sphere which is in agreement with the numerical simulation undertaken by Dharmakumar et al., stating that the change in the bubble size due to change in pressure caused changes in the effective spin-spin relaxation rate

$1/T_2^{\text{eff}}$ (or R_2^{eff}). The presence of the microbubbles perturbed the external magnetic field and a change in the bubble size results in a differing spatial extent of this field perturbation. The protons at the bubble surrounding experience a dephasing because they sample different magnetic field strengths while diffusing. The greater the field perturbations sampled by the proton, the greater the extent to which the MR signal decays due to dephasing, which yields image contrast to the pressure. Therefore, as the bubble size decreases due to the pressure increase, the proton samples lesser field perturbations that cause it to experience less dephasing, hence the increase in the MR signal.

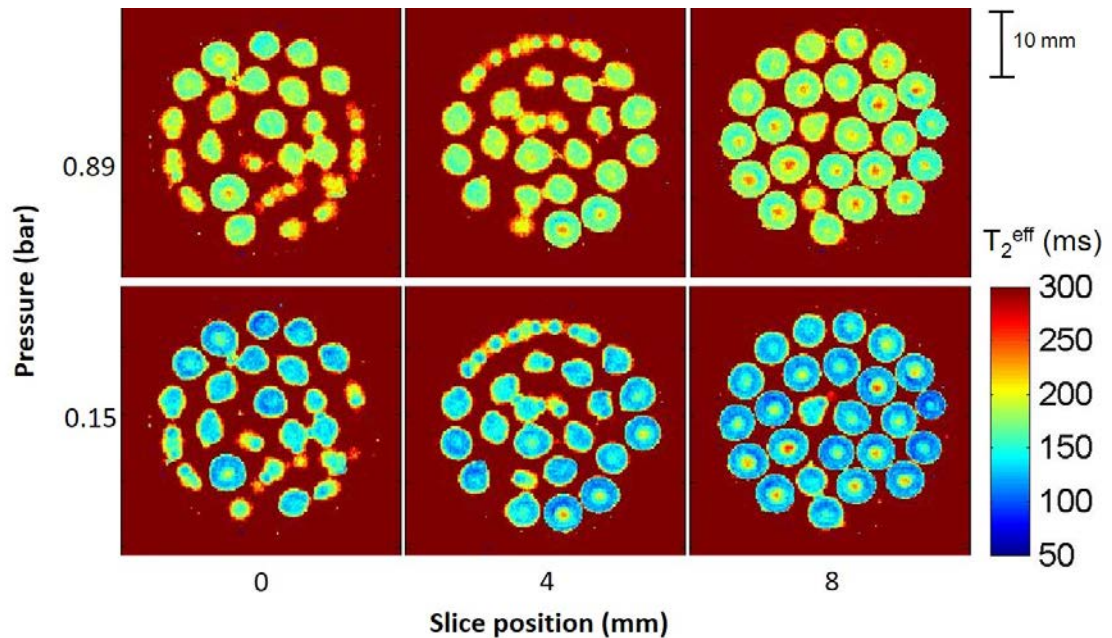


Figure 4.5 – Two sets of the three-slice MSME images taken at different pressures showing the T_2^{eff} values within the alginate spheres with microbubbles. The image is an axial slice taken from the centre of the sample, which also reveals a spatial gradient of the T_2^{eff} between the centre and the periphery of the spheres.

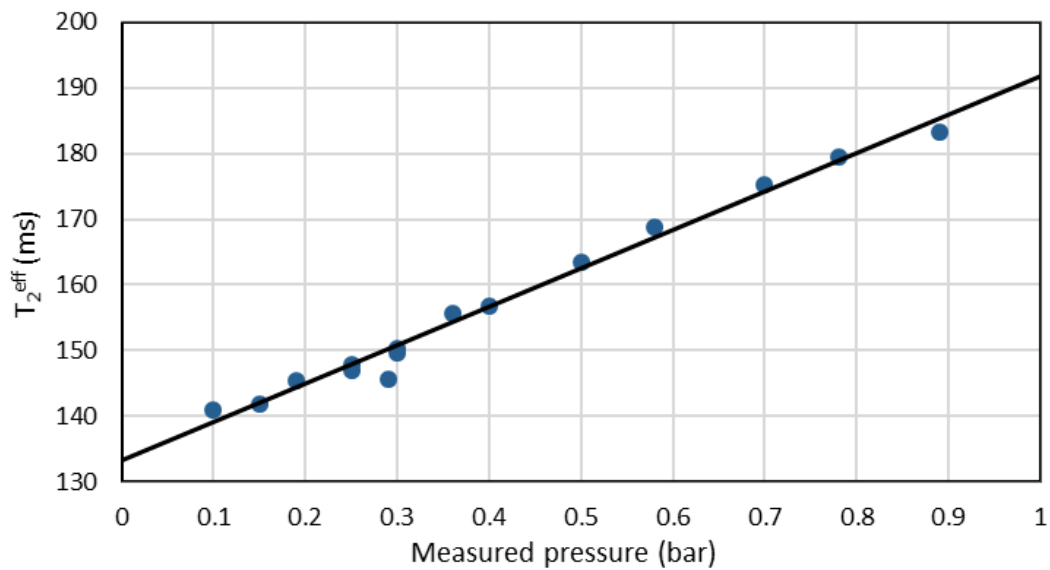


Figure 4.6 – Graph showing a linear correlation between effective transverse relaxation time, T_2^{eff} , of microbubble-loaded alginate spheres with the pressure change. The T_2^{eff} value increases linearly as the pressure applied increases. The solid line denotes a trend line providing the best fitting of the data (blue circles). The spheres exhibit a sensitivity of 43 % T_2^{eff} change per bar.

On the images, a spatial gradient is also revealed between the centre and the periphery of the spheres. In order to demonstrate these spatial variations and the extent of the T_2^{eff} change to the pressure change in both regions, we divided each T_2^{eff} image by the first one measured (Figure 4.7). Then, this effect is further demonstrated in Figure 4.8 by plotting the T_2^{eff} values in both regions as the pressure increases. It is seen that the T_2^{eff} value in the centre of the alginate sphere is constantly higher compared to the periphery. Both of these regions contribute to the increase in the T_2^{eff} value of the whole alginate spheres when the pressure is increased, with the periphery exhibits a higher sensitivity, which is up to 58 % T_2^{eff} change per bar whilst the centre exhibits 24 % change per bar (Figure 4.8). The sensitivity to pressure changes of these two regions within the spheres is further explored in the next chapter.

In addition, there is no measurable change of spin density (Figure 4.9), as expected, with pressure, which constitutes further evidence that the change in MR signal is mostly caused by the size changes of gas-filled microbubbles as the pressure changes.

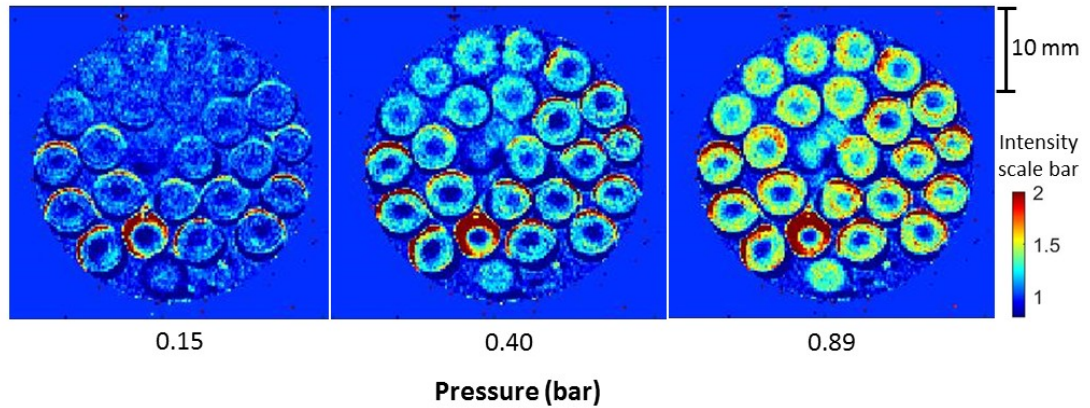


Figure 4.7 – Three of the T_2^{eff} division images, the same slice but at different pressures, revealing the spatial variations between the centre and the periphery of alginate sphere and demonstrating the sensitivity difference between the two regions to the pressure change. These images are produced by dividing each T_2^{eff} image with the first image acquired, at a pressure value 0.1 bar.

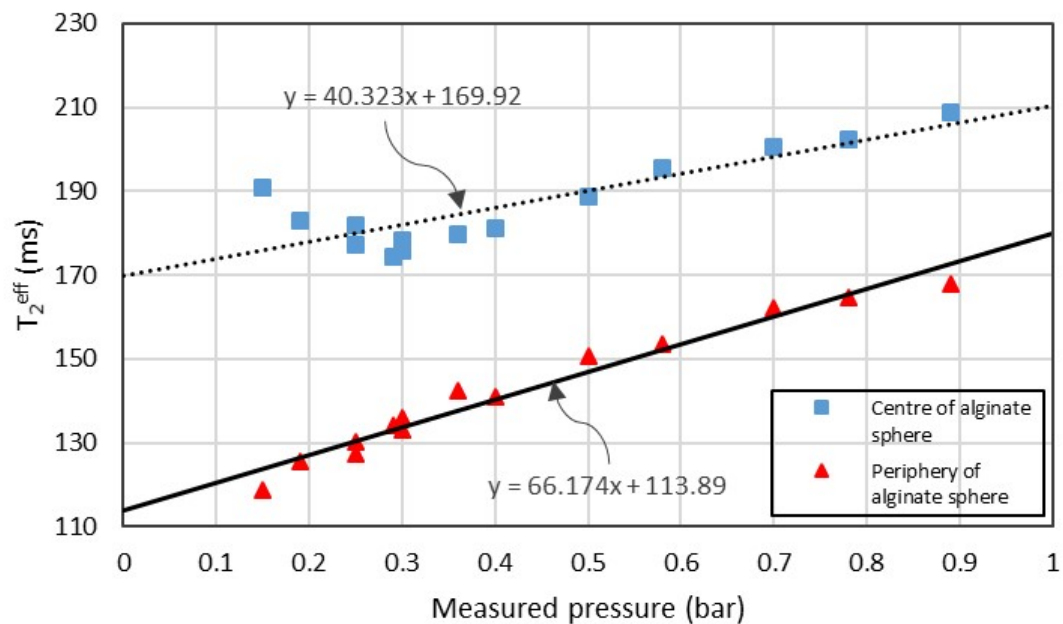


Figure 4.8 – Graph showing the T_2^{eff} changes in the centre and the periphery of alginate sphere to the pressure change. In both regions of the sphere, the T_2^{eff} value increases linearly as the pressure applied increases. The linear lines (the dotted line for the centre and solid line for the periphery) best fitted the data and the gradients and y-intercepts for both lines are presented in the form of $y=mx+c$ equations. The sensitivity of the two regions derived from the linear lines is 24 % T_2^{eff} and 58 % change per bar in the centre and periphery, respectively.

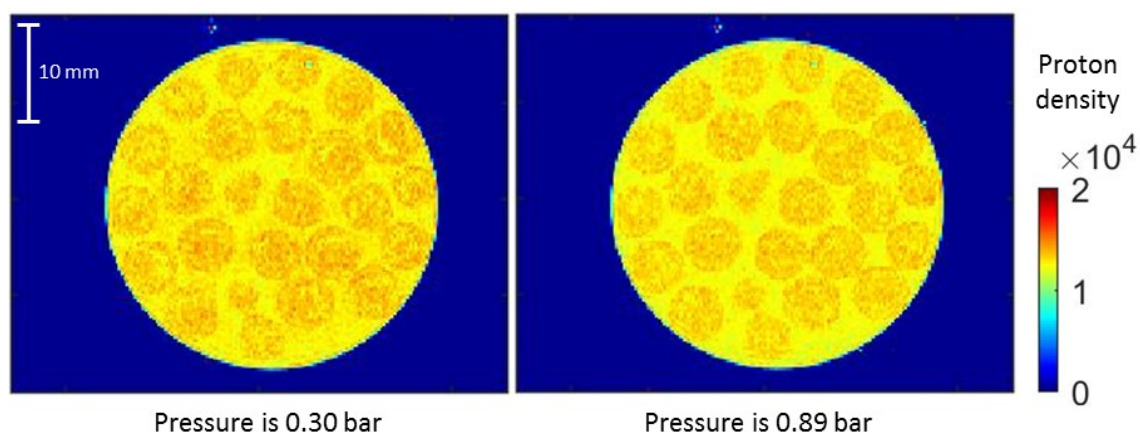


Figure 4.9 – The images showing the proton density of the sample taken at two different pressures, demonstrating there is no measurable change as the pressure change.

4.4 Conclusions

A pressure-sensitive contrast agent was produced from alginate spheres with entrapped microbubbles and its functionality was tested with MRI. In this experiment, the pressure was applied to the system and gradually increased while the MR images were simultaneously taken. The T_2^{eff} mapping results show an excellent linear correlation with the externally applied pressure, the T_2^{eff} within the contrast agent increased as the pressure increased. This result is consistent with the initial finding demonstrated by Alexander et al., although they were using less stabilised microbubbles (air-filled) with polydisperse size preparations, where the relaxation rate ($1/T_2^{\text{eff}}$) was seen inversely proportional to the pressure change (Alexander, McCreery et al. 1996). Also, the theoretical study demonstrated by Dharmakumar et al. (2002) is in agreement with this outcome. As the pressure increases, the size of the bubble decreases, the magnetic field perturbation is being altered, therefore the MR signal too.

Additionally, we have also found that the sensitivity to pressure changes is different between the centre and the periphery of the alginate spheres, where the periphery exhibits a higher sensitivity, which is up to 58 % T_2^{eff} change per bar whilst the centre exhibits 24 % change per bar. We believe that the predominant reason for this is due the difference of the microbubbles distribution between these two regions. As a conclusion, the results we obtained in this chapter demonstrate that this contrast agent

can be used as a non-invasive technique for measuring pressure within a human body, particularly for gastrointestinal study. In the next chapter, with an aid of a rapid MRI sequence, we explore the ability of this contrast agent in measuring rapid pressure changes.

References

1. ALEXANDER, A.L., McCREERY, T.T., BARRETTE, T.R., GMITRO, A.F. and UNGER, E.C., 1996. Microbubbles as novel pressure-sensitive MR contrast agents. *Magnetic Resonance in Medicine*, **35**(6), pp. 801-806.
2. DHARMAKUMAR, R., PLEWES, D.B. and WRIGHT, G.A., 2002. On the parameters affecting the sensitivity of MR measures of pressure with microbubbles. *Magnetic Resonance in Medicine*, **47**(2), pp. 264-273.

CHAPTER 5

MRI SENSITIVITY OF MICROBUBBLE-LOADED ALGINATE SPHERES TO PRESSURE VARIATION

5 MRI SENSITIVITY OF MICROBUBBLE-LOADED ALGINATE SPHERES TO PRESSURE VARIATION

5.1 Introduction

In the previous chapter, we have demonstrated using an MSME sequence that the alginate sphere with microbubbles can provide the MRI scan to sense changes in pressure. Here, we explore the ability and the MR sensitivity of this novel contrast agent to measure a rapid pressure change *in-vitro*. In order to achieve this, the fast MR imaging sequence called Rapid Acquisition with Relaxation Enhancement (or RARE) was adopted allowing the acquisition of images while the pressure within the system was being rapidly changed. In parallel, the stability of the contrast agent was also assessed, by repeatedly cycling the applied pressure several times (whilst acquiring the RARE images).

In order to use this contrast agent for measuring pressure changes in the human stomach, it must endure the human stomach conditions whilst maintaining its functionality. Hence, this study includes the measurement of the sensitivity of the alginate spheres with microbubbles in different environments mimicking the human stomach acid and temperature. On top of that, the sensitivity of this contrast agent is also observed using a 3-T whole body scanner intended to be used for the *in-vivo* experiments involving human volunteers. Both data acquired by the 2.35T Biospec Bruker and the 3T Philips Achieva scanners are presented in this chapter.

5.2 *In-Vitro* Studies at 2.35 Tesla Using a Small Animal Scanner

The image acquisitions performed for this section were carried out using a Biospec 2.35T Bruker small animal MR scanner (Figure 3.1) at the Physics Department of the Nottingham Trent University.

5.2.1 NMR Signal Changes to Rapid Pressure Cycling in Water

5.2.1.1 Sample Preparations

Two preparations of alginate spheres were produced following the method described in Chapter 2. The two preparations were made identical except for the presence of

microbubbles; one preparation was without microbubbles and the other with microbubbles entrapped. The spheres were loaded into a twin-compartment sample holder (the same as used in section 3.2.2) to facilitate the simultaneous assessment of both preparations.

5.2.1.2 Experimental Set-up

The Swagelok tubing was connected to the two-compartment sample holder, containing the two preparations of alginate spheres with and without microbubbles, and to a pump and a pressure gauge (Figure 5.1). The inlets of the two individual compartments were interconnected at the same distance of 50 cm allowing identical pressure changes to be simultaneously applied to both preparations. Optimised RARE images were acquired with pressure cycling between 0 and 1 bar, at echo time $TE = 10$ ms every 7 seconds, and effective echo time, $TE^{eff} = 400$ ms. It has been previously demonstrated that to achieve a maximum MR sensitivity, the effective echo time is optimised when $TE^{eff} = 2T_2^{eff}$ (Morris, Bencsik et al. 2008). Hence, the value of the TE^{eff} of our RARE sequences was adjusted accordingly, from the previous experiment described in section 3.2.4.2.

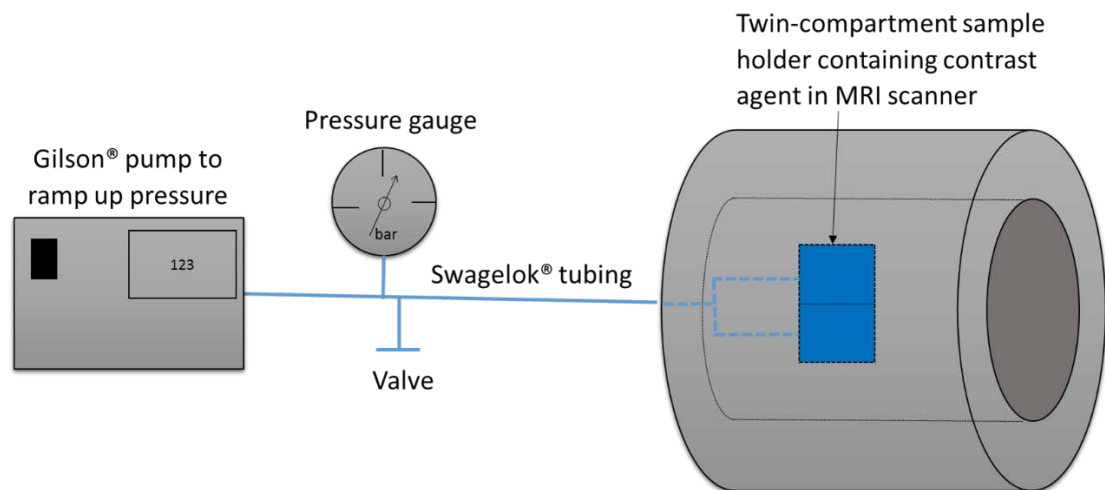


Figure 5.1 – Illustration showing the equipment set-up for the experiment measuring the MR sensitivity of the alginate spheres with and without microbubbles to pressure changes. A twin-compartment sample holder containing both alginate spheres preparations was connected to a pump and pressure gauge with Swagelok tubing.

5.2.1.3 Results

On the RARE images, the signal intensity coming from the alginate spheres with microbubbles at 0 bar is lower to that coming from the alginate spheres without microbubbles by a factor of approximately 2.5, indicating, as expected, that the T_2^* is decreased in the presence of the microbubbles (Figure 5.2). In monitoring the MR sensitivity to pressure, the lower MR intensity pixels were selected, thereby eliminating the water solvent from the analysis to ensure that the signal intensity is solely coming from the spheres. The signal intensity of the first MR image is relatively high due to the T_1 recovery effect, hence, we took the mean signal intensity of the second and the third images, where the magnetisation had reached its steady state while there was no measurable pressure applied, to calculate the sensitivity of the contrast agents to the pressure change. Essentially, we analysed the percentage of the relative signal intensity change compared with the alginate spheres 'at rest'.

Using this strategy, the MR signal intensity in the spheres with entrapped microbubbles exhibits changes of approximately 40 % signal change per bar. On the contrary, the signal intensity remains constant (to within 1 % due to noise and scanner electronic drift) throughout the experiment in the spheres without microbubbles, demonstrating that the signal change is indeed due to the presence of the microbubbles. In the preparation with microbubbles, there is a 10 % signal drift most probably due to bubble destruction, however, the sensitivity remains as high as 25 % change per bar, towards the end of this 17-min long experiment after 12 pressure cycles (Figure 5.3).

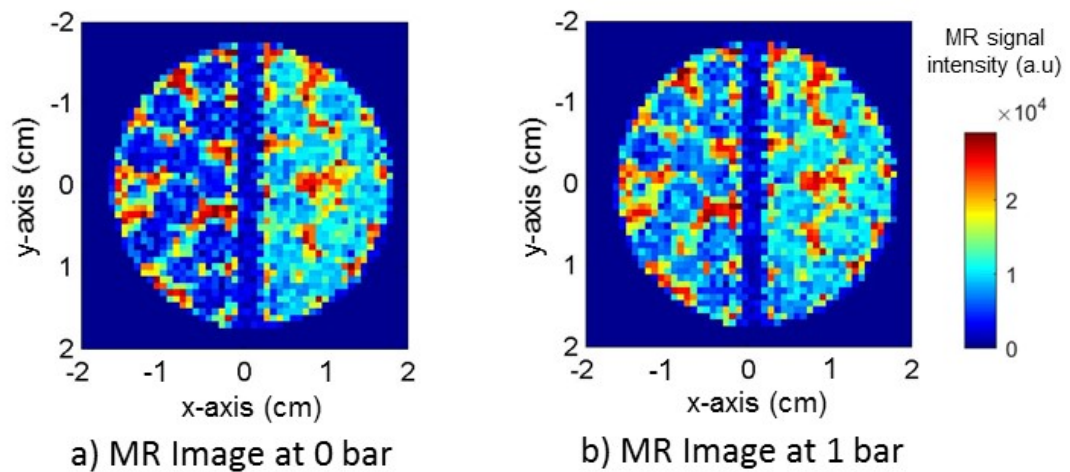


Figure 5.2 – Two RARE images showing both compartments containing alginate spheres with (left) and without (right) microbubbles acquired at different pressure values; 0 bar in image a) and 1 bar in image b). At 0 bar, the signal intensities coming from the alginate spheres with microbubbles are much lower compared to the counterpart alginate spheres without microbubbles. At 1 bar, the signal intensities of the alginate spheres with microbubbles increase whilst the ones without microbubbles remain the same.

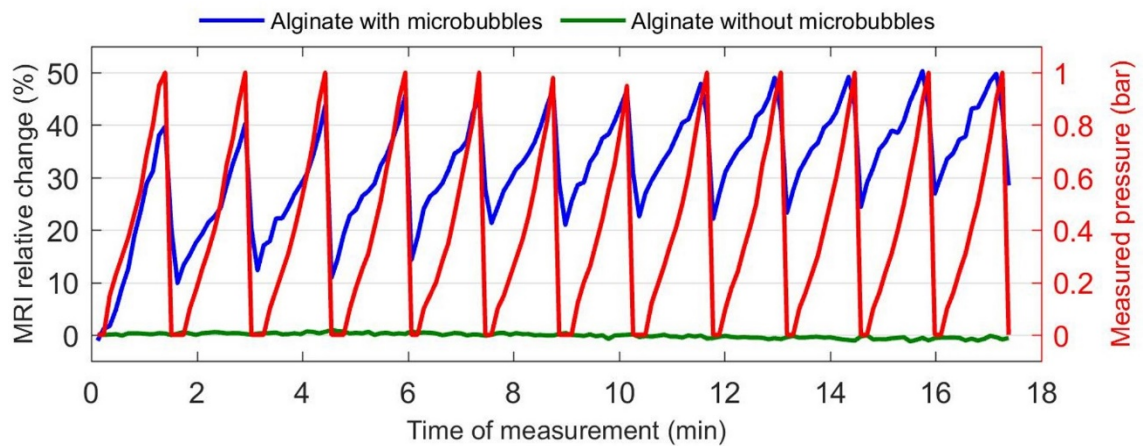


Figure 5.3 – Graph showing the sensitivity of both alginate spheres with and without microbubbles. The MR signal intensity changes coming from alginate spheres with bubbles initially typically shows 40 % signal change per bar, whilst the signal intensity remains constant in alginate without bubbles. The percentage of the MR signal intensity change is relative to the second and the third images, where the magnetisation had reached its steady state while the measured pressure was still zero. The red curve shows the measured pressure.

5.2.2 MRI Sensitivity with Different Bubbles Densities, and Effect of an Acid

Simulating Gastric Conditions

It has been demonstrated by previous workers through a numerical simulation that the pressure sensitivity of the microbubbles can be further enhanced by increasing its density (Bencsik, Al-Rwaili et al. 2013). Although we have demonstrated in the previous experiment that the alginate spheres with microbubbles exhibited a maximum pressure sensitivity up to 40 % signal change per bar, it would be desirable if this sensitivity can be further enhanced to maximise its ability in assessing small pressure changes within the human stomach, a pressure range between 30 – 82 mmHg or 39 – 109 mbar (Bortolotti, Annese et al. 2000). Here, we explore this effect on two different microbubbles densities entrapped in alginate spheres, expecting to see an increase in the sensitivity for a higher bubbles density. At the same time, the effect of an acid solution, that is similar to the gastric secretions existing in the stomach, is also observed on these preparations.

5.2.2.1 Sample Preparations

In this experiment, two preparations of alginate spheres with different bubble densities were used; one preparation containing approximately twice more bubbles than the other did in terms of gas volume fraction, to demonstrate the resulting increase in the MR sensitivity to pressure changes. In order to achieve this, two vials containing 1 ml of phospholipid solution each were shaken using the usual capsule mixing device to yield the same amount of microbubbles in both vials. Then, both microbubbles preparations were placed into separate containers with different amounts of sodium alginate gel, one with 10 ml and the other is twice more volume (20 ml), before the two preparations were respectively dropped into separate calcium lactate solutions resulting in the creation of alginate spheres with different bubble densities (4.5 % and 8.3 %). Then, the two different alginate sphere preparations were loaded into a separate cell of the two-compartment sample holder (same as discussed in section 3.2.2).

Separately, an acid solution mimicking the human gastric conditions was prepared following the steps described in section 2.4.1. Then, 20 ml volume of this solution withdrawn into a syringe.

5.2.2.2 Experimental Set-up

The main challenge for setting-up this experiment is that, in the acid solution, the alginate spheres are seen to exhibit a decrease in the T_2^* , which has also been mentioned in the previous study (Hoad, Rayment et al. 2009). In our initial attempt, we prepared the sample by suspending the alginate spheres in the acid solution before placing it into the scanner, but then the effect of the acid has already taken place before the scanning was started. By the time the first MR image was acquired, about 5 minutes after the spheres' first contact with the acid, a substantial decrease in the MRI signal intensity had already taken place.

In order to overcome this issue, we came up with a solution, by incorporating some additional assembly to the previous set-up described in section 5.2.1.2.; a syringe, an isolation valve and an outlet valve were also connected to the system, allowing the flushing with the simulated gastric acid solution (held in the syringe) (Figure 5.4). This would enable us to run the MR image acquisition, first, when the spheres reside in water suspension, and then, while flushing and immediately after the flushing of the acid solution into the system, replacing the water.

The optimised RARE images with $TE^{\text{eff}} = 400$ ms were acquired with pressure cycling between 0 and 1 bar, at $TE = 10$ ms every 7 seconds, initially, in the presence of water. Subsequently, the pressure cycling was stopped, then, the outlet valve and the isolation valve were released, and the water surrounding the alginate spheres was flushed out and replaced with the solution simulating gastric acid before the pressure cycling was resumed. A 20-ml volume of the acid solution, which was double from the volume capacity of the sample holder, was used to ensure a complete flushing of the water from the system was achieved.

In addition, necessary precautionary measures have also been considered regarding health and safety issues in handling the acid solution while running the experiment. Specified personal protective equipment (PPE), consisted of gloves, safety goggles and laboratory coat, was used at all time while handling this solution.

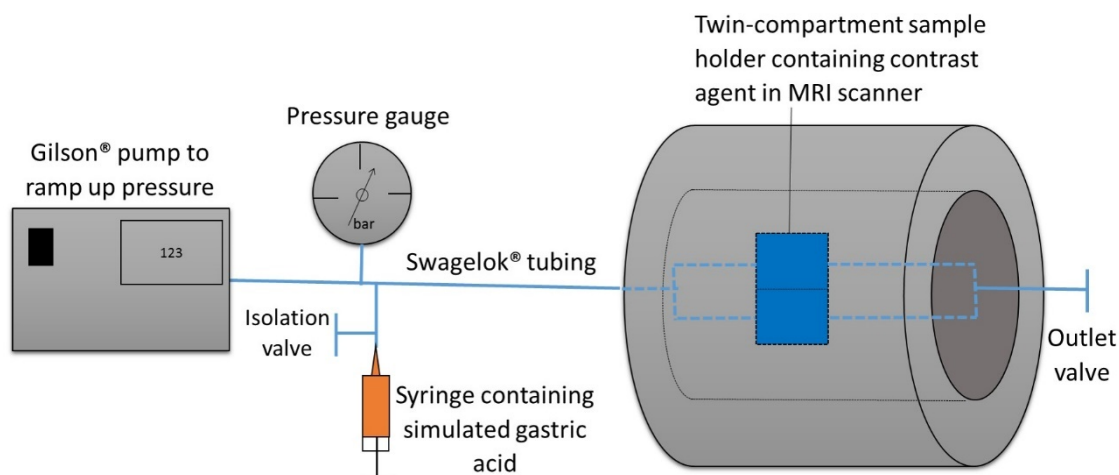


Figure 5.4 – Illustration showing the equipment set-up for the experiment measuring the MR sensitivity of the contrast agent in a simulated gastric solution. The syringe is connected to the assembly, through isolation valve, enabling the flushing of the simulated gastric acid solution into the system.

5.2.2.3 Results

In comparing two different bubbles densities, in the initial pressure cycle with the presence of water, the sensitivity of alginate spheres with twice higher bubbles density is approximately 45 % change per bar, and 35 % in the lower density preparation (Figure 5.5). This difference is less than expected, a 200 % increase has been demonstrated in previous work (Bencsik, Al-Rwaili et al. 2013) for an increase of twice of the bubble density. This is probably because at high enough density, the field gradients of individual bubbles will start overlapping, and the increase in MR sensitivity is not linear with bubble density anymore. At the same time, the signal drift, approximately 50 % over 10 pressure cycles, is observed more prominently in the higher bubble density, where it is only 11 % in the lower bubble density, suggesting that the bubble destruction due to pressure is higher as the experiment progresses, in the higher bubble density preparation. For further validation in the future, images of the contrast agents before and after of the pressure cycling can be acquired to be able to quantitate the signal change that caused by the bubbles destruction. Overall, although there is a slight increase of MR sensitivity with bubble density, the result suggests that there is no great benefit in exploring even higher values of bubble density.

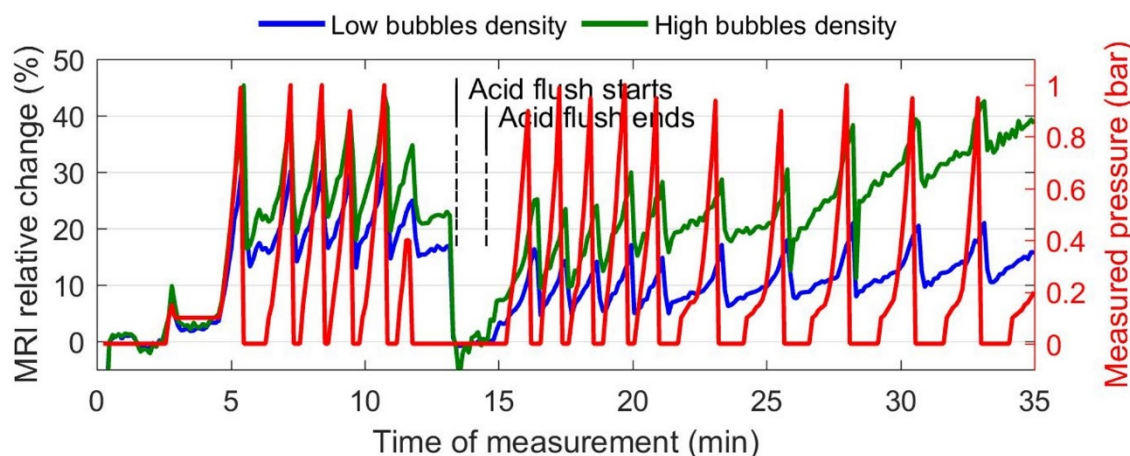


Figure 5.5 – Comparison of the sensitivity to pressure changes between low and high microbubbles densities in water suspension and in simulated gastric solution. Approximately 29 % sensitivity increase can be seen in the alginate spheres with twice more bubbles. There is a 50 % decrease in the sensitivity of the contrast agents when the solution mimicking gastric acid replaced the water suspending the spheres. The MRI relative change is calculated by comparing the signal intensity with the start of the pressure cycling within the water, and the acid. This means the relative signal change in water (corresponds to the time measurement up to 13 min) is computed relative to the zero pressure in the water and the relative signal change in acid (corresponds to the time measurement 14 min onwards) is relative to the zero pressure in the acid. The start and the end of the flushing of the acid solution into the system are indicated by vertical dotted lines. The red curve shows the measured pressure.

Following the introduction of simulated gastric acid, there is a decrease in the overall signal intensity of the samples. In a previous study carried out by Reyman and co-workers, it was shown that in lower pH condition, the transverse relaxation time in alginate spheres considerably decreased, and it was further suggested that this was due to the shrinking and the formation of a denser acid gel network (Rayment, Wright et al. 2009). This phenomenon suggests that the ‘free’ water molecules within the spheres are being expelled due to the shrinking of the alginate gel, hence the significant decrease on the observed signal intensity. This can be further demonstrated by observing the proton density changes within the spheres following the exposure to the acid solution, however, we have not explored this in our experiment.

At the same time, we anticipated that the shrinking of the alginate gel affects the flexibility of the microbubbles within the gel, which explains the 60 % decrease of the

sensitivity of the contrast agent in the acid solution. Nevertheless, we have demonstrated that following the alginate spheres being dipped in the acid, the contrast agents and especially the one with a lower microbubbles density are still very much functional for a time duration of at least 20 minutes.

5.2.3 MRI sensitivity at Body Temperature, 37 °C

5.2.3.1 Sample Preparations

The contrast agent comprising of the alginate spheres with microbubbles was prepared following the steps explained in Chapter 2. Then, the contrast agent was placed in a one-compartment sample holder in water suspension at room temperature.

5.2.3.2 Experimental Set-up

The set-up is similar to the previous experiment in section 5.2.2, which has an outlet valve and syringe connected (Figure 5.4), enabling the flushing of warm water into the system. However, in this experiment, one-compartment sample holder was used to contain the alginate spheres with microbubbles. Optimised RARE images were acquired simultaneously with pressure cycling between 0 and 1 bar, at TE = 10 ms every 7 seconds. Firstly, the pressure was cycled for approximately 12 min, with a cycle taking place every 3 minutes. Then, the pressure cycling was stopped. The fluid surrounding the alginate spheres was then flushed out and replaced with water at 37 °C, before resuming the pressure cycling.

The initial water surrounding the alginate spheres at room temperature was flushed out and replaced with 20 mL of water at 37 °C, which was twice than the volume of the sample holder, to ensure the fluid was completely replaced with warm water. However, we could not be certain that the spheres were actually at 37 °C, as we could not directly measure the temperature in the sample while running the experiment. We expected that there is a drop in the temperature of the water at 37 °C when it was flushed through a long thin tube to get into the main chamber of the sample. Perhaps for future reference, the temperature of the water coming out of the system should be monitored and keep the flushing through the sample with warm water until the outlet temperature reached 37 °C.

5.2.3.3 Results

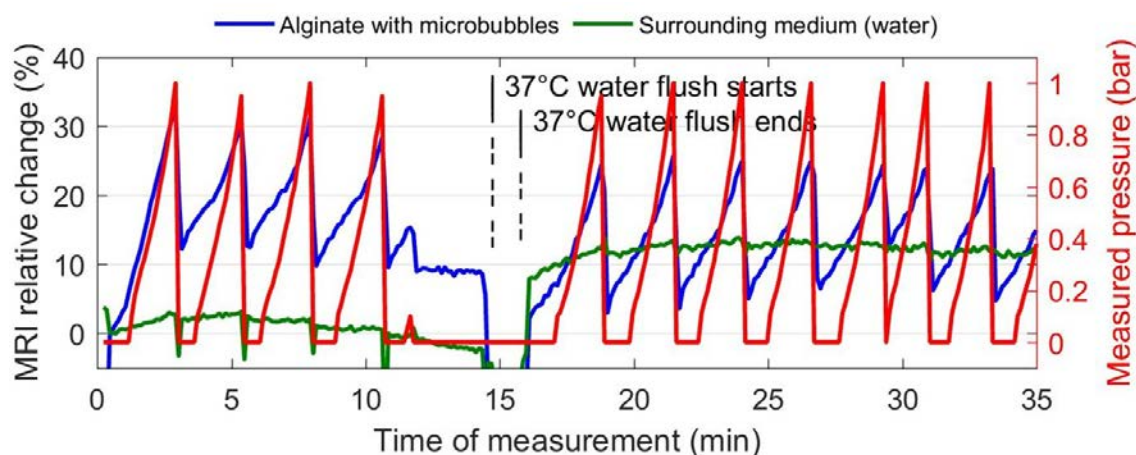


Figure 5.6 – Graph showing the MR sensitivity of the alginate spheres with microbubbles to pressure changes in distilled water at room (18°C) and body temperature, 37 °C. The sensitivity of the contrast agent in a warm surrounding water remains the same as in room temperature. The time of measurement up to 14.5 min corresponds to the relative signal change from alginate spheres in water at 18°C and from 15 min onwards at 37°C. The MRI relative change is calculated by comparing the signal intensity with each of the start of the pressure cycling. This means the relative signal change at temperature 18 °C is computed relative to the mean signal intensity at zero pressure (acquired at the beginning of experiment), and the relative signal change in water at 37 °C is relative to the mean signal intensity at zero pressure in water at 37 °C (acquired at the time 15.6 & 15.7 min). The start and the end of the flushing of the water in water at 37 °C into the system are indicated by vertical dotted lines. The red curve shows the measured pressure.

In the first pressure cycle at room temperature, the sensitivity exhibited is approximately 35 % signal change per bar, and then gradually decreased to 28 % change per bar after four pressure cycles. When warm water at 37 °C was introduced, the sensitivity further dropped to 26 % signal change per bar and then remains the same for at least another 15 min of observation (Figure 5.6). In accordance to the ideal gas law, the increase of the temperature will increase the volume of the microbubbles, causing the increase on its size which consequently changes the pressure sensitivity. The correlation between the bubble size and the pressure sensitivity has been estimated by Dharmakumar et al. through numerical simulations, showing the sensitivity increased with the expanse of the bubble, until it reached the size limit (2 μm radius), also known as critical bubble radius, which the sensitivity is then decreased beyond this point

(Dharmakumar, Plewes et al. 2002). This theoretical study has been further validated by Bencsik et al. which showed the maximum sensitivity to pressure changes can be achieved, indeed, by having the microbubbles at an optimum size (Bencsik, Al-Rwaili et al. 2013), although there is no experimental study available, to date, to offer sufficient data in order to conclude upon the applicability of these theoretical works.

Furthermore, this result is significant evidence that the phospholipid microbubbles are robust enough in keeping the contrast agent stable and functional at body temperature. It is known that each type of phospholipid has a unique transition temperature, a temperature that induces a change in phase of the phospholipid. For example, DPPC, which is the main component of our microbubble shell has a transition temperature at about 41 °C (Avanti Polar Lipids 2017), which means only microbubbles experiencing higher temperatures than this will break as the phospholipids disperse (Zuo, Chen et al. 2016). This temperature is proportional to the length of the hydrophobic chain of the lipids, and it has been demonstrated that the increase in the length of this chain contributes to the increase in the stability of the microbubbles (Borden, Longo 2002).

Additionally, there is a slight increase, approximately 10 %, in the signal intensity of the water solvent after the flushing, which further demonstrates the temperature increase within the sample. The temperature dependency of the transverse relaxation time of water has been previously observed, which showed an increase in the relaxation time with increasing temperature (Vesanen, Zevenhoven et al. 2013).

5.3 *In-Vitro* Studies at 3 Tesla using Whole Body Scanner

The MRI experiments in this section were carried out on the 3T whole body scanner Philips Achieva in the Sir Peter Mansfield Imaging Centre at the University of Nottingham. Several *in-vitro* experiments were performed simulating the stomach conditions and aiming to optimise the MRI sequences as a step towards the *in-vivo* experiments. Besides, the experiments discussed here can also be used to further validate the results that have been achieved in our previous experiments using a 2.35T small animal scanner.

5.3.1 Assessing the Sensitivity of Contrast Agent in Water Suspension at 37 °C

In this experiment, the MR sensitivity to pressure of the alginate spheres with microbubbles in water suspension was investigated by varying the effective echo time TE^{eff} , and comparing them with the signal coming from the alginate spheres without microbubbles using the RARE sequence. Afterwards, the sensitivity coming from the centre and the periphery of the spheres were also analysed and compared.

5.3.1.1 Sample Preparations

Two preparations of alginate spheres, with and without microbubbles, were placed in a water suspension, in a one-compartment sample holder with 100 ml capacity, at room temperature (Figure 5.7). It was easy to keep these two preparations separate in the container because, in water, alginate spheres with microbubbles float while the others sink. An hour before the experiment, the sample was placed in a warm water bath at 37 °C, identical to the body temperature. Then, it was immediately wrapped up in foam before it was placed in the head coil of the scanner, vertically, with the floating alginate spheres residing on the top of the cylindrical sample holder.

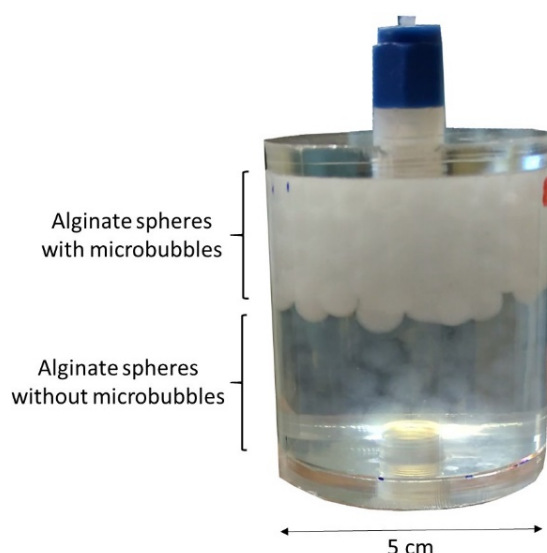


Figure 5.7 – Homemade sample holder containing alginate spheres with and without microbubbles. The natural buoyancy causes the spheres with microbubbles to float whilst the others sink; keeping the two preparations fully separated in the container.

5.3.1.2 Experimental Set-up

The sample was connected to a pressure gauge and a pump. Immediately after the pump was switched on, MR images were acquired using the RARE sequence in the transverse plane with 3 slices at 5 mm thickness, acquired every 7 seconds. The pressure was cycled between 0 and 1 bar, for approximately 5 minutes, with a complete cycle took about 3 minutes. This experiment was repeated several times with different effective echo times, TE^{eff} (400 ms, 500 ms and 600 ms), to explore the effect on the sensitivity.

5.3.1.3 Results

By using the RARE sequence, the MR sensitivity to pressure changes can be maximised by varying the effective echo time TE^{eff} . Image processing was undertaken in Matlab® to select specific pixels and analyse the MR signal coming from a single sphere to demonstrate the optimum TE^{eff} value that can yield the maximum sensitivity to pressure changes (Figure 5.8). The signal changes were found to be most sensitive at $TE^{eff} = 500$ ms, approximately 23 % changes per bar, compared to $TE^{eff} = 400$ ms and $TE^{eff} = 600$ ms (Figure 5.9). In previous theoretical studies (Dharmakumar, Plewes et al. 2002, Bencsik, Al-Rwaili et al. 2013), it was found that the sensitivity increased with an increase in the field strength. The result obtained from this experiment is surprisingly lower than the sensitivity from the 2.35T scanner, where it exhibited up to 40 % signal change per bar. However, the stability of the sensitivity on this scanner is better than what we have seen on the 2.35T Biospec and there is hardly any signal drift seen throughout the measurements with excellent SNR.

At the same time, we analysed the signal changes coming from a much larger rectangle that encompasses both the alginate spheres and the surrounding water. The sensitivities exhibited from this method are 15 %, 14% and 12 % signal changes per bar, respective to the TE^{eff} values 400 ms, 500 ms and 600 ms (Figure 5.10). The sensitivity yielded from this method is approximately 60 % lower compared to the single sphere analysis.

For the next part of the experiment, we analysed the MR signal from a single pixel intensity coming from the centre of a sphere and another single pixel intensity coming from the periphery of a sphere (Figure 5.8) and the result is shown in Figure 5.11. The signal intensity in the centre of the sphere is constantly higher indicating that the T_2^*

value is higher in this area as compared to the periphery of the spheres (Figure 5.11 a)), as seen in the previous experiments. We anticipated that the microbubbles density is higher in the periphery. This is consistent with the common feature exhibited by these spheres that we observed where the periphery exhibits higher sensitivity to pressure changes, which is up to 55 % signal changes per bar whilst the centre exhibits less than 20 % changes per bar (Figure 5.11 b)). Nevertheless, both these two areas contribute to the overall sensitivity of the alginate spheres with microbubbles to the pressure changes in the experiment where large volumes of the meal will be used to monitor pressure changes.

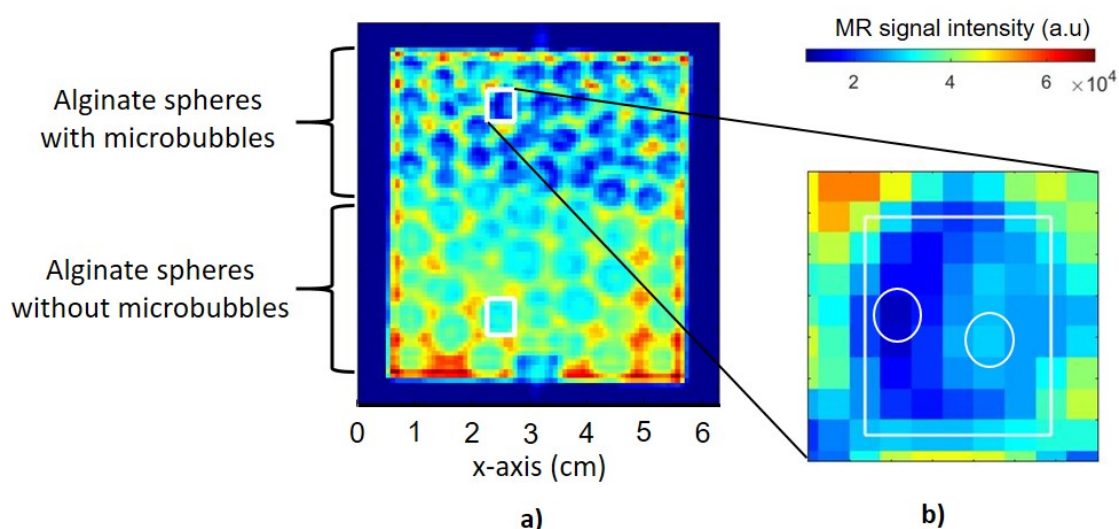


Figure 5.8 – a) One of the RARE images acquired at $TE^{eff} = 500$ ms using the 3T Philips Achieva whole body scanner, when the pressure applied at 0 bar. The MR signal intensity differences can be seen at the top and bottom of the specimen, showing alginate spheres with and without microbubbles well separated in the container. The two white squares represent the pixels selections for the signal intensity analysis coming from a single sphere for both preparations. b) Zoomed image of the selected sphere with microbubbles and the two circles represent the pixels selection for the signal intensity analysis coming from the centre (high intensity) and the periphery (low intensity) of the sphere.

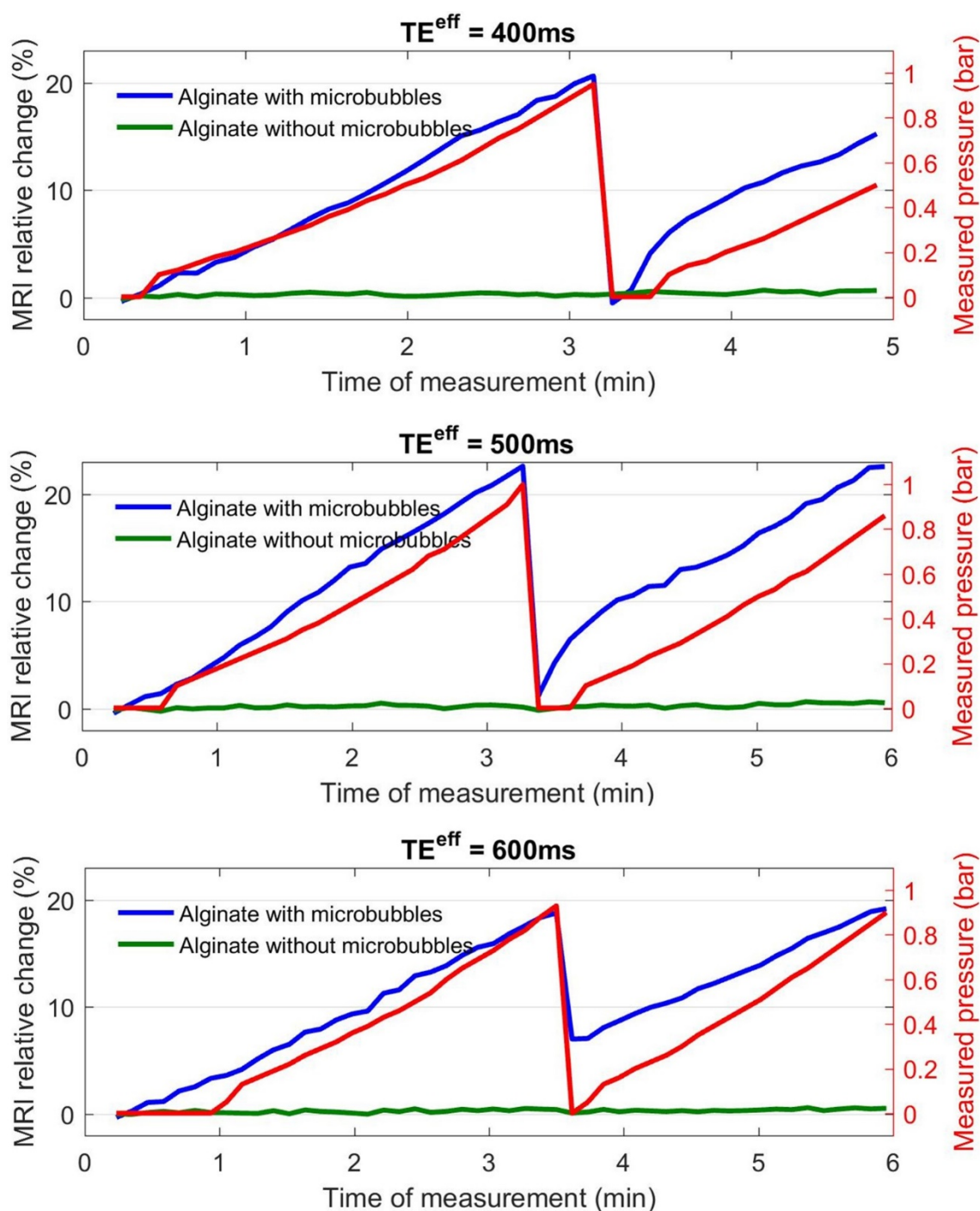


Figure 5.9 – Graphs showing the sensitivity of the alginate spheres with and without microbubbles for different TE^{eff} values of the RARE sequence. The signal intensity change is coming from the pixels representing a single sphere for each preparation as shown in Figure 5.8. The sensitivity of the alginate spheres with microbubble is highest at $TE^{eff} = 500$ ms with 23 % signal changes per bar, whilst the signal intensity coming from the alginate sphere without microbubbles remains zero. The MRI relative change is calculated by comparing the signal intensity with the start of the image acquisition and pressure cycling (measured pressure 0 bar). The red curves show the measured pressure. At very low pressures, the MR sensitivity is seen better than that of the pressure gauge.

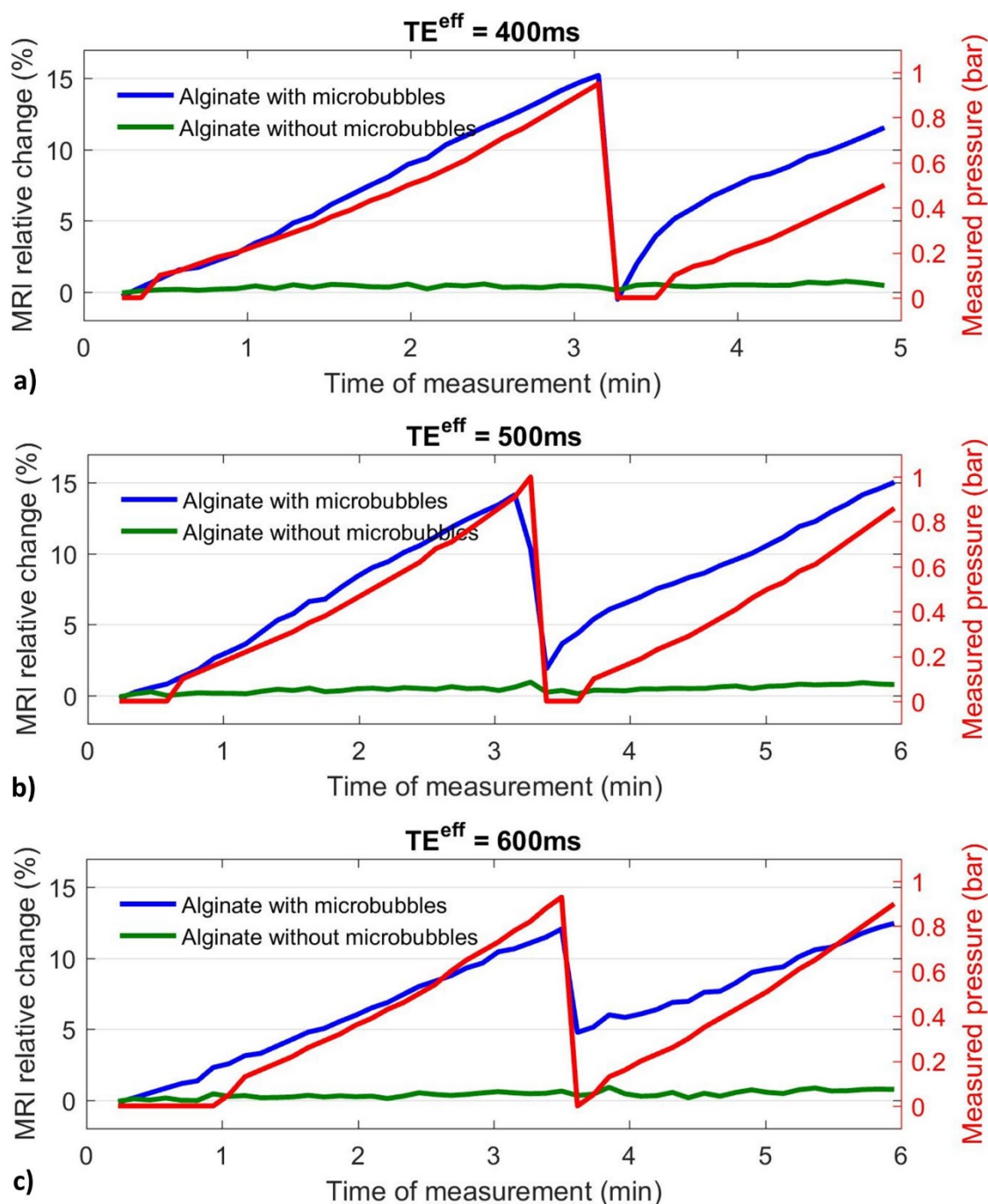


Figure 5.10 – Graphs showing the sensitivity of the alginate spheres with and without microbubbles for different TE^{eff} values of the RARE sequence, by selecting a large rectangle encompasses the pixels representing the alginate spheres and the surrounding water. The sensitivity of the alginate spheres with microbubbles to the pressure change is approximately 60 % lower as compared to the single sphere analysis in Figure 5.9. The signal intensity coming from the alginate sphere without microbubbles remains zero.

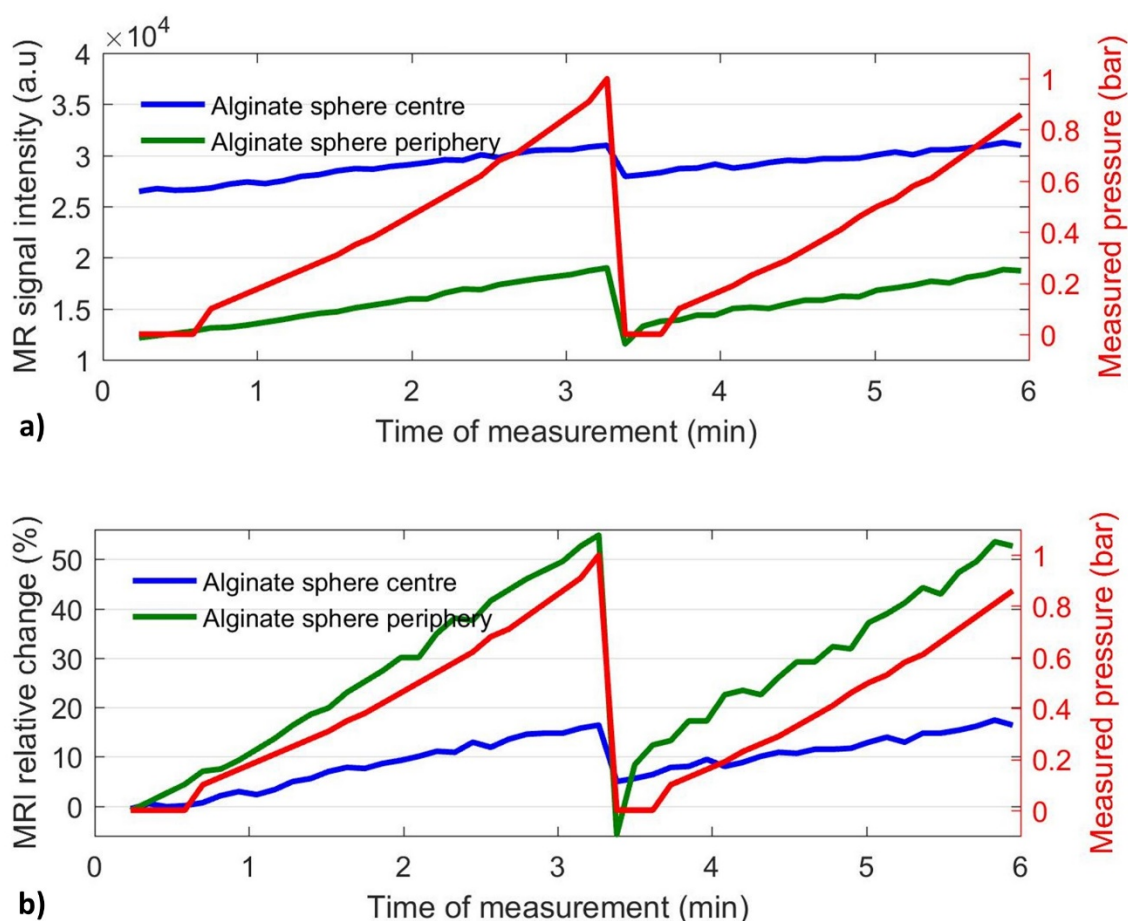


Figure 5.11 – Comparing the sensitivity at the centre and at the periphery of one alginate sphere with microbubbles. a) The absolute signal changes revealing the signal intensity from the centre of the sphere constantly higher than the periphery. b) Relative signal change showing the periphery is more sensitive to pressure than the centre of the sphere. The red curves show the measured pressure. The MRI relative change is calculated by comparing the signal intensity with the start of the image acquisition and the pressure cycling (pressure 0 bar).

5.3.2 Assessing the Sensitivity of the Contrast Agent in Simulated Gastric Solution

5.3.2.1 Sample Preparations

The sample preparation was similar to the previous experiment in section 5.3.1.1, with the contrast agent only consisting of the alginate spheres with microbubbles. This time, after the sample was wrapped up in a foam, it was then placed in a glass beaker to prevent acid spillage on the MR scanner in case of any leakage from the sample, before it was placed in the head coil of the MR scanner.

5.3.2.2 Experimental Set-up

The sample holder had an inlet and an outlet allowing the liquid medium being flushed when required and enabling the sample to be connected to a pressure gauge and a pump (Figure 5.12). Immediately after the pump was switched on, MR images were acquired using the RARE sequence in a transverse plane with 3 slices at 5 mm thickness, every 7 seconds. The pressure was continuously cycled between 0 and 1 bar while running the MR scanning, with a cycle applied every 4 minutes.

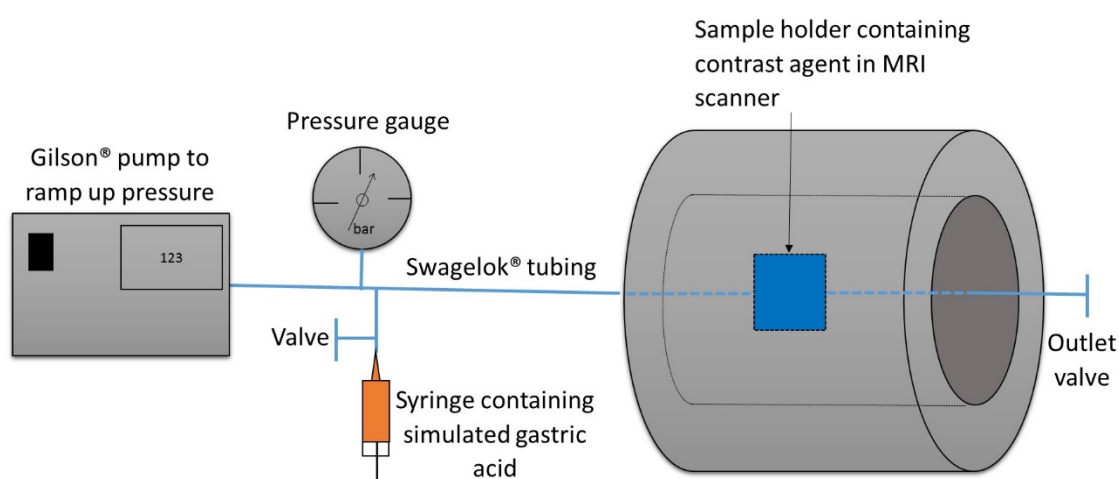


Figure 5.12 – Illustration showing the equipment set-up for the experiment measuring the sensitivity of the contrast agent in a simulated gastric solution. A single-compartment sample holder containing the alginate spheres with microbubbles was connected to a pump and pressure gauge by Swagelok nylon tubing. It also connected to a syringe and an outlet valve accommodating the flushing of the simulated gastric acid solution into the system.

5.3.2.3 Results

Firstly, we analysed the MR signal coming from a large rectangular section of the sample in water solvent, highlighted with a white rectangle on MR images in Figure 5.13. The signal changes exhibited up to 28 % changes per bar when accounting for all pixels within the rectangle. However, by dismissing the pixels that represent the water solvent, the sensitivity goes up as high as 35 %, which can be understood as resulting from the sensitivity solely coming from the alginate spheres with microbubbles (Figure 5.14). About the same sensitivity has been demonstrated in the previous experiments presented in this chapter using the 2.35T Biospec MR scanner.

In a subsequent MR acquisition, when the acid was introduced into the system replacing the water surrounding medium, it is seen that the contrast agent is still functional in the new medium, but the sensitivity is decreased to 17 %, a phenomenon we have also seen in our previous experiments using the Biospec scanner in section 5.2.2, where it was also seen to drop to 17 % signal change per bar.

The spheres are also seen to be shrinking in the acid solvent because alginate creates a tighter gel network in acidic condition. For this, we have estimated the volume shrinkage to be approximately 8 % within the 20 minutes of this experiment, using a simple pixel intensity threshold to discriminate the volume of solvent from that covered by the gel. This effect can also be seen in the RARE images where the space occupied by the spheres in acid solution decreased over time (Figure 5.13).

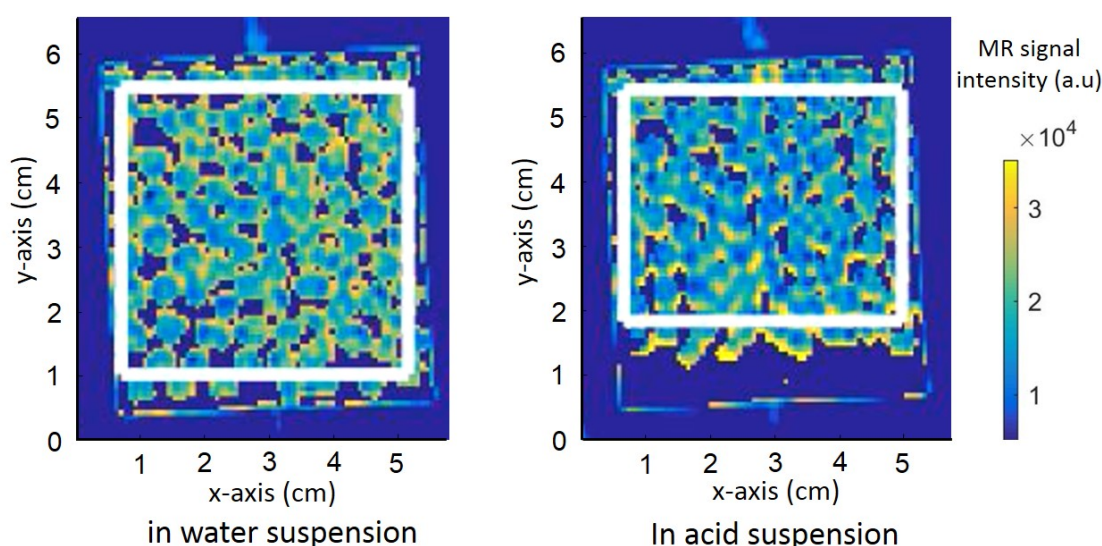


Figure 5.13 – RARE images of alginate spheres with microbubbles suspended in two different solvents, water (left) and simulated gastric acid (right). In both these images, the solvent (water and acid) is dismissed for signal analysis so that the sensitivity is solely coming from the spheres. The space occupied by the spheres in acid suspension is decreased, demonstrating the shrinking of the spheres. The white squares represent the pixels selections for the signal intensity analysis.

In this particular experiment, after an acidic solution was introduced into the system, some instabilities can be seen on the pressure cycle (Figure 5.14b) due to the insufficient time duration of releasing the pressure at the valve (tap), which was approximately 4 m

away from the specimen. The first release of the pressure produced the MR signal intensity drop much lower than the second release, indicating that the sample was still under pressure although the pressure gauge reading was zero. This is evidenced by the second cycle where an instantaneous and unusual increase of the MR signal intensity was exhibited, compared to the other two following cycles, upon the introduction of the pressure. During the experiment, the second release was done by opening the tap for a time duration at least 1 minute longer than the first release, giving enough time for the pressure within the sample to drop to zero. Additionally, a similar effect is also observed in the fourth and fifth cycle (time of measurement approximately at 18 minutes), however, in this case, the pressure gauge reading was immediately increased to 0.6 bar after the pressure was introduced, indicating that this part was caused by a blockage due to a movement of some of the spheres into the tubing when the pressure was released.

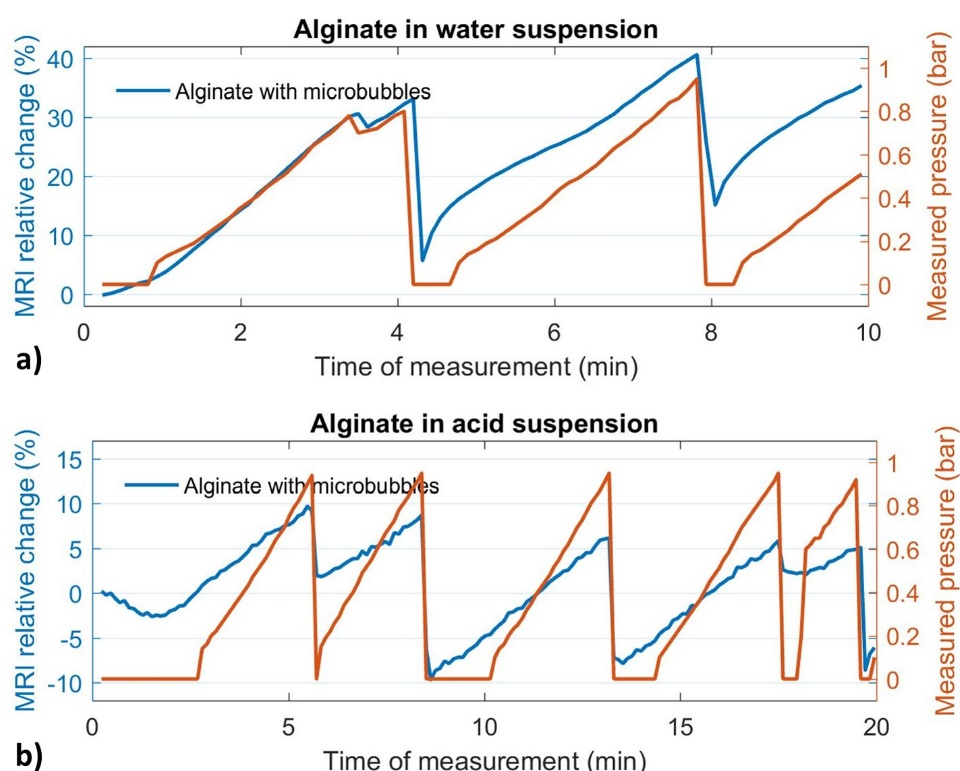


Figure 5.14 – Graphs showing two subsequent experiments measuring the sensitivity of alginate spheres with microbubbles in a) water and b) acid simulating gastric solution. The MRI relative change is calculated by comparing the signal intensity with the start of the image acquisition and the pressure cycling (pressure 0 bar). The red curve shows the measured pressure.

5.3.3 MRI sensitivity in locust bean gum and acid solution simulating gastric conditions

Due to the buoyant characteristic of the alginate spheres with microbubbles, it is a challenge to distribute them evenly once they reside in the human stomach because they naturally float when placed in a water suspension. Hence, a locust bean gum has been used as a suspending medium to prevent them from floating too quickly. In this experiment, the sensitivity of the alginate spheres with microbubbles suspended in a 2 % w/v locust bean gum is investigated.

5.3.3.1 Sample Preparations

The alginate spheres with microbubbles were prepared and placed in a water suspension. Separately, a locust bean gum solution (2 % w/v) was prepared following the steps in section 2.4.2 and placed in a beaker. Then, 250 ml of alginate spheres with microbubbles were mixed gently with 250 ml of locust bean gum solution, in a plastic bottle, 500 ml capacity, at room temperature, simulating the actual volume ratio to be ingested by a human volunteer. In order to eliminate as much as possible of trapped air bubbles within the mixture, a gentle stirring was used when mixing the alginate spheres into the locust bean gum to encourage large bubbles to rise to the surface. Once they rose to the surface of the preparation, they were then removed by scooping out with a spatula. There were only very few large air-trapped bubbles left after insertion of the meal into the bottle. An hour before the experiment, the sample was placed in a warm water bath at 37 °C.

5.3.3.2 Experimental Set-up

The sample was connected to Swagelok nylon tubing and immediately wrapped up in foam before it was placed in the body coil, which will be used for the study on the human volunteer, of the MR scanner. An inlet was created enabling the bottle to be connected to a pump and a pressure gauge, allowing the pressure being changed during MRI scanning. Immediately after the pump was switched on, MR images were acquired using the RARE sequence at $TE^{eff} = 500$ ms, with 3 slices at 5 mm thickness, every 7 seconds. The pressure was continuously cycled between 0 and 1 bar until the MRI scanner sequence was finished in 10 min, with a cycle applied every 5 minutes. Due to the large

volume of the specimen and the flexibility of the bottle, there was far more water volume (about 140 ml) required to be pumped into the system to reach the usual 1 bar pressure.

After the first set of scanning completed, the bottle was taken out from the scanner and then 50 ml of the sample was scooped out of the bottle and replaced with acid simulating gastric solution at 37 °C. Subsequently, the bottle was immediately reconnected to the initial set-up and another set of RARE images were acquired with the pressure cycling for 20 min.

At the end of the first pressure cycle, we found that, even though the pressure gauge dropped rapidly to zero, the specimen was still under pressure. This was evidenced by the fact that switching the pump back on resulted in an immediate rise of the pressure read by the gauge. We concluded that, when releasing the pressure, some locust bean gum was brought back into the Swagelok tubing, thereby blocking fluid flow and preventing the pressure from being released from the meal.

5.3.3.3 Results

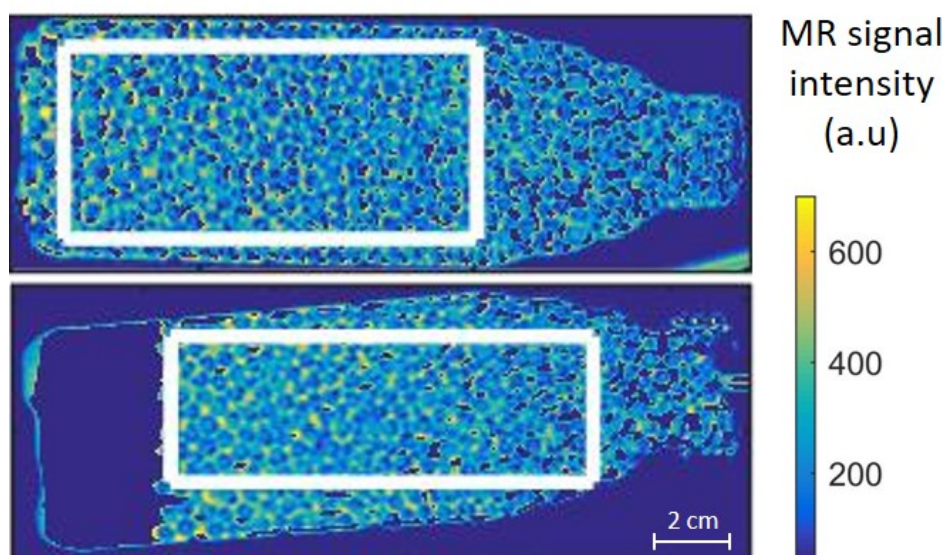


Figure 5.15 – RARE images of alginate spheres with microbubbles in locust bean gum, without (top) and with (bottom) the acid simulating gastric solution. The white rectangles representing the ROI selections for the signal intensity analysis.

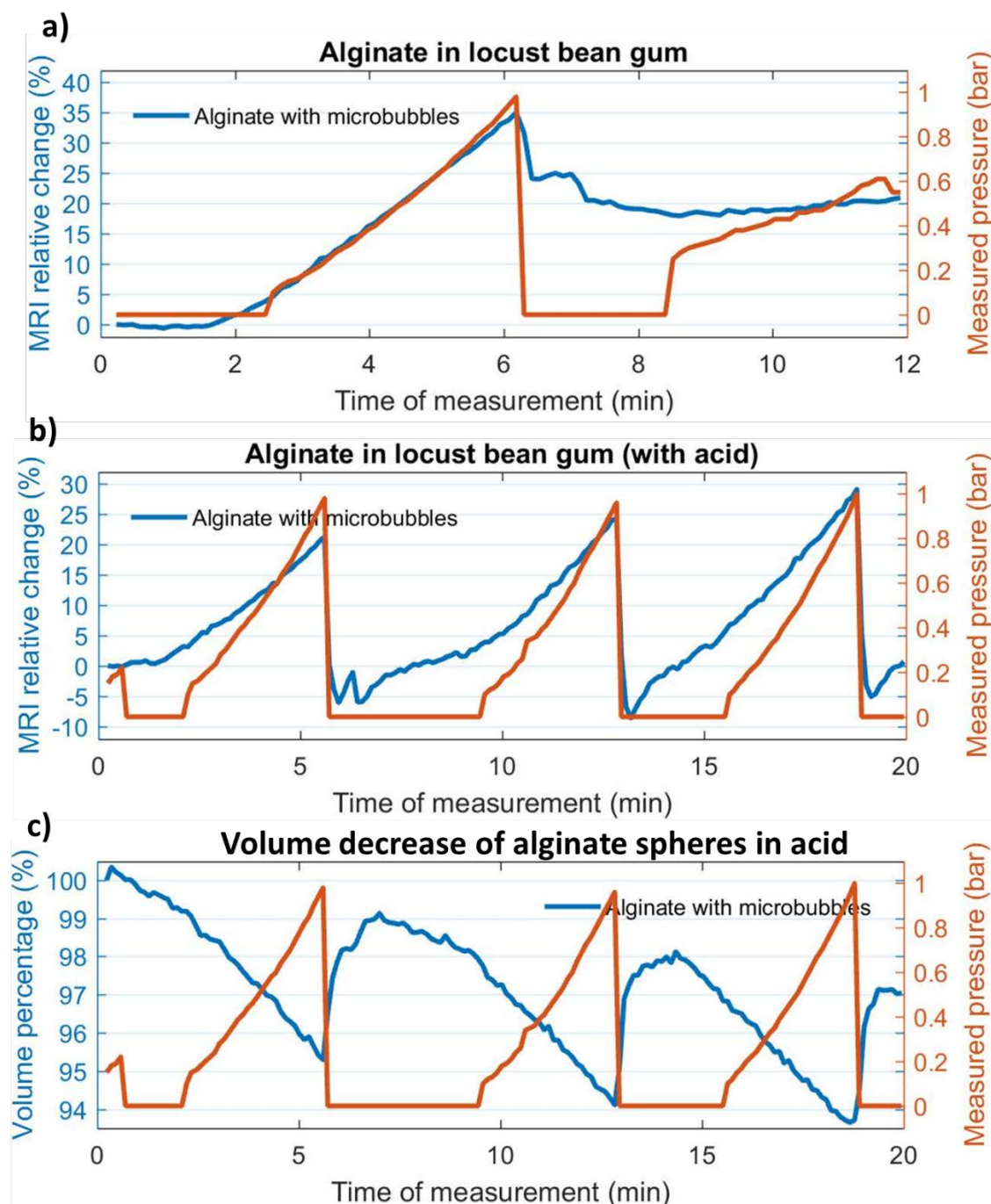


Figure 5.16 – a) The sensitivity of the alginate spheres with microbubbles suspended in the locust bean gum, without a solution simulating gastric acid. The MRI relative change is calculated by comparing the signal intensity with the start of the image acquisition and the pressure cycling (pressure 0 bar). b) The sensitivity of the alginate spheres with microbubbles suspended in the locust bean gum, with a solution simulating gastric acid. c) The volume of the spheres decreases 3 %, due to the effect of acid on the sample, within 20 min observation. This effect can be identified by observing the decrease of the peak on the plot every time the pressure is being released from 1 to 0 bar.

The locust bean gum with a 2 % w/v concentration successfully kept the spheres from physically rising within the sample holder. This is a major improvement from our initial locust bean gum preparation with a 1 % w/v concentration, which was not viscous enough to immobilise the alginate spheres with microbubbles, which were seen to rise within a minute.

The MR signal was analysed by selecting a large rectangular section of the sample, highlighted with white rectangles on the MR images (Figure 5.15). The signal changes exhibited up to 35 % changes per bar, prior to adding the acid (Figure 5.16 a)). Then, the MR sensitivity of the contrast agent in a locust bean gum with the simulated gastric solution drops to 22 % (Figure 5.16 b)). The decrease of the signal intensity is seen, due to the effect of the acid, by observing the MR signal taking place at zero pressure. However, the sensitivity to the pressure change is seen to increase over time, with the maximum MR signal reached the highest pressure, 1 bar, exhibits a remarkable steady state, probably due to the signal increase coming from bubble damage somewhat compensating the signal decreasing coming from the acid.

Over time, the spheres are seen to be shrinking after the acid solvent is added to the specimen. Again, we estimated the volume change by using Matlab® image processing to discriminate the volume of locust bean gum from that covered by the spheres, by setting a pixel intensity threshold. The results show that the acid-driven volume shrinkage is approximately 3 % within the 20 min of this experiment (Figure 5.16 c)), which is much less compared to the previous experiment in section 5.2.2 where the alginate spheres were not suspended in a locust bean gum, resulting in a 8 % volume shrink. The thick gel of locust bean gum somewhat works as a protection layer, which slows down the effect of the acid on the alginate spheres. Overall, the locust bean gum with 2 % w/v concentration has been demonstrated to be useful in immobilising the spheres, whilst maintaining the robust signal sensitivity of this contrast agent.

5.4 Conclusions

A pressure sensitive MR contrast agent has been created and tested. It comprised of gas-filled microbubbles suspended in soft-solid alginate spheres, which has been specifically tailored to investigate the pressure changes in the human stomach. Dynamic

measurements have been used to test its functionality in several conditions including in a solvent mimicking the human gastric solution at body temperature. This novel contrast agent yielded a high level of sensitivity, up to 40 % MR signal change per bar.

At the same time, a suitable suspension medium for the spheres, which made of a locust bean gum, has found to be useful for immobilisation while keeping its robust sensitivity. The primary issue was the rapid motion of the alginate spheres upwards due to their buoyancy in an aqueous suspending media. This has been overcome in this work by using a 2 % w/v concentration of locust bean gum. In addition, this gel is seen to slow down the acidification of the alginate spheres when it is dipped in the simulated gastric solution, which can be a great benefit when the contrast agent resides in the human stomach for *in-vivo* investigation. As the acid solution is seen to degrade the pressure sensitivity of these spheres, this gel can help in keeping the spheres functional for a longer period in the stomach. As a conclusion, with the combination of MR imaging, this contrast agent can be used as a novel technique in demonstrating pressure changes in the human stomach.

References

1. AVANTI POLAR LIPIDS, 2017-last update, 16:0 PC (DPPC) [Homepage of Avanti Polar Lipid, Inc.], [Online]. Available: <https://avantilipids.com/product/850355/> [04/01, 2017].
2. BENCSIK, M., AL-RWAILI, A., MORRIS, R., FAIRHURST, D.J., MUNDELL, V., CAVE, G., McKENDRY, J. and EVANS, S., 2013. Quantitation of MRI sensitivity to quasi-monodisperse microbubble contrast agents for spatially resolved manometry. *Magnetic Resonance in Medicine*, **70**(5), pp. 1409-1418.
3. BORDEN, M.A. and LONGO, M.L., 2002. Dissolution behavior of lipid monolayer-coated, air-filled microbubbles: Effect of lipid hydrophobic chain length. *Langmuir*, **18**(24), pp. 9225-9233.
4. BORTOLOTTI, ANNESE, COCCIA and BORTOLOTTI, M., 2000. Twenty-four hour ambulatory antroduodenal manometry in normal subjects (co-operative study). *Neurogastroenterology & Motility*, **12**(3), pp. 231-238.
5. DHARMAKUMAR, R., PLEWES, D.B. and WRIGHT, G.A., 2002. On the parameters affecting the sensitivity of MR measures of pressure with microbubbles. *Magnetic Resonance in Medicine*, **47**(2), pp. 264-273.
6. HOAD, C., RAYMENT, P., COX, E., WRIGHT, P., BUTLER, M., SPILLER, R. and GOWLAND, P., 2009. Investigation of alginate beads for gastro-intestinal functionality, Part 2: In vivo characterisation. *Food Hydrocolloids*, **23**(3), pp. 833-839.
7. MORRIS, R.H., BENCSIK, M., NESTLE, N., GALVOSAS, P., FAIRHURST, D., VANGALA, A., PERRIE, Y. and MCHALE, G., 2008. Robust spatially resolved pressure measurements using MRI with novel buoyant advection-free preparations of stable microbubbles in polysaccharide gels. *Journal of Magnetic Resonance*, **193**(2), pp. 159-167.
8. RAYMENT, P., WRIGHT, P., HOAD, C., CIAMPI, E., HAYDOCK, D., GOWLAND, P. and BUTLER, M.F., 2009. Investigation of alginate beads for gastro-intestinal functionality, Part 1: In vitro characterisation. *Food Hydrocolloids*, **23**(3), pp. 816-822.

9. VESANEN, P.T., ZEVENHOVEN, K.C.J., NIEMINEN, J.O., DABEK, J., PARKKONEN, L.T. and ILMONIEMI, R.J., 2013. *Temperature dependence of relaxation times and temperature mapping in ultra-low-field MRI*. 235, pp. 50-57.
10. ZUO, Y.Y., CHEN, R., WANG, X., YANG, J., POLICOVA, Z. and NEUMANN, A.W., 2016. Phase Transitions in Dipalmitoylphosphatidylcholine Monolayers. *Langmuir*, **32**(33), pp. 8501-8506.

CHAPTER 6

DEMONSTRATING SPATIAL PRESSURE GRADIENT USING MICROBUBBLE-BASED MRI CONTRAST AGENTS

6 DEMONSTRATING SPATIAL PRESSURE GRADIENT USING MICROBUBBLE-BASED MRI CONTRAST AGENTS

6.1 Practical Motivation

A non-invasive technique for direct MR measurement of the dynamic pressure in the stomach is highly desirable as it can be beneficial in helping the clinicians to further understand the condition of diseases such as functional dyspepsia, which is normally associated with chronic disorder of sensation and movement (also known as peristalsis) in the upper digestive tract, including stomach. In the past, gas phase MRI has been demonstrated as a suitable method to assess a spatial gradient for fluid pressure measurements (Bencsik, Ramanathan 2001), but this method is not suitable for medical applications. In addition, in the previous chapters, we have successfully demonstrated that by using MRI as the imaging tool, gas-filled microbubbles suspended in alginate spheres can be used as a method to monitor pressure changes. Although, various studies (Alexander, McCreery et al. 1996, Dharmakumar, Plewes et al. 2005, Bencsik, Al-Rwaili et al. 2013) have previously investigated the potential of microbubbles as a pressure probe in MRI, a spatial pressure gradient has never been demonstrated within a medical application. In a publication in 2007, a pressure gradient effect has been demonstrated with microbubbles, however, the bubbles preparation was not monodisperse and they were suspended in a medium, and were seen to rise within minutes (Morris, Bencsik et al. 2007). Besides, the study was conducted in a porous medium consisting of a structure similar to sandstones, which was not in a medical application set-up.

In this chapter, we use gas-filled microbubbles suspended in two different media, a viscous liquid gellan gel and the soft-solid alginate gel spheres, to map a pressure gradient with the aid of MRI for *in-vitro* studies, in order to demonstrate their capability to be used as a method to measure spatially varying pressure changes in the human stomach. The MR image acquisition is performed using the RARE sequence to be able to achieve a rapid measurement (less than 1 second) of the MR signal intensity of the contrast agent whilst the externally applied pressure changes.

6.2 Microbubbles in Gellan Gel

6.2.1 Introduction

It has been previously demonstrated that gellan gel can be used as a suspending medium keeping the gas-filled microbubbles immobilised for more than 40 hours (Morris, Bencsik et al. 2008), and exhibiting a sensitivity up to 23 % signal change per bar (Bencsik, Al-Rwaili et al. 2013). It suggested that this contrast agent can be used as a non-invasive technique for a direct MR measurement of a fluid pressure. In this study, we use this similar contrast agent preparation (microbubbles suspended in gellan gel) to demonstrate a spatial pressure gradient effect.

6.2.2 Sample holder design

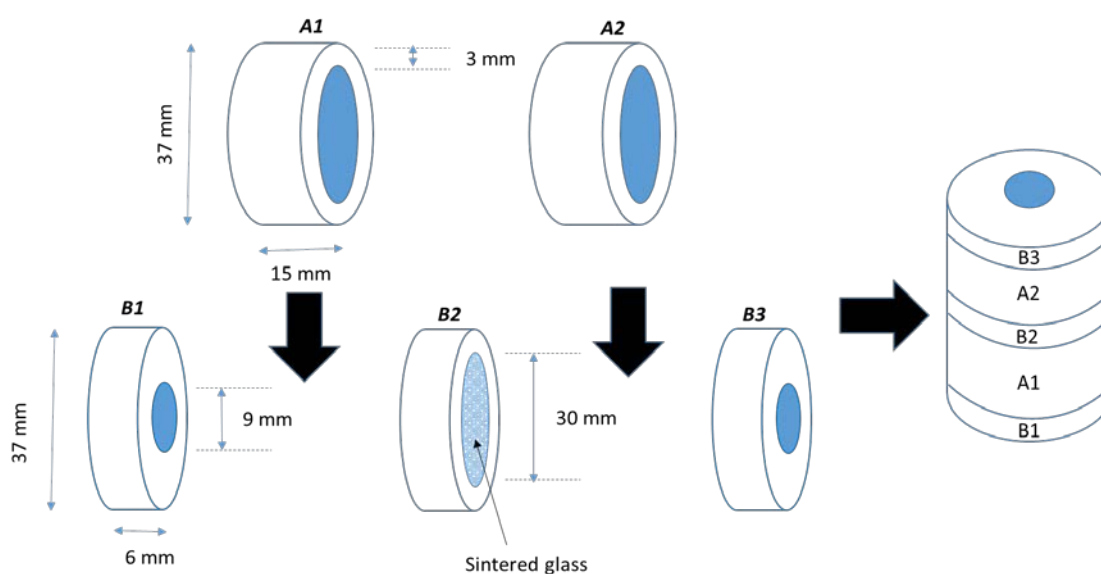


Figure 6.1 – Diagram showing the design of the sample holder which comprised of two compartments separated by a sintered glass disc with pores (5-15 μm). The finished product is shown in Figure 6.2, loaded with the microbubbles contrast agent.

A cell which is comprised of two compartments was manufactured from transparent acrylic tubing. The design of this homemade sample holder is shown in Figure 6.1. The main parts of the cell, labelled as A1 and A2 in the diagram, were built from two round tubes, with 3 mm wall thickness, 15 mm length and 37 mm outer diameter. Next, a piece of acrylic was laser cut to form three disks, each with a diameter 37 mm and thickness 6 mm, labelled as B1, B2 and B3. Then, circular apertures were formed at the centre of

each of these disks with diameters 9 mm, 30 mm and 9 mm on B1, B2 and B3 respectively. Afterwards, a 3-mm thick sintered glass disc (AM Glassware, Aberdeen, Scotland) with 30 mm diameter and 5-15 μm pores was attached to the circular aperture on disk B2. Finally, all parts were glued together as shown in Figure 6.1, by using an acrylic adhesive (RS components, Northants, UK). Before it was further used for the experiment, the integrity of the sample holder was tested by filling it with water and pressurising it up to 4 bar.

6.2.3 Sample preparations

In this particular experiment, the microbubbles were suspended in gellan gel (2 % w/v), which works as a bubble immobilisation medium. The mixture of the microbubbles and gellan gel was prepared following the protocol fully described in Chapter 2 (section 2.2). Then, this mixture was loaded into the two-compartment sample holder (Figure 6.2).



Figure 6.2 – The two-compartment sample holder, separated by a sintered glass with micropores, filled with microbubbles suspended in gellan gel, ready for MRI pressure gradient experiment.

6.2.4 Pre-MRI experiment set-up

Due to the use of an MRI-incompatible pressure gauge, it was difficult to measure the actual pressure in both compartments during the MRI measurement. In order to demonstrate the time duration of the pressure transient from one compartment to another, the timings were measured prior to the MRI scanning. The equipment was set-up as shown in Figure 6.3, outside the MRI scanner. The assessment shows that there is a 60 seconds delay in the time course of the pressure measured in each compartment, meaning the pressure is only seen to change in the second compartment one minute after the pressure is ramped up in the first one. Following the pump switching off, approximately eight minutes are required for both compartment pressures to

equilibrate (Figure 6.4). This demonstrates the existence of a pressure gradient in the sample holder.

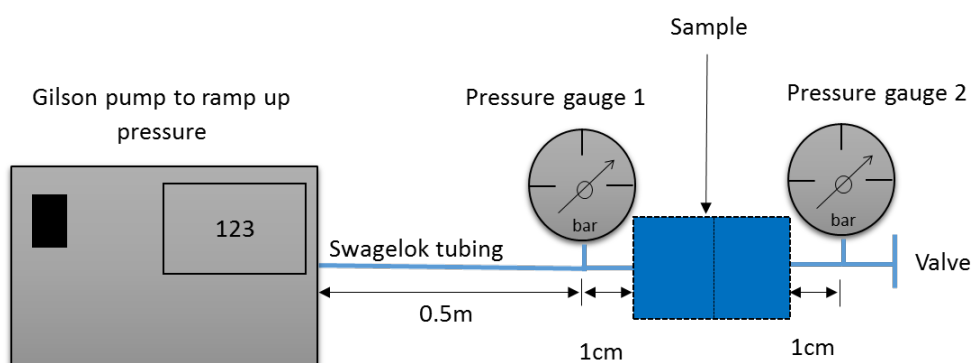


Figure 6.3 – Illustration showing the equipment set up to assess a pressure gradient between two compartments of the sample holder. The tubing was filled with gellan gel and the pump supplied a flow in order to ramp up the pressure within the system.

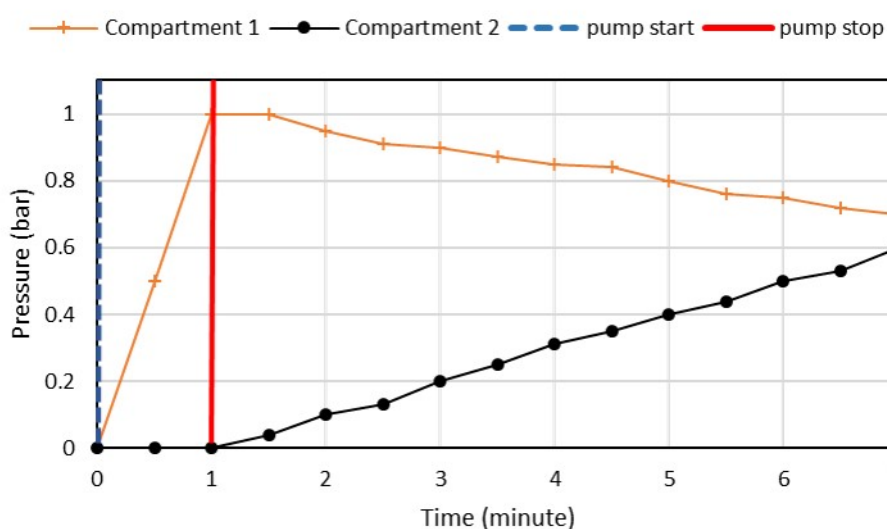


Figure 6.4 – The time course of the measured pressure demonstrating a pressure gradient between the two compartments of the sample holder. It demonstrates that there is a one-minute delay between the two compartments and it takes approximately eight minutes for the pressure to equilibrate within both compartments.

6.2.5 Experiment set-up

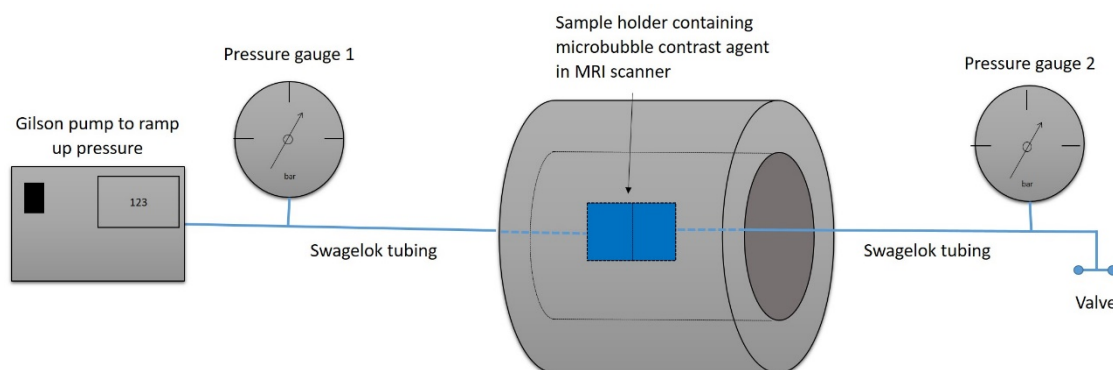


Figure 6.5 – Illustration showing the equipment set-up for the pressure gradient experiment with MRI. The two-compartment sample holder containing microbubbles suspended in gellan gel was connected to a pump by Swagelok® tubing. The pressure gauges were placed at both sides of the compartments to measure the pressure change, however, it was not possible to measure the actual pressure within both compartments because of the use of the MRI-incompatible pressure gauges which were placed outside the 5 Gauss line of the polarising field (approximately 4 m away from the sample).

The sample was connected to a pump and the full experiment setup is shown in Figure 6.5. Firstly, without applying any pressure yet, the effective transverse relaxation time, T_2^{eff} , of the microbubble contrast agent was measured by using the MSME sequence at $TE = 10$ ms and $TR = 3000$ ms using a Bruker Biospec 2.35T MR scanner. The MSME image of the sample showing the T_2^{eff} value is displayed in Figure 6.6, and the average T_2^{eff} value (170ms) from this measurement is used to optimise the next MRI sequence for the subsequent image acquisition.

Then, the pump was set to flow at 50 ml/min rate, to supply an increasing pressure to the system, while the outlet was closed. Immediately after the pump was switched on, MR images were acquired simultaneously using the RARE sequence ($TE=10\text{ms}$, RARE Factor = image size = 64, $TE_{\text{eff}} = 2T_2^{\text{eff}} = 340\text{ms}$).

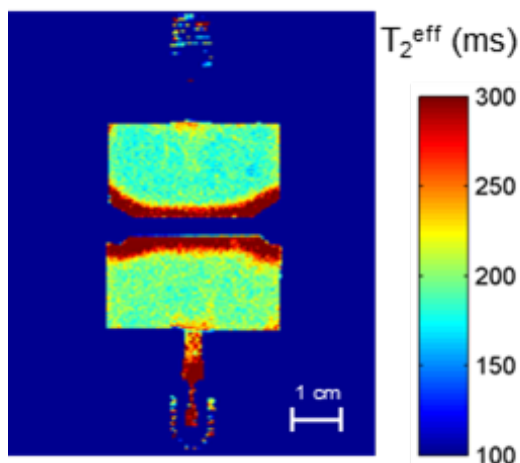


Figure 6.6 – T_2^{eff} image of both compartments filled with microbubbles suspended in gellan gel showing the T_2^{eff} value before any pressure is being applied to the system. The average T_2^{eff} value from this measurement is then used to optimise the RARE sequence in the next MR acquisition with the pressure.

6.2.6 Results

Figure 6.7 shows two RARE MRI images of both compartments taken at different times and demonstrates the spatial pressure gradient. At 6 seconds after switching on the pump, the signal intensity in both compartments was almost identical, compared to the signal taken at 290 seconds where the signal intensity in compartment 1 was greater by a factor of 1.5.

We analysed the signal intensity and produced plots of its changes over the course of time within these two compartments (Figure 6.8). For the signal analysis, the field of views (FOV) were selected using ImageJ processing program (NIH, Maryland, USA), in order to prevent an image artefact contributing into our analysis. The artefact was caused by the gel when it was driven into the sample to ramp up the pressure. On the image in Figure 6.7, we identify this as a ‘compression artefact’.

Figure 6.8 shows the change in MR signal intensity due to the variation of pressure across the two compartments. The signal intensity in compartment 1 started to increase 150 seconds after the pump was turned on. This was followed, 30 seconds later, by a signal increase in compartment 2. This 30-second delay is slightly faster compared to the time delay we obtained in the pre-experiment in section 6.2.4, where the pressure in compartment 2 is seen to increase one minute after the pump switched on in compartment 1. This discrepancy shows that, at very low pressures (below than 0.1 bar), the MR sensitivity is better than the sensitivity of the pressure gauges we used, in

sensing the pressure change. In the future, the use of a higher sensitivity pressure gauge should be taken into consideration.

Following that, the signal intensity in compartment 1 increased more rapidly which indicates an increasing spatial pressure gradient between both compartments. As the pump was stopped, the signal intensity in compartment 1 decreased whilst in compartment 2 it continued to rise, indicating that the pressure was still equilibrating. This is in agreement with the result acquired in the pre-experiment in section 6.2.4, however, a longer MRI measurement could be performed to observe the signal intensities in both compartments reaching the equilibrium as seen in the pre-experiment, where the pressure in both compartments was seen to equilibrate approximately 8 minutes after the pump was switched off.

Although, the sample was connected to the pressure gauges while acquiring the MR images, the actual pressure within both compartments was only indirectly measured due to the use of a non-MRI compatible pressure gauge, which was placed outside the 5 Gauss line of our polarising magnet. Hence, in the future, we propose to use a suitable pressure reading method in order to enable a direct measurement of the pressure transient between the compartments.

This particular work has been presented as a poster at the International Conference on Magnetic Resonance Microscopy 2015, Munich, Germany (Appendix A).

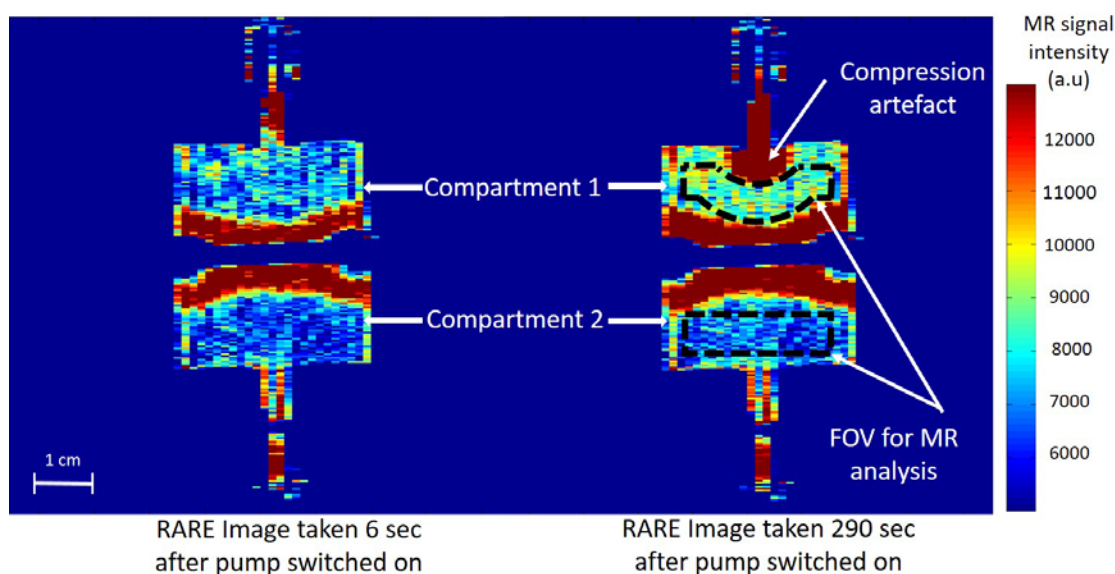


Figure 6.7 – RARE MR images showing both compartments at time 6 seconds and 290 seconds respectively, showing signal intensity changes and demonstrating a pressure gradient effect.

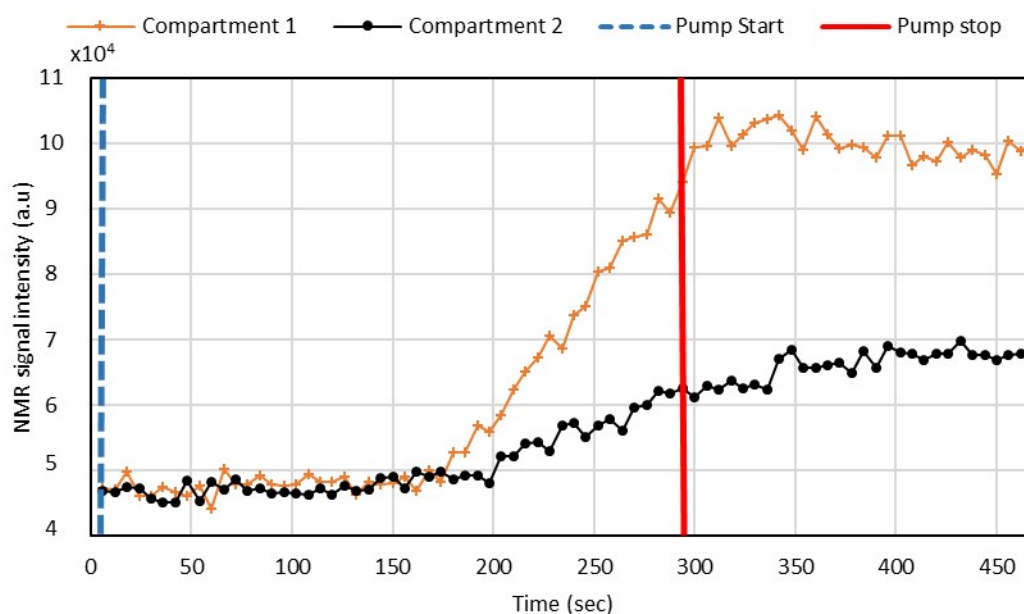


Figure 6.8 – MR signal intensity changes to pressure in both compartments, containing microbubbles suspended in a Gellan gel. When the pump was switched off (solid red line), the signal intensity in compartment 2 (black circle) continue to rise whilst it started to decrease in compartment 1 (yellow cross).

6.3 Microbubbles Entrapped in Alginate Spheres

6.3.1 Introduction

With the intent of measuring pressure changes in the human stomach, it is crucial that the contrast agent is capable of measuring the dynamic pressure changes in different areas within this organ. Although we have demonstrated that the microbubbles suspended in a viscous liquid gellan gel is capable of sensing the spatial pressure gradient, it would be a challenge to achieve this in the human stomach because this fluid solution's pressure would nearly instantaneously equilibrate throughout the meal volume. Hence, we use a large collection of soft-solid alginate spheres with entrapped microbubbles as an artificial meal to overcome this issue allowing the measurement of pressure changes to local compression. In this way, the microbubbles are immobilised in an elastic gel network whilst maintaining its compressibility and flexibility. In this experiment, we intend to demonstrate through *in-vitro* experiment that this contrast agent can be used to measure a pressure gradient spatially and temporally. We are hoping to be able to sense the local pressure in this meal without the need to have the low permeability disc that we previously used in section 6.2.

6.3.2 Experimental Set-up

In this experiment, the contrast agent consists of alginate spheres with entrapped microbubbles. The spheres were sieved from the water suspension and then placed into an empty 50-mL plastic bottle. Additionally, a deflated balloon was connected to an air pump, enabling pressure to be applied to the balloon, and then placed into the plastic bottle containing the alginate spheres (Figure 6.9). This way, upon inflation, the balloon can compress the spheres as it changes size, at varying locations within the vessel, hopefully allowing different alginate spheres to experience different pressures in a way similar to what we anticipate to see in the case of them residing in the human stomach.

The sample was imaged using an optimised RARE sequence in a sagittal plane with nine contiguous, 4 mm thick slices. We monitored signal intensity changes from within the spheres for 23 min as the pressure was cycled between 0 and 1 bar, in order to expand the balloon to different sizes. A bicycle pump was used to expand the balloon quickly

until the pressure reached 1 bar, and the pressure was slowly released, in steps of 0.1 Bar.

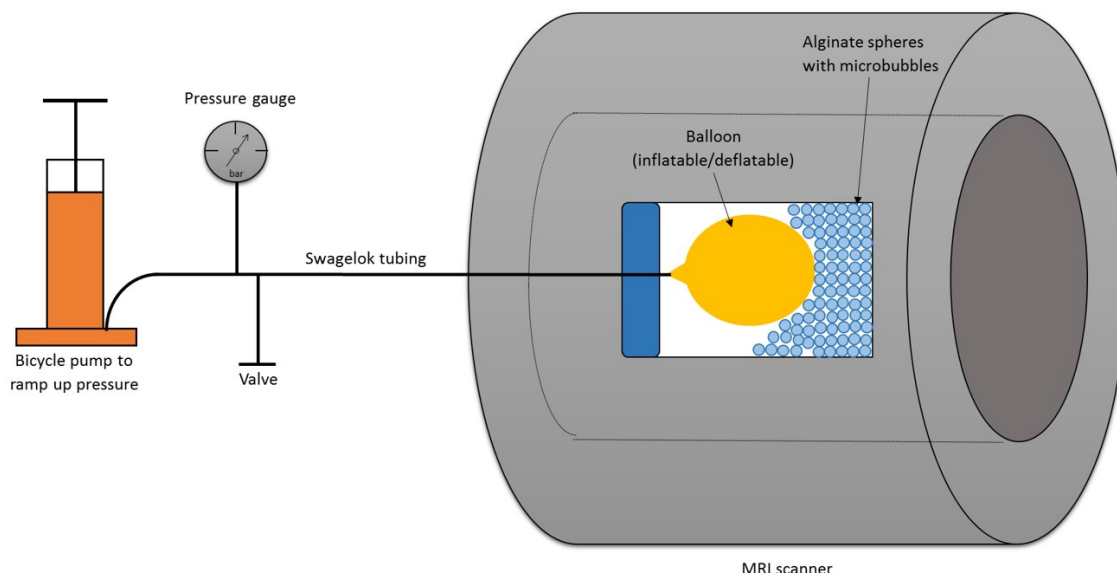


Figure 6.9 – Illustration showing the experimental setup to demonstrate a pressure gradient using alginate spheres with microbubbles entrapped. The pump is used to inflate the balloon, which then compresses the alginate spheres providing a variation of applied pressure in different locations within the sample container. The valve is used to release the air allowing the balloon to deflate slowly whilst MRI images of the sample are acquired.

6.3.3 Results

Figure 6.10 shows one of the sets of nine-slice RARE images taken when the pressure within the balloon was at 0.7 bar demonstrating that the microbubbles-loaded alginate spheres located in different parts of the bottle exhibit differing signal intensity suggesting spatial pressure gradients throughout the sample.

We further analysed the mean signal intensity changes coming from the alginate spheres with microbubbles on each slice of the data set as the pressure is ramped up and down, thereby changing the balloon size, and then provided a plot for each of the image slices (Figure 6.11). The result demonstrates differing signal changes at differing slices, as the pressure within the balloon changes. The maximum signal change exhibited on the image at slice position 24 mm and the minimum at 4 mm, respectively, with 30 %

and 15 % signal changes as the pressure within the balloon gradually changed from 1 bar to 0 bar.

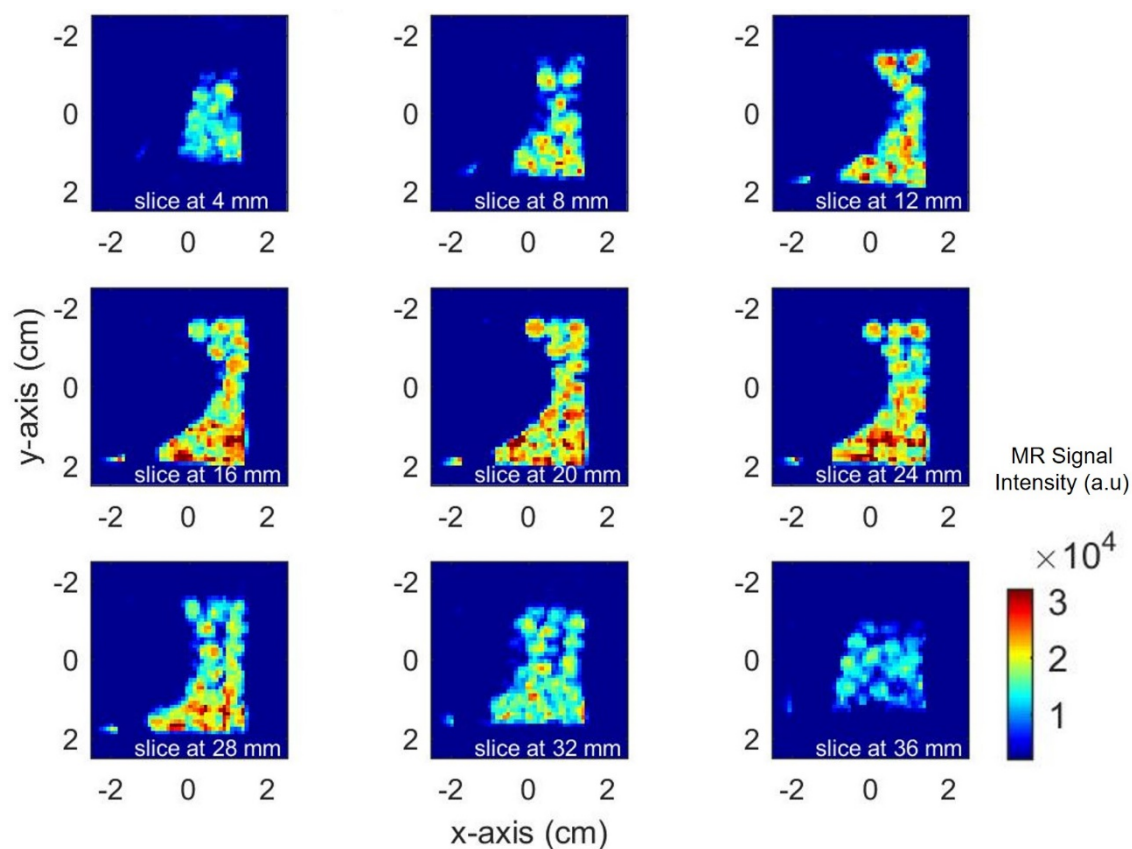


Figure 6.10 – One of the sets of the nine-slice MR images taken when the pressure in the balloon is 0.7 bar, showing the alginate spheres throughout the sample differing in MR signal intensity (SI). The percentage signal change of each of the slice is shown in Figure 6.11.

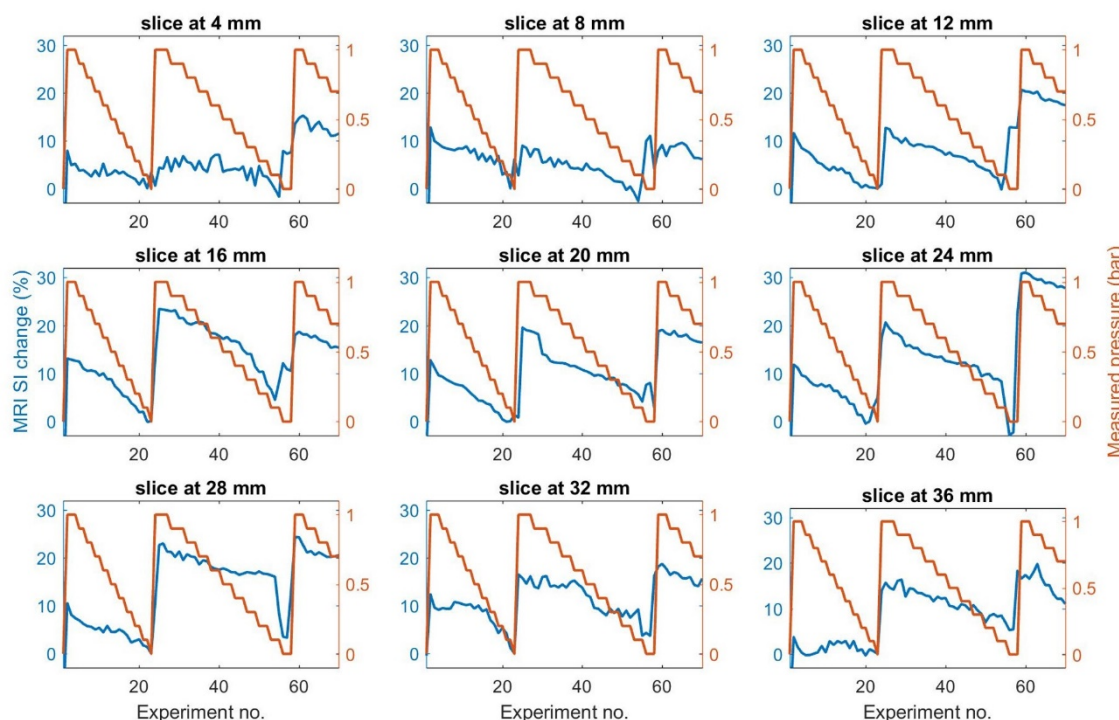


Figure 6.11 – Each plot is corresponding to a specific slice of the RARE images, showing the MR signal intensity (SI) percentage change exhibited on all nine different image slices, throughout the sample, as the pressure is cycled between 0 and 1 bar. The blue and red curves represent the MR SI percentage change and measured pressure, respectively. The highest SI change is seen on the image at slice 24 mm and the lowest at slice 4 mm. This shows that this contrast agent can demonstrate a pressure gradient on the sample.

6.4 Conclusions

In these *in-vitro* studies, MR imaging using a rapid RARE sequence demonstrates a spatial pressure gradient on the specific specimens using our microbubble-based contrast agents, which to the best of our knowledge has never been demonstrated before. In the first experiment, by using microbubbles suspended in a gellan gel with 2% w/v concentration, we show that the MR signal intensity and its time course are different in a two-compartment sample holder separated by a sintered glass with pores (Figure 6.7 & Figure 6.8). This effect is associated with the size change of the microbubbles due to the pressure gradient between the two compartments, which affects the overall T_2^* . It demonstrates that the microbubble contrast agents can be used as a fluid pressure measurement tool which shows potential as an agent in clinical prospects for measuring pressure changes within the human stomach.

The second experiment reveals that the alginate spheres with entrapped microbubbles exhibit a variation in the MR signal intensity in different locations when the pressure is applied, demonstrating their capability in sensing the localised pressure changes (Figure 6.11). This work shows a great potential for microbubble-based contrast agents to measure pressure changes spatially and temporally using MR imaging. It also promises that this method can be very useful in medical applications, particularly in measuring a rapid and localised pressure change within the human stomach.

References

1. ALEXANDER, A.L., McCREERY, T.T., BARRETTE, T.R., GMITRO, A.F. and UNGER, E.C., 1996. Microbubbles as novel pressure-sensitive MR contrast agents. *Magnetic Resonance in Medicine*, **35**(6), pp. 801-806.
2. BENCSIK, M., AL-RWAILI, A., MORRIS, R., FAIRHURST, D.J., MUNDELL, V., CAVE, G., MCKENDRY, J. and EVANS, S., 2013. Quantitation of MRI sensitivity to quasi-monodisperse microbubble contrast agents for spatially resolved manometry. *Magnetic Resonance in Medicine*, **70**(5), pp. 1409-1418.
3. BENCSIK, M. and RAMANATHAN, C., 2001. Direct measurement of porous media local hydrodynamical permeability using gas MRI. *Magnetic Resonance Imaging*, **19**(3-4), pp. 379-383.
4. DHARMAKUMAR, R., PLEWES, D.B. and WRIGHT, G.A., 2005. A novel microbubble construct for intracardiac or intravascular MR manometry: a theoretical study. *Physics in Medicine and Biology*, **50**(20), pp. 4745-4762.
5. MORRIS, R.H., BENCSIK, M., NESTLE, N., GALVOSAS, P., FAIRHURST, D., VANGALA, A., PERRIE, Y. and MCHALE, G., 2008. Robust spatially resolved pressure measurements using MRI with novel buoyant advection-free preparations of stable microbubbles in polysaccharide gels. *Journal of Magnetic Resonance*, **193**(2), pp. 159-167.
6. MORRIS, R.H., BENCSIK, M., VANGALA, A.K. and PERRIE, Y., 2007. Three-dimensional fluid pressure mapping in porous media using magnetic resonance imaging with gas-filled liposomes. *Magnetic Resonance Imaging*, **25**(4), pp. 509-512.

CHAPTER 7

MRI *IN-VIVO* STUDIES

7 MRI *IN-VIVO* STUDIES

7.1 Introduction

In previous chapters, we have demonstrated through *in-vitro* experiments that the alginate spheres with microbubbles exhibited a sensitivity of up to 40 % signal changes per bar at the field strength of 2.35T and 3T, showing promising potential as a pressure probe for MRI examinations. Following this, we carried out further *in-vivo* investigations on healthy volunteers to demonstrate the capability of this microbubble-based contrast agent to sense spatially varying pressure changes in the human stomach. The expected pressure exerted in the stomach on its meal, within the antrum region, during the digestive period is ranging between 30 and 82 mmHg (40 to 109 mbar) (Bortolotti, Annese et al. 2000). It is known that the symptoms of the patients related to functional dyspepsia disease, such as nausea, vomiting and belching, are enhanced with the stomach distention (Tack, Caenepeel et al. 2001). This related to the alteration of the physical responses of the stomach to ingestion of food (Farre, Vanheel et al. 2013).

For *in-vivo* studies, the contrast agent is prepared in the form of a meal to be consumed by the volunteers before being further scanned with MRI. An initial scanning is performed using the RARE sequence which resulted in severe motion artefacts. We therefore further explored the BTFE sequence. In this chapter, five *in-vivo* investigations are carried out and for the purpose of the MRI sequence optimisation, several *in-vitro* experiments are also undertaken in between. All of the experiments involving MRI scanning in this chapter were carried out using the 3T Philips Achieva whole-body scanner at the Sir Peter Mansfield Imaging Centre (SPMIC), at the University of Nottingham.

7.2 Study Design

7.2.1 Selection of Participants

The ethical approval for the *in-vivo* studies was acquired from the ethics committee of the University of Nottingham. The participation into the study is entirely voluntary and all the volunteers gave written informed consent. At the time of writing this document, four volunteers (two males, two females, age range 25-55 years) were

recruited, for five *in-vivo* studies. All volunteers had no history of gastrointestinal disease and were suitable for MRI scanning. In the process of designing the study, the eligibility criteria were written to reduce any possible bias resulting from spurious results in subjects with specific underlying conditions, which may alter intra-gastric pressure:

Inclusion criteria:

- Age between 18 and 55 years
- Able to give informed consent

Exclusion criteria:

- Pregnancy
- History of pre-existing gastrointestinal disorder, including but not limited to:
 - Inflammatory Bowel Disease
 - Coeliac Disease
 - Pancreatitis
 - Active Gallstone disease (biliary colic, cholecystitis)
 - Diverticulitis
 - Cancer of the gastrointestinal tract
 - Irritable Bowel Syndrome
- Reported history of the previous resection of any part of the gastrointestinal tract other than appendix or gallbladder
- Any medical condition making participation in the study potentially compromising e.g. diabetes mellitus, respiratory disease limiting ability to lie in the scanner
- Contraindications for MRI scanning
- Reported alcohol dependence
- Inability to lie flat or exceed scanner limits of weight (120 kg in our case)
- Poor understanding of English language
- Participation in any medical trials for the past 3 months
- History declared by the candidate of food allergy to nuts and shellfish

7.2.2 The Contrast Agent Meal

The production of the alginate spheres was carried out following the protocol described in chapter 2 (section 2.3.1) using food grade ingredients in a food safe physiology laboratory (ERD145B) at the Nottingham Trent University. Prior to this, the researchers involved in the meal preparation obtained a food hygiene certificate. The 500 ml meal consisted of a mix of alginate spheres and locust bean gum with a volume ratio of 1:1 is prepared for each of the volunteers.

7.2.3 Study Arrangement

7.2.3.1 Participant Preparations

On the day of the study, the participants arrived at the SPMIC after a minimum of 6 hours fast. This was to attempt to reduce subject variability and factors that can affect gastrointestinal function. Participants were allowed a cup of water on the morning of the study if it was consumed at least an hour before coming to the test centre. Then, the participant was instructed to change into MRI compatible loose clothing before going through the meal ingestion and the MRI protocols.

7.2.3.2 Meal Ingestion Protocol

The 500 ml contrast agent meal, warmed up to 37 °C, was separated into two parts (250 ml each) and placed into plastic cups. Before consuming it, participants were asked to consume a high-fat content meal, 50 ml of Calogen® (Nutricia, UK), to rapidly turn the stomach from a fasted into a fed state and to help retain the alginate meal in the stomach for a longer time duration (Hoad, Rayment et al. 2009). After 15 minutes, the participants were asked to eat, as much as they felt comfortable, of the first part of the contrast agent meal (250 ml of the microbubble alginate spheres) within a 10-min period. The volunteers were instructed to ingest the spheres without chewing to retain its shape and functionality in sensing pressure in the stomach. They then underwent an approximately 10-min long MRI scan. Immediately after this scan, the participants were asked to eat as much as they felt comfortable of a further 250 ml of the meal within 10 min. Another approximately 20-min MRI scan was then taken. Throughout the investigations, slight changes in the protocol were occasionally carried out based on

individual studies, which will be further explained in each of the experiments. Finally, the participant is free to go after the MRI scanning is done.

7.2.3.3 MRI Protocol

Initially, the MRI scanning was performed using the RARE sequence. However, after undertaking the study on the first volunteer, we found this sequence was greatly susceptible to motion artefacts, naturally caused by breathing and the internal organs' involuntary movements. Hence, in the subsequent experiments we moved on to using a gradient echo sequence with a faster imaging acquisition, Balanced Turbo Field Echo (BTFE) which also known as TrueFISP. In this study, the typical time duration of the acquisition of k-space for the RARE is between 300 to 500 ms, and for the BTFE is around 90 ms. In addition, a spin echo pulse, which also known as a T_2 prep time, is applied as a preparation pulse before the acquisition of the BTFE sequence (Hoad, Cox et al. 2010) to make sure that T_2^* contrast is left to take place in the contrast agent.

7.3 Flavour Enhancement of the Contrast Agent

While working on the ingredients of the contrast agent, volunteers found its taste was rather plain and not sufficiently appealing to the palate. The taste is important in helping the participants to feel comfortable in consuming the meal, however, it is also crucial that any additional ingredient will not impede the MR signal and the sensitivity of the contrast agent in sensing the pressure. In an attempt to enhance the flavour, we tried adding commercially available sweetener (Tesco, UK) and vanilla extract flavouring (Dr. Oetker, Germany) in the locust bean gum (LBG) solution.

7.3.1 Experimental set-up

The LBG solutions (2 % w/v concentration) were prepared following the procedure described in section 2.4.2. For this experiment, three samples of the LBG solutions were prepared; (1) with sweetener and vanilla flavouring (2.5 % and 0.8 % w/v concentration respectively), (2) with sweetener (0.8 % w/v concentration) and (3) without any additive flavour or sweetener (plain). Each of these LBG solutions was filled into separate 50 ml plastic test tubes. MRI scanning was then carried out with the RARE sequence ($TE^{eff} = 500$ ms) using the 3T Philips scanner.

7.3.2 Results

The RARE image with colour scale signal intensity is shown in Figure 7.1. The result demonstrates that the signal intensity of the LBG is decreased with the addition of the sweetener and flavouring. As compared to the plain LBG, the decrease is about 13 % in the LBG with sweetener, whilst a dramatic drop, approximately 50 %, of the signal intensity takes place in the LBG with sweetener and vanilla flavour. In terms of taste, we found that it was only slightly improved by adding sweetener into the LBG and further enhanced with the vanilla flavour. However, considering the effect on the signal intensity, we decided not to add any of these taste enhancers to our contrast agent meal for the subsequent experiments. In order to enhance the experience and the process of consuming the meal without affecting the signal and sensitivity, the volunteers for the *in-vivo* studies are provided with a variety of strongly scented foods (chocolate and lemon) or warm solutions (vanilla and lemon) for them to smell whilst eating the contrast agent. The purpose is to help to stimulate their olfactory senses while consuming the meal.

In the future, further exploration on different flavours that could enhance the taste with less effect on the MR signal of the meal would be very helpful in providing a better experience for the participants (or patient) in consuming the contrast agent meal.

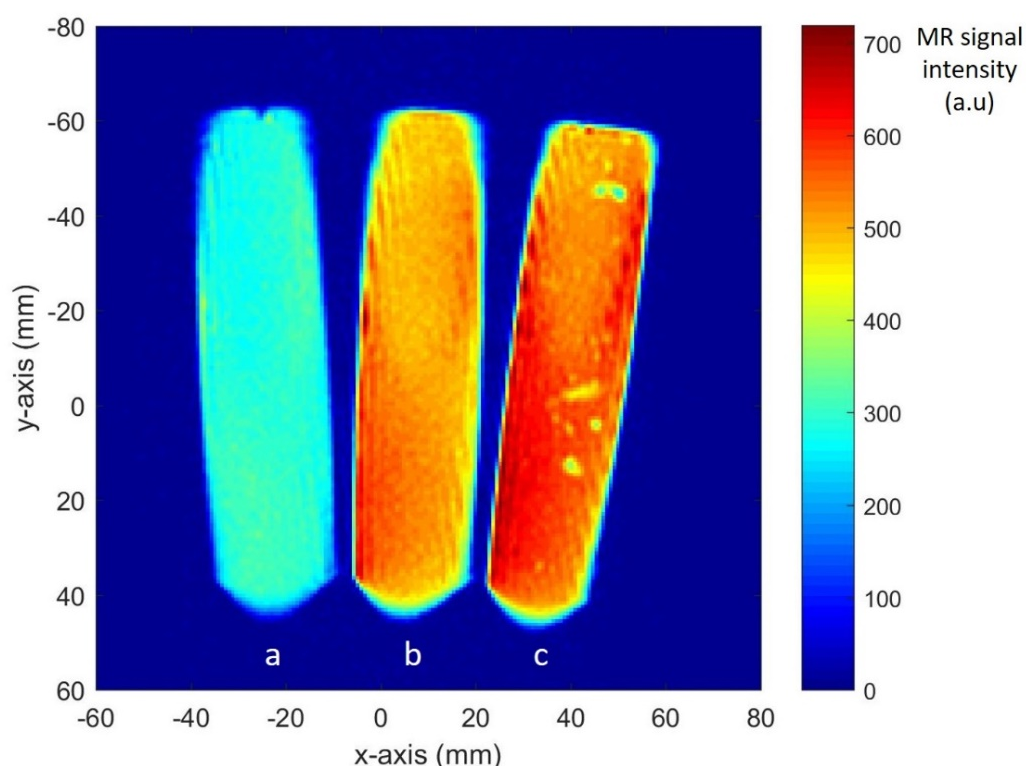


Figure 7.1 – The RARE images of three locust bean gum solutions (2 %) in 50 ml plastic test tubes, a) with sweetener and vanilla flavour, b) with sweetener and c) without any sweetener or flavour (plain). The signal intensity of the LBG solutions in a) and b) decreased 50 % and 13 % respectively compared to c) the plain LBG.

7.4 *In-Vivo* Investigation using the RARE Sequence

7.4.1 Method

The alginate spheres with microbubbles (250 ml) were prepared the day before the MRI procedure and suspended in distilled water in a 500 ml glass bottle before it was stored in a fridge. On the day of the MRI study, a 250 ml LBG solution (2 %) was prepared 3 hours before the investigation. The alginate spheres were sieved out of the glass bottle, eliminating the water suspension, and then mixed with the freshly prepared LBG which resulted in a total volume of 500 ml of contrast agent. The meal was divided equally into two portions and placed into separate plastic cups. After being given a briefing regarding the procedure, the volunteer was instructed to ingest the meal following the ingestion protocol described in section 7.2.3.2. The volunteer consumed approximately 80 % and

40 % of the first and second part of the meal, respectively, which resulted in a total volume of an ingested meal of approximately 300 ml.

The participant was positioned in the scanner with a slightly tilted orientation; left side of the body lifted higher than the right side, in order to help to channel the meal within the stomach towards the antrum. This enabling the observation of the stomach muscle wall contraction on this region on the MR images, while the spheres experience the resulting pressure variations. Two sets of dynamic MRI scans were acquired using the RARE sequence, mainly to explore the effect of varying the value of TE^{eff} . The first one was acquired every 7 seconds with three slices imaged at 5 mm thickness and $TE^{eff} = 500$ ms, and the second measurement with one slice imaged at $TE^{eff} = 300$ ms.

7.4.2 Results

In the first step of the analysis, the MR images were inspected, slice by slice, and an ROI corresponding to the part of the stomach containing the largest part of the meal was manually selected by using the ImageJ processing program. In doing so, we noticed large deviations from frame to frame, due to motion artefact caused by breathing. This effect is further quantitated when the mean of the MR signal intensity in the selected ROI was analysed, frame by frame (Figure 7.2). Unfortunately, when motion artefact takes place, the pixel intensity loss is severe, and resulting in the exhibited change up to 300 % (Figure 7.3).

The signal variations that we are trying to harvest are expected to be much smaller than those presently measured and probably dominated by the motion artefact, and should be around 1.6 and 4.3 % when considering the typical 40 % per bar sensitivity of this contrast agent. At this point, it is clear that the limitation of the study is presently within the artefact most probably caused by breathing. Therefore, in the next experiments we worked at improving and somewhat overcoming this effect by exploring different MRI sequences, which are less susceptible to the motion artefact, by providing means of acquiring k-space in much shorter time durations.

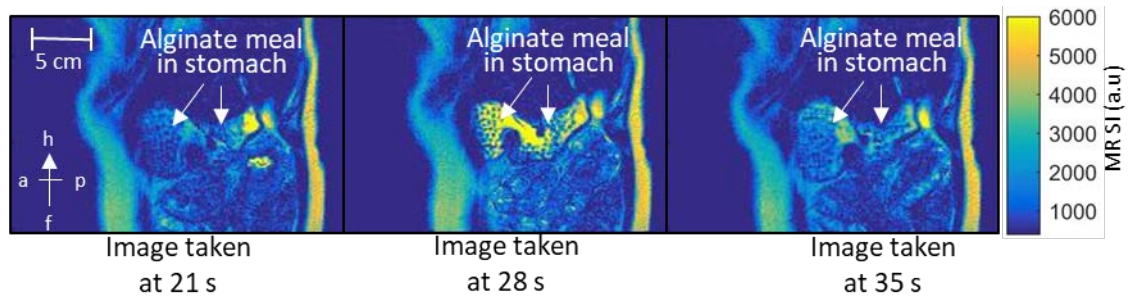


Figure 7.2 – Three consecutive sagittal RARE images acquired with $TE^{eff} = 500$ ms, and respectively taken at 21, 28 and 35 seconds of the measurement. This demonstrates large deviations, from frame to frame, of the area of the meal in the stomach captured by the selected slice, mainly caused by breathing motion as well as large deviations in MR signal intensity. The letters h, f, a and p indicate the directions relative to the position of the volunteer in the scanner, and respectively stand for head, feet, anterior and posterior.

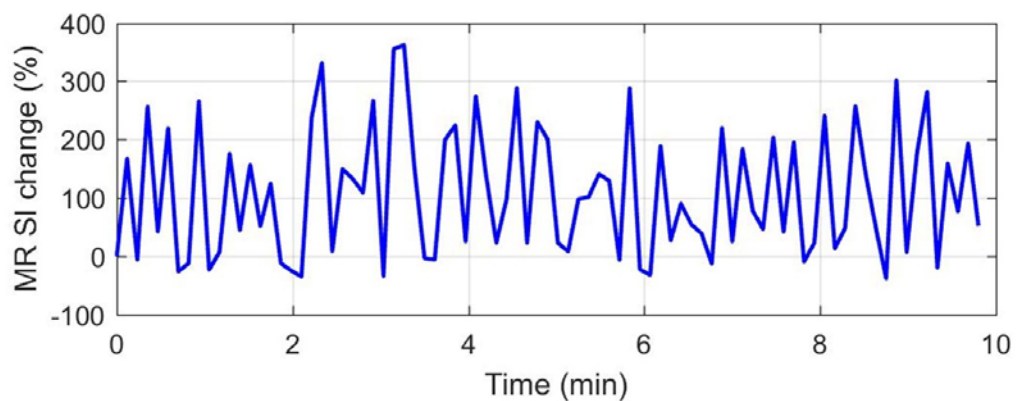


Figure 7.3 – Graph showing the percentage of the mean signal intensity variation over the meal is really high (between 100 to 300 % changes) probably due to movement artefact caused by breathing during the time duration of the k-space acquisition 500 ms.

7.5 Exploring HASTE and BTFE Sequences to Minimise the Effect of Movement

Artefacts

We need to be able to assess the signal intensity changes related to motion (or other sources) and not due to pressure changes, in order to explore and quantitate different MRI sequences aimed at reducing the unwanted artefacts. This was achieved by running more *in-vivo* studies with an artificial meal identical to the one already used, but not

comprising of any microbubbles. In such a meal, any MR signal changes will not be due to pressure changes.

7.5.1 Method

A 500 ml contrast agent meal, consisting of the alginate spheres without microbubbles suspended in LBG solution, was prepared and then ingested by the volunteer following the standard experimental protocol (section 7.2.3.2). The total amount of the contrast agent consumed by the volunteer on this occasion was approximately 54 % (270 ml).

The dynamic MRI images were acquired using two different sequences, Half-Fourier Acquisition Single-shot Turbo Spin Echo Imaging (HASTE), and Balanced Turbo Field Echo (BTFE). HASTE is another Turbo Spin Echo sequence, which is very similar to RARE. It uses a half Fourier transform acquisition, which is used to reduce the data acquisition time by acquiring only a part of k-space. Whilst, the BTFE is a gradient echo sequence. One data set with three-slice images was acquired using HASTE (TR = 991 ms) at $TE^{eff} = 400$ ms and another set with single-slice images using the BTFE sequence (TE = 1.71 ms, TR = 3.4 ms) with T_2 prep time = 50 ms.

7.5.2 Results

For the image analysis, we first compared the signal intensity change coming from two different methods of ROI selection, one using manual selection by hand drawing the edge of the meal and another one by selecting a smaller elliptical area within the stomach (Figure 7.4), which is similar to the technique previously used in 7.4.2. By using the ImageJ software, both of the selection methods were performed on the data set acquired with the BTFE sequence. Then, the ROI selection was further uploaded into Matlab® and processed to analyse the signal intensity changes.

The percentage of signal intensity change for this study performed by comparing the intensity relative to the mean signal intensity of the second and the third images, where the magnetisation had reached its steady state. The elliptical ROI exhibits less variation in the meal mean signal intensity, as shown in Figure 7.5. For the BTFE images, the full stomach selection shows an overall variation of 7 %, while the elliptical area selection only shows a change of 5 %. By further neglecting the odd outlier seen at 0.9 minute of the measurement, the percentage change drops to less than 2 %, which clearly

demonstrates that the elliptical selection is a better route in gaining a stable ROI for the analysis from one frame to another.

The main reason for this is likely to reside in that the elliptical area selection can be taken near the centre of the stomach where the meal is more homogeneous, decreasing the effects of the edge-artefacts, which is more susceptible to the movement normal to the stomach wall. At the same time, this selection method also allows two separate ROIs to be targeted simultaneously for comparison, and in particular, within the body of the stomach and the antrum. Although the elliptical ROI method has the drawback that there are fewer pixels accounted for signal analysis compared to the hand-drawn ROI, we moved on to performing the subsequent analysis in this particular study with the elliptical area selection due to the lower signal variation exhibited.

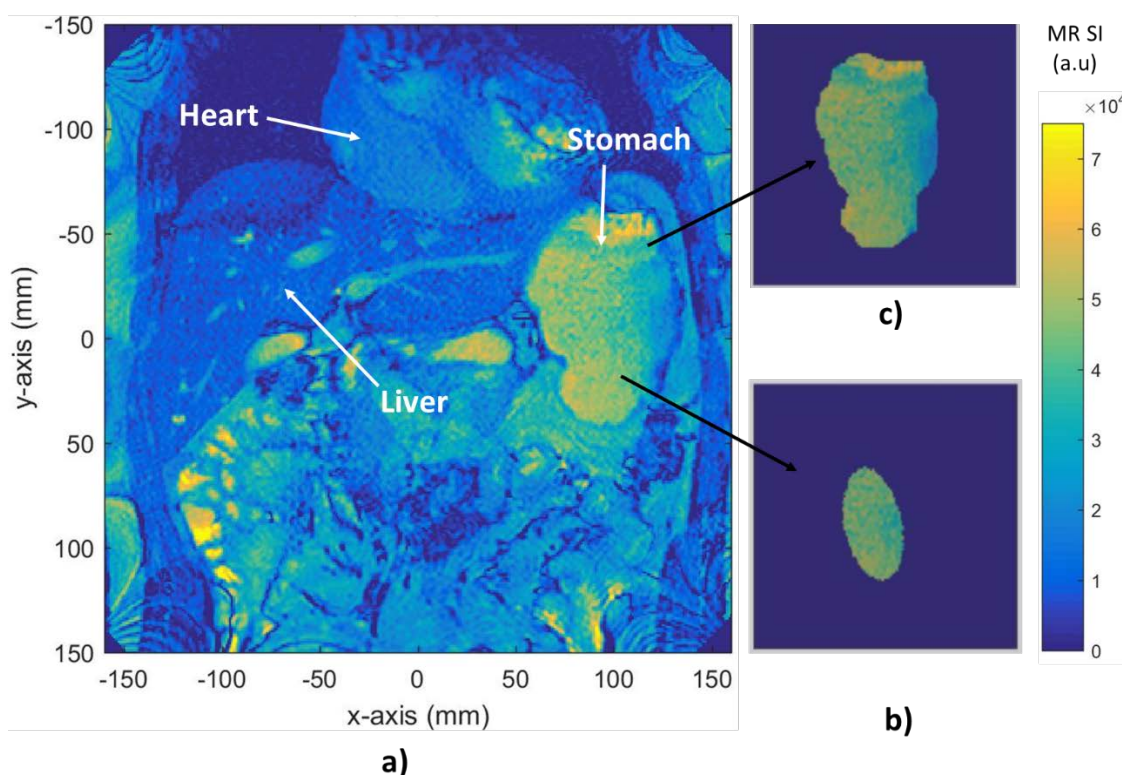


Figure 7.4 – a) BTFE coronal MRI image showing the meal (alginate spheres without microbubbles) in the stomach, and the surrounding organs. Two ROI selection methods are used to analyse the signal intensity change, b) elliptical and c) hand-drawn ROI selections. The corresponding signal intensity changes are plotted on the graph in Figure 7.5.

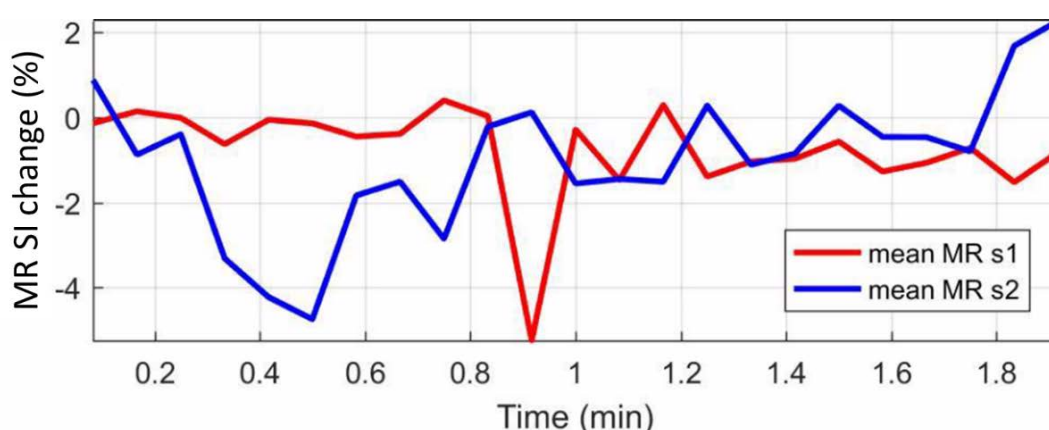


Figure 7.5 – Plot showing the comparison between two ROI selection methods, in terms of signal intensity changes. The elliptical selection (S1 – red curve) demonstrates less signal variation compared to the hand-drawn selection around the edge of the stomach (S2 – blue curve), demonstrating that the first method is less susceptible to the movement artefact.

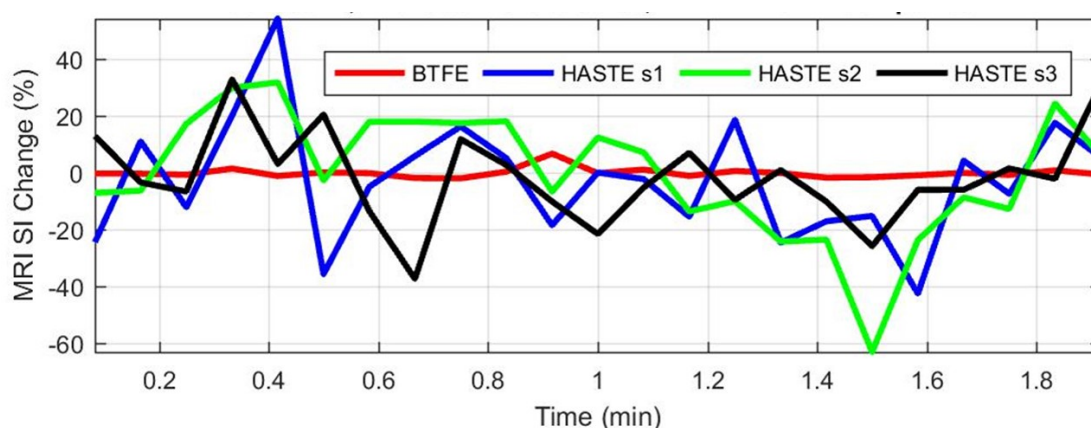


Figure 7.6 – The mean signal intensity comparison between the BTFE (single slice) and the HASTE (three slices) sequences. The signal variation coming from the BTFE sequence is dramatically reduced to 2 %, compared to the HASTE which exhibits signal changes between 20 to 50 %.

The mean signal intensities of the meal within an elliptical ROI for both BTFE and HASTE were calculated and displayed for comparison (Figure 7.6). This was done for the single-slice BTFE images and for all of the three slices HASTE images. In addition, since the dynamic acquisition for HASTE data set was taken for only 2 consecutive minutes, the comparison can only be observed within this time frame. As a result, the motion artefact

is more prominent in HASTE, where the signal intensity change fluctuates between 20 % to 50 %. In contrast, it is only 2 % on the BTFE images. We can therefore conclude that, the BTFE is the most appropriate MR sequence to be used for our investigation with regards to its effectiveness in reducing the motion artefact. However, due to its ultrafast scanning of k-space, a preparation pulse is required, for us, with the BTFE, to make sure that some T_2^* contrast is left to take place in the contrast agent. This preparation pulse is known as the T_2 -prep time, and the investigation on varying the length of this time is further discussed in section 7.6.3.

In the next *in-vivo* experiment, with the microbubbles present in the meal, a percentage change is expected to be higher than the value that currently measured (without microbubbles), due to the effect of the pressure in the stomach being sensed by the meal. Although the BTFE sequence is showing promise in reducing the motion artefact, unfortunately, another issue has arisen when the study undertaken with the meal comprises of microbubbles. Due to the meal high heterogeneity with the presence of microbubbles, a different part or portion of the meal that is being interrogated provides different mean signal intensity. This issue will be fully discussed in section 7.7, where the improvements obtained with the use of the respiratory triggering.

We also further analysed the images, by normalising the signal intensity relative to the mean of the highest signal intensities found in the meal, assuming it is a representative of the LBG. It may therefore be possible to somewhat compensate the motion artefact by ensuring that the MR signal strength coming from the LBG alone is scaled to a constant value. The normalisation method allows us to effectively enhance the signal change due to the pressure change, provided that the percentage of pixels that we are using is representative of the LBG only. However, a problem will occur when this percentage is increased to the point that it is no longer representative of the intensity of LBG and starts to include important data such as the periphery of the spheres. At this point, the normalisation will then deteriorate the sensitivity of the contrast agent to pressure changes, hence, an optimum value should be further calculated.

In this endeavour, firstly, we investigated the effect of the normalisation in the BTFE images by comparing the signal change in the meal, by taking off the top 5, 10, 15 and 20 % of the signal intensity. The MR signal coming from the LBG alone is not expected

to exhibit much deviation, except the drift due to the effect of the acid. Surprisingly, as the percentage of the signal intensity taken to represent the average intensity of the LBG increases the percentage of the intensity change within the meal is shown to reduce (Figure 7.7). This further evidenced the meal heterogeneity contributes to the signal intensity change, when the analysis performed from one image to another.

The figures showing the effect of changing the pixels accounted for as the LBG with differing percentages is shown in Figure 7.8. By taking the 10 % normalisation as an example, the signal intensity percentage change in the alginate spheres without microbubbles was found to be around 1 %, compared to the one without normalisation which is around 2 %. In this particular study, the 20 % normalisation appears to be most effective in reducing the signal variations coming from the meal without microbubbles. For the meal with microbubbles where the meal heterogeneity is expected to be much higher, perhaps the normalisation could be used to further reduce this effect.

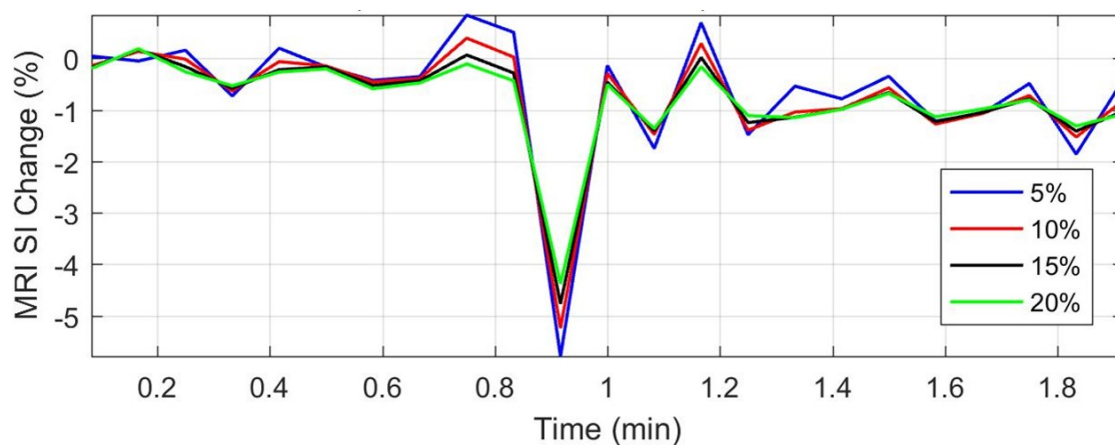


Figure 7.7 – Plot showing the effect of normalising the signal intensity to the highest intensity found on the image of alginate spheres without microbubbles meal, in an attempt to scale the signal intensity coming from LBG to a constant value. The signal intensity change observed by removing the top 5, 10, 15 and 20 % of the signal intensity, respectively represented by the blue, red, black and green curves.

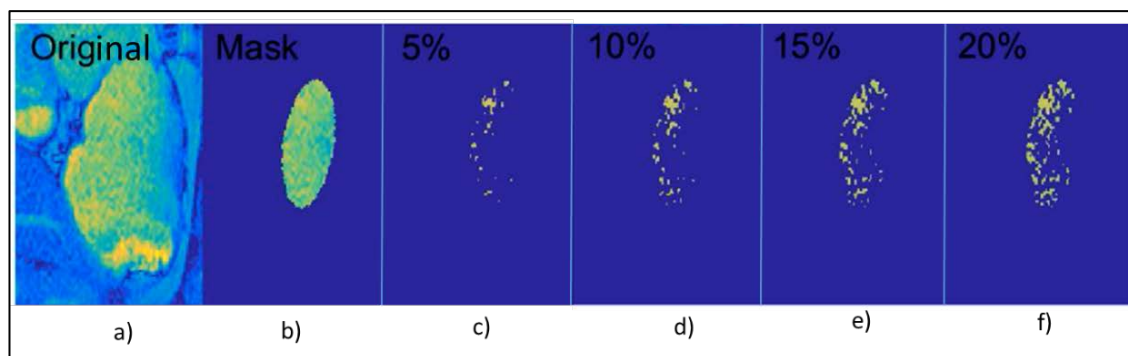


Figure 7.8 – a) MR image of the meal within the stomach. b) The ROI selection (mask) used for analysis. The images c) to f) showing the pixels accounted for LBG, when different percentages (5, 10, 15, 20 %) are explored for the normalisation.

7.6 Optimisation of the BTFE Sequence in Sensing Pressure Changes in the Human Stomach

7.6.1 *In-Vivo* Study: Varying the Image Resolution

In the previous section, we have demonstrated the BTFE sequence effectively reduced the motion artefact as compared to the HASTE and the RARE sequences, hence we moved on to use this sequence as our imaging method in the consequent studies. In order to optimise the sequence, we explore a variation of spatial resolutions in an attempt to further minimise the motion artefact. In this experiment, we gradually decreased the spatial resolution, hoping to reduce the motion artefact. It is known that high image resolution has high sensitivity to motion artefacts and often requires longer acquisition time that again worsens the movement artefact.

7.6.1.1 Method

As usual for our *in-vivo* investigations, 500 ml of the contrast agent meal (250 ml alginate spheres with microbubbles mixed with 250 ml locust bean gum) was prepared. Then, in this particular experiment, the volunteer was instructed to ingest the whole meal at once, instead of taking half-and-half as for the previous two volunteers. This was to try to avoid a scanner problem taking place when taking the bed out and in, in the middle of the experiment, which caused an issue with the previous volunteer, not allowing further scanning until 'new patient' registration was logged in. Exceptionally, this

particular volunteer managed to consume the whole volume of the meal, before entering the MR scanner in a supine position.

In this study, six sets of dynamic MR images were obtained using the BTFE sequence with a single-slice image taken every 3 seconds for 5 minutes, mainly differing in the resolution of the image from experiment to experiment. The acquisition was started with the highest resolution (0.826) and it was then decreased gradually, in each subsequent experiment. The followings are the sequence details:

Data set	T ₂ -prep time (ms)	Slice thickness (mm)	FOV (mm x mm)	Image size (x,y)	Image resolution (pixel/mm)	Slice orientation
1	100	5	340 x 403	337 x 336	0.826	Coronal
2	100	5	340 x 400	268 x 264	0.520	Coronal
3	100	5	340 x 352	236 x 230	0.454	Axial
4	100	5	340 x 402	203 x 202	0.300	Coronal
5	100	5	340 x 401	203 x 202	0.300	Coronal
6	120	5	340 x 400	159 x 158	0.185	Coronal

Table 7.1 – Details of parameters used for the BTFE sequence, mainly exploring different image resolutions and the effect on the sensitivity of the contrast agent meal.

7.6.1.2 Results

The signal intensity analysis was carried out by selecting two ROIs of the meal, within two different regions in the stomach (antrum and body of the stomach, see Figure 7.9). In all of the data sets, the MR signal intensity changes in the antrum are systematically higher compared to those seen in the main body of the stomach, respectively around 7 to 10 % and 4 to 5 % (Figure 7.10). The data also shows that the MR signal changes exhibited are higher than previously seen in the study on the meal without microbubbles, regardless of the spatial resolution value explored, which is anticipated as this sensitivity difference could be due to the effect of the pressure exerted by the stomach.

Unfortunately, due to the presence of the microbubbles, spatial heterogeneity in the meal is further enhanced and this also contributed to the signal change.

Following that, we performed a normalisation, as previously explained in section 7.5.2, by removing 10 % of the highest signal intensity as a representative of LBG signal intensity. Initially, a sensitivity increase was expected, however the signal changes are instead decreased to approximately between 4 to 6 % in the antrum and between 2 to 3 % in the body of the stomach (Figure 7.10). In an attempt to explain this, it is possible that the variation in the appearance of LBG on the acquired images contributes to the alteration of the signal intensity from slice to slice of the image.

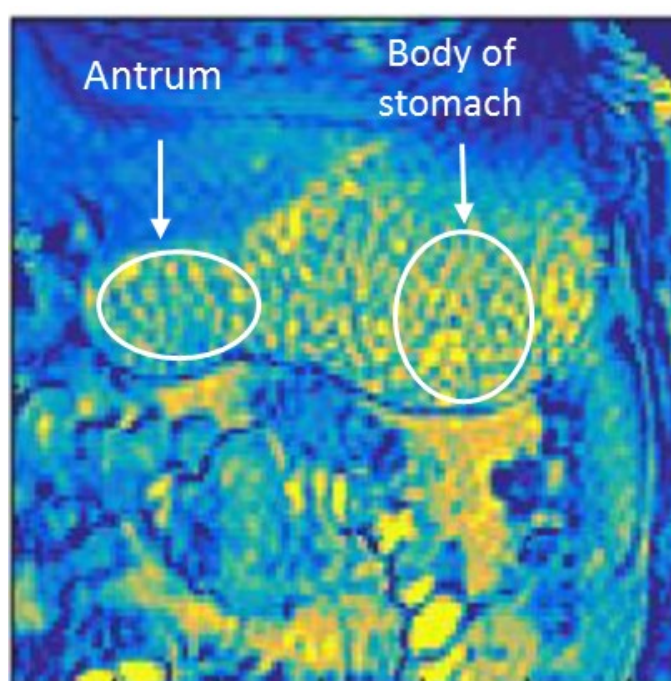


Figure 7.9 – ROI selections within the meal (alginate spheres with microbubbles) in different regions in the stomach for signal intensity analysis.

By having a closer look at the data, in the instances where the volunteer held their breath, at the beginning and within the experiment (specifically on Figure 7.10f at 2.5 minutes of the measurement), the signal in the antrum is seen to exhibit signal changes substantially larger than that seen in the main body of the stomach, within the expected

range of sensitivity to pressure changes (4 %). This is perhaps evidence of stronger pressure changes in the antrum compared to the main body of the stomach.

The outcome of varying the image resolution demonstrates that the signal fluctuation is seen to remain the same in all of the resolution values explored in this experiment (Figure 7.10), except in Figure 7.10d where the signal change exhibited up to 20 % which mainly due to the large variation of the meal volume captured by the selected image slice. Even with the lowest resolution that we have explored (0.185 mm/pixel), the images are still clear enough to allow a clear selection of the meal within the two main regions of the stomach.

Unfortunately, none of these experiments, however, was taken in exactly identical MR conditions to those in the previous volunteer with the meal without microbubbles (section 7.5), in terms of the MR sequence parameters. Hence, we cannot make a direct comparison or conclude that the signal intensity changes in this study are solely due to the pressure changes in the stomach. In fact, the high signal stability in instances where the volunteer is known to hold their breath clearly demonstrates that we are still severely suffering from either motion artefact, or from the slice collecting a signal from differing areas of the meal.

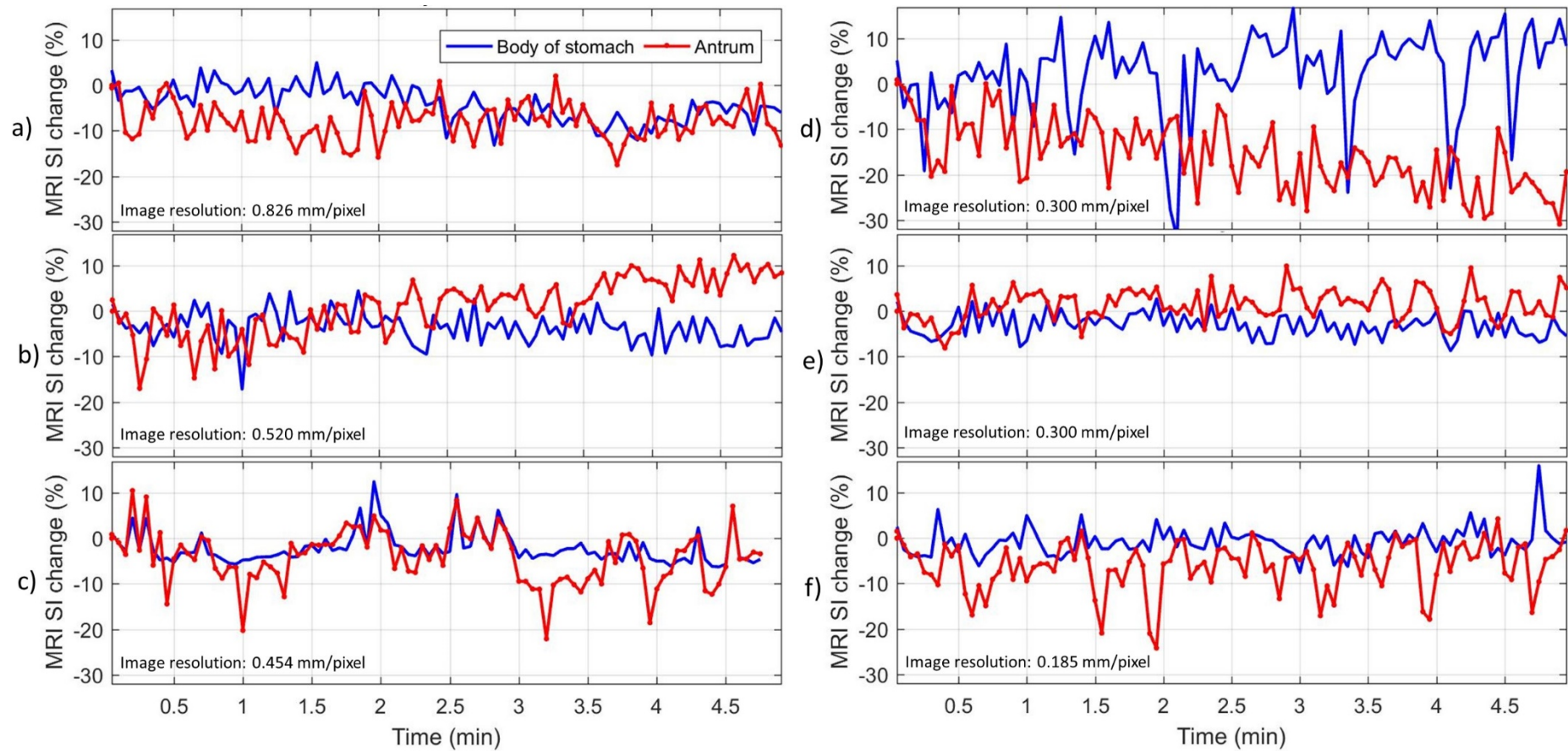


Figure 7.10 – Plots showing the signal intensity changes within the meal (alginate spheres with microbubbles) on different regions in the stomach (antrum and body of stomach), when varying the image resolution, a) 0.826, b) 0.520, c) 0.454, d) 0.300, e) 0.300 and f) 0.185 mm/pixel. There is no obvious change in the signal fluctuation when lowering the resolution. The signal variation is higher in the antrum compared to the region in the body of the stomach, typically by a factor of 2.

7.6.2 *In-Vitro* Experiment: Varying the Slice Thickness of the BTFE Sequence

In this *in-vitro* study, we acquire the MRI images and observe the signal intensity change to pressure changes by varying the slice thickness. Furthermore, without any pressure being applied, we also perform another experiment to quantitate the signal intensity change as the slice selection being moved throughout the sample. We anticipate that it is possible the variation in the appearance of the meal on different image slice (meal heterogeneity) contributes to the alteration of the signal intensity from slice to slice of the dynamic images in the previous studies.

7.6.2.1 Experimental set-up

Alginate spheres with microbubbles were prepared and suspended in distilled water, then loaded into a 100-ml Perspex container before being placed in a water bath at 37 °C. The sample was further connected to a pump and placed in the 3T MRI scanner in a vertical orientation. For the first part of the experiment, the MR images were obtained using the BTFE sequence (T_2 -prep = 100 ms) varying the slice thickness (5 mm, 7 mm, 8 mm, 10 mm, 12 mm and 15 mm) while externally applying pressure changes. In the second part, we acquired the BTFE images by changing the slice location in a vertical direction towards the bottom of the sample, without applying any pressure. For this part of the experiment, two data sets were obtained with different slice thicknesses (5 mm and 15 mm) and the slice selection was moved in 5 mm increments across the sample, resulting in eight slices in each set.

7.6.2.2 Results

Square ROIs were selected for the analysis, as shown on one of the images in

Figure 7.11a. In the first part of the experiment, in order to quantitate the sensitivity of the contrast agent when increasing the slice thickness, the mean MR signal intensity from the ROIs were analysed and relative MR signal changes to the signal found in the first image that had reached the longitudinal magnetisation steady state is shown, as a function of the applied pressure. In order to perform a processing realistic of the situation where the meal resides in the stomach, there was no signal thresholding undertaken, used as an attempt to dismiss the LBG from the analysis in *in-vitro* studies in the previous chapters. This is because all pixels will have some contribution from the

alginate and some from the locust bean gum when the slice is thick enough. Since the thresholding is meaningless for the thickest slice, it was not used in any of the other slice thickness values for the consistency of the processing strategy.

The results show small sensitivity changes to the slice thickness, as it remains more or less around 40 % (standard deviation 2.08 %) signal change per bar in all experiments (Figure 7.12). This suggests that in order to minimise the effect of movement in causing artefact on the MR images and the meal spatial heterogeneity, which are the main limiting factor in the *in-vivo* study, it is safe to increase the slice thickness, which does not result in substantial sensitivity loss.

In the experiment where the selected slice was moved throughout the sample, without applying any pressure, we show the relative signal change from one slice to another, using the first slice as the reference in Figure 7.11b. As a result, the signal intensity varies substantially, up to 25 % over a 30 cm displacement (Figure 7.13). This could be due to the alginate spheres with microbubbles tend to float when residing in water causing more fluid to accumulate towards the bottom of the sample. These particular results suggest that breathing-induced displacements of the selected slice are most probably the origin of some of the large signal changes that we have seen in our *in-vivo* studies, so far, and certainly substantiates the need to do respiratory-gated MRI.

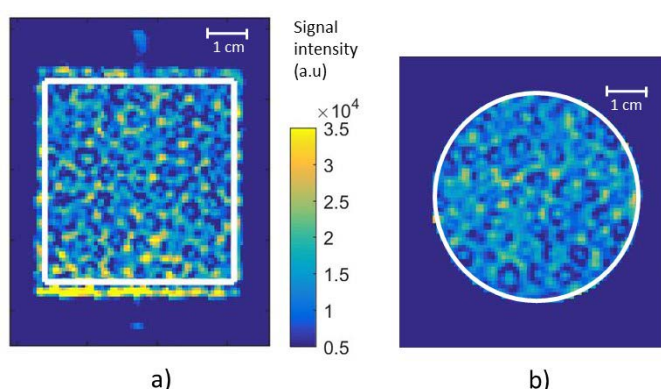


Figure 7.11 – MRI images taken with the BTFE sequence at 5 mm slice thickness a) measuring the signal intensity change to the pressure change, with a measured pressure at 0 bar for this particular image, and b) the first slice used as a reference to demonstrate the signal intensity change as the selected slice moved throughout the sample, when there is no pressure being applied. White rectangle and circle show the selected ROI for the analysis of the signal intensity.

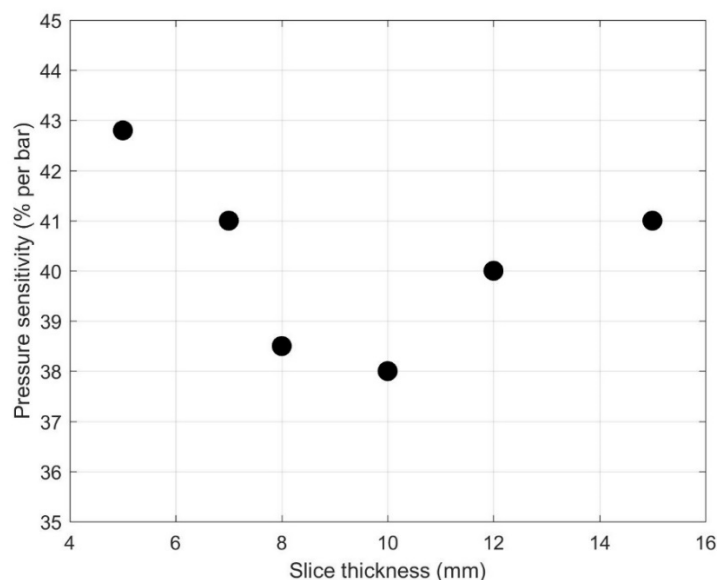


Figure 7.12 – Plot showing the relationship between the sensitivity of alginate spheres with microbubbles to pressure change, as a function of the MR image slice thickness. The sensitivity exhibited around 40 % (standard deviation 2.08 %) signal change per bar in all experiments.

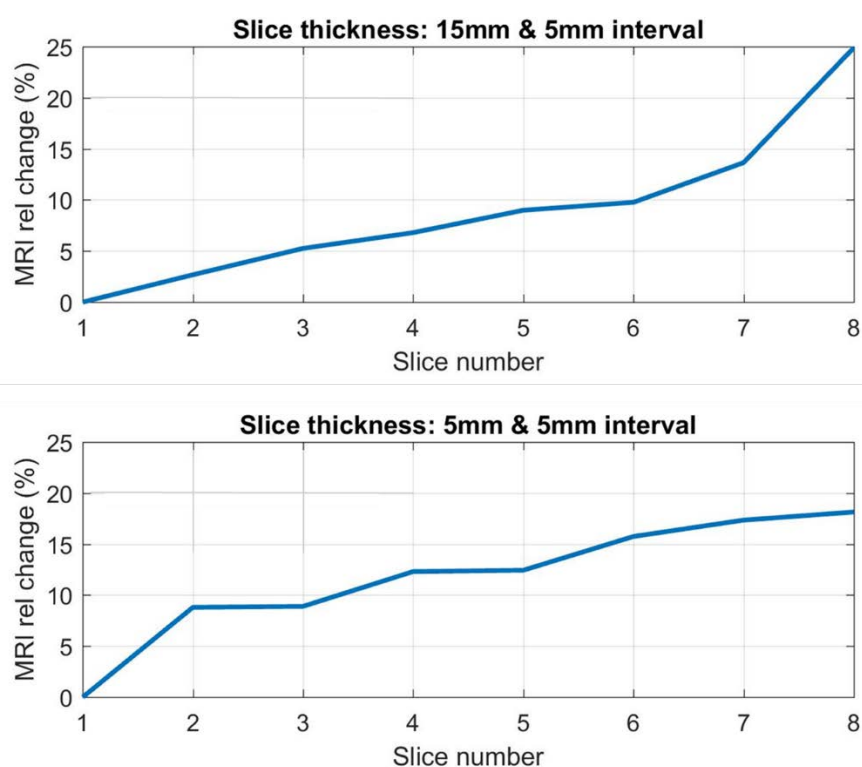


Figure 7.13 – Plots showing the signal intensity change by shifting the position of the selected slice within the sample, when there is no applied pressure.

7.6.3 *In-Vitro* Experiment: Varying the T_2 prep Time of the BTFE Sequence

In our study, the T_2 prep time is a time delay which is applied as a preparation pulse before the acquisition of the BTFE sequence (Hoad, Cox et al. 2010) to make sure that T_2^* contrast is left to take place in the contrast agent. Here, we explore the effect of varying the T_2 prep time on the sensitivity of the contrast agent in sensing the pressure changes.

7.6.3.1 Experimental set-up

The sample was prepared and the experiment was set up identically to the earlier study described in section 7.6.2. In this experiment, the images were acquired using the BTFE sequence with two alternating T_2 prep time values within one acquisition, resulting in fifty MR images taken within a 5-minute long measurement. This was repeated several times by varying the values of the pair of the T_2 prep times, which were 20, 50, 75, 100, 125 and 150 ms. All the T_2 -prep times were repeated three times with the exception of 75 ms and 125 ms, where time constraints only allowed to acquire a single experiment.

Although a difficulty occurred during the experiment, a blockage caused by spheres entering the tubing, this was solved by taking out the sample from the scanner, removing and reconnecting the tubing, after the blockage was flushed out. Then, the sample was replaced into the scanner upside down, so that the water was driven into it from the bottom, avoiding any possible floating alginate being driven back into the tubing when releasing the pressure.

7.6.3.2 Results

The MR images were analysed and the change in our contrast agent's MR sensitivity to the change in the T_2 -prep time is demonstrated. The results showed that the overall mean signal intensity in the sample is increased with decreasing in T_2 -prep times (Figure 7.14), as expected, as the T_2^* attenuation effect is stronger with increasing values of time delay.

Furthermore, the sensitivity to the pressure change as a function of the T_2 -prep time values is shown in Figure 7.15, which demonstrates a trend of increasing sensitivity with increasing T_2 -prep time, as expected. However, the T_2 prep time values of 75 and 125

ms, which were acquired in the same data set, show unusually high sensitivity to pressure even though the signal intensity they exhibit is well within the trend of the exponential decay curve with T_2 -prep time in Figure 7.14. We are not certain about the reason for this but we anticipate it could be due to our bubble size having an optimum T_2^{eff} value producing the best sensitivity to pressure. We further investigated this in the following *in-vivo* study (section 7.7.1) to try to clarify if this effect was genuine, but there was no sensitivity enhancement demonstrated.

From the overall results of this experiment, we have shown that 50 ms is the best viable T_2 -prep time value as it exhibits very similar sensitivity to that obtained at 100 ms. This lower T_2 -prep time, 50 ms, is further advantageous as it is expected to decrease the susceptibility to movement when compared to 100 ms.

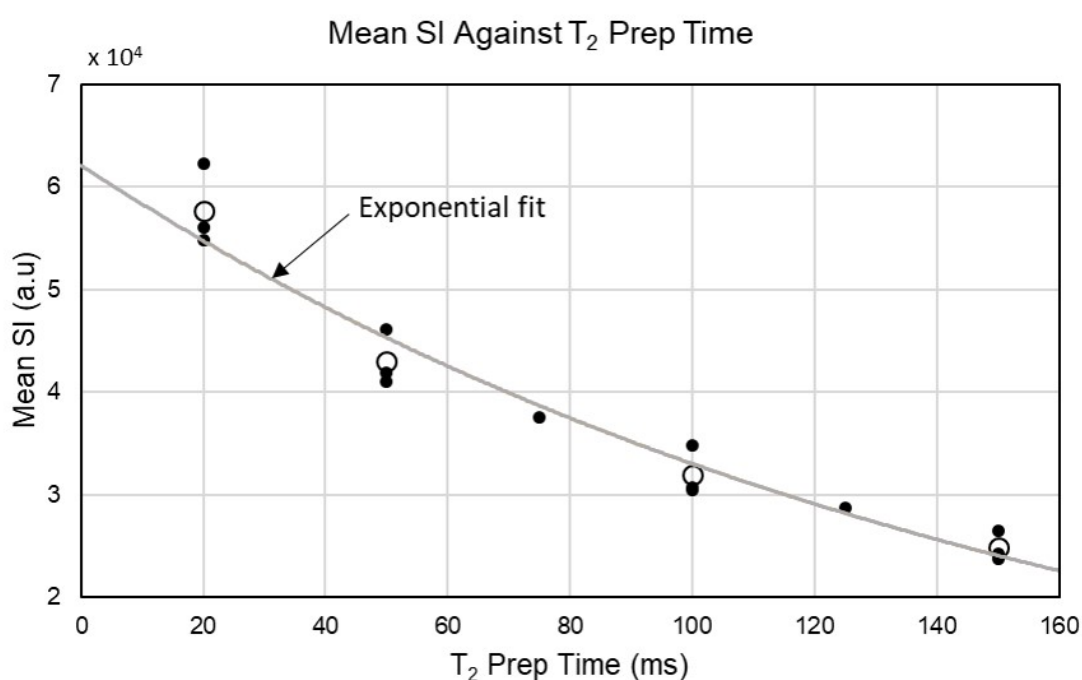


Figure 7.14 – The plot showing the overall mean signal intensity decrease in the sample containing alginate spheres with microbubbles with increasing T_2 prep time. Each of the measurements repeated three times (solid circles), except for 75 ms and 125 ms with only one experiment each. The mean value of the three repeats (hollow circles) and their exponential fit (solid line) are also provided, with estimated T_2^* value 166 ms.

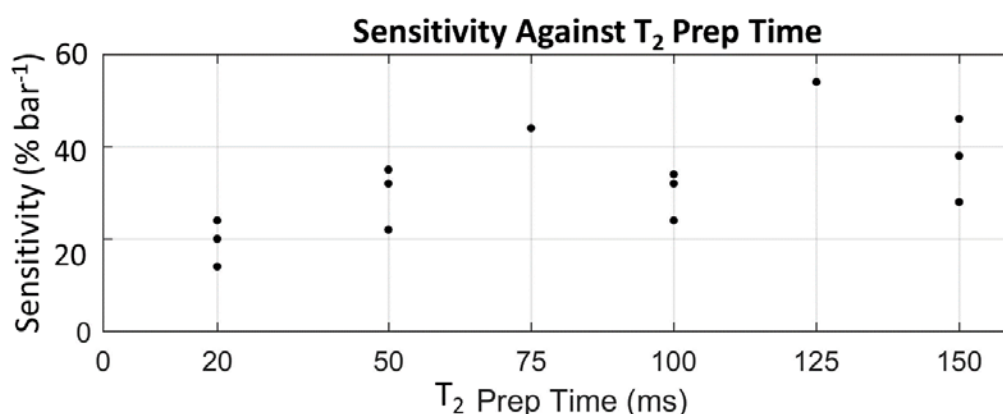


Figure 7.15 – The plot showing the sensitivity of this contrast agent to pressure changes as the T_2 prep time is changed. Each of the measurements repeated three times, except for 75 ms and 125 ms with only one experiment each.

7.7 *In-vivo* Investigations of the Alginate Spheres Using the BTFE Sequence with Respiratory Triggering

During normal breathing, the stomach moves and causing a selected slice captures a slightly different location of the tissue in each of the MR images, which in our case, also contributes to the signal variations in the meal, hindering the accurate quantitation of the signal that solely coming from the pressure change in the stomach. Our strategy to overcome this issue is by incorporating the MR image acquisition with the respiratory triggering. This involves in tracking the respiratory cycle motion and acquiring images within a selected interval of the cycle. This way, the acquired dynamic images are expected to be more constant, from one image to another. The experiment, firstly, performed on the alginate spheres without microbubbles to establish any MR signal changes will not be due to pressure changes. Then, a further investigation carried out on the meal with the presence of the microbubbles.

7.7.1 *In-Vivo* Study on Alginate Spheres without Microbubbles

7.7.1.1 Method

The meal consisted of the alginate spheres without microbubbles in locust bean gum. The total amount ingested by the volunteer was about 250 ml. For this study, the

volunteer was in a supine position and the images were obtained in the coronal plane using the BTFE sequence with and without the respiratory triggering. In addition, the images were also acquired with two different slice thicknesses, 10 mm and 15 mm, and two different T_2 -prep times, 50 and 75 ms, exploring their effect in optimising the sequence to better reduce the movement artefact.

7.7.1.2 Results

For the image analysis, the software was written to allow ROI tracking from frame to frame performed on interpolated images, with eight additional pixels in both dimensions, by using a cross-correlation analysis with the interpolated image of the first frame on the selected ROIs. A square-shaped ROI (Figure 7.16) from the meal was selected, and another one from a small section of the liver, served as a reference because signal intensity within this region is expected to have less deviation. The ROI tracking was undertaken to try to have the selected ROIs within the exact same tissue area in each of the acquired dynamic images, in spite of small horizontal and vertical shifts taking place in the raw images.

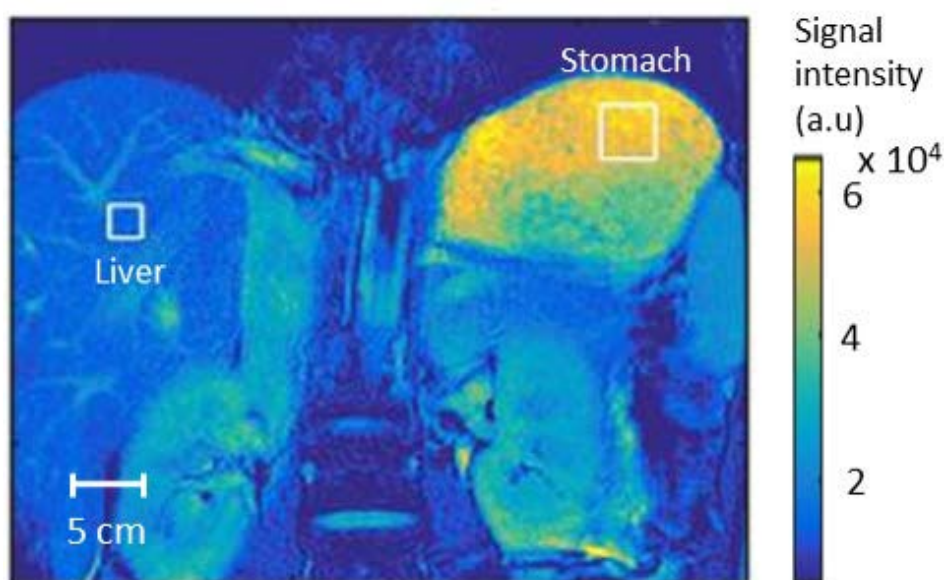


Figure 7.16 – a) MR image acquired showing the meal (alginate spheres without microbubbles) in the stomach with the surrounding organs. The white squares indicate the selected ROIs for signal intensity analysis, in the liver and in the meal (stomach).

When comparing the experiments with and without the use respiratory triggering, the MR images clearly appear more stable and less affected by the movement artefact with the use of the respiratory gating. The percentage of signal intensity change without the respiratory triggering is about 6 to 8 %, decreasing to about 2 to 3 % with the respiratory-gating (Figure 7.17). However, there are also a few images exhibiting very large artefacts, coming from rare instances where the scanner failed at tracking the volunteer's respiration. In addition, large susceptibility artefacts appeared on all the images caused by blood flow and lung displacement which affect the signal substantially. The affected regions were avoided from the signal analysis and not included in the signal deviations exhibited by the data shown on the graphs.

In this particular study, the pressure change within the stomach should not bring any effect because the meal consisted of the spheres without microbubbles. However, the signal variations still measured in this meal with the use of respiratory triggering could be originating from T_1 partial recovery (Figure 7.18), since the value of the repetition time, TR, was not set constant with the use of this technique. This could be affected by the change in respiration rate and depth of the participant over time. The signal intensity change in the meal follows the TR quite closely, probably due to its long T_1 , whilst the liver does not, probably due to its short T_1 . Additionally, a signal drift can be seen in the meal which most possibly caused by the effect of the stomach acid. However, this also appeared in the liver, which was not expected, could be caused by the scanner electronic drift. For the next *in-vivo* study, when using the meal with the presence of microbubbles, the signal intensity change is expected to be higher than this, due to the effect of the pressure in the stomach.

In the experiment investigating the effect of changing the slice thickness between 5 mm to 10 mm, we only found a very minimal effect with a reduction in the signal variation about 1 % (Figure 7.19). This result is in agreement with the *in-vitro* experiment result in section 7.6.2.2, where the variation in the slice thickness did not bring any strong effect on the sensitivity of the contrast agent to pressure. When increasing the T_2 -prep time from 50 to 75 ms, there is no deterioration of the signal changes, probably because the T_2^* sensitivity is developing in the tissue without the application of the field gradients.

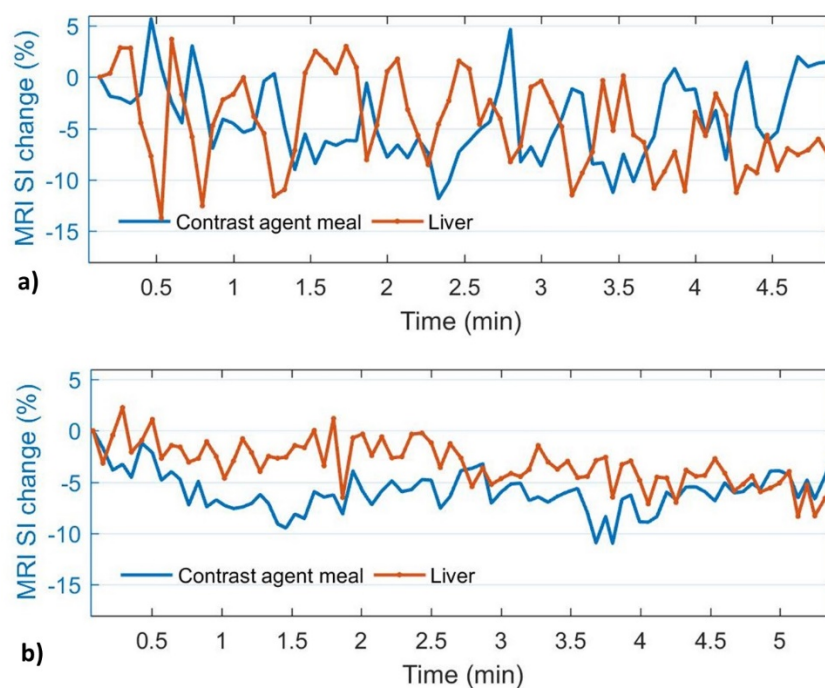


Figure 7.17 – The signal intensity change in the meal (alginate spheres without microbubbles) and in the liver (a) without and (b) with the respiratory triggering. The signal fluctuation is more prominent in the images acquired without the respiratory triggering, approximately 6 to 8 %, compared to its counterpart with the respiratory triggering, only around 2 to 3 % signal changes. The imaging parameters for both data sets are as follow; T_2 -prep time = 50 ms and slice thickness = 10 mm.

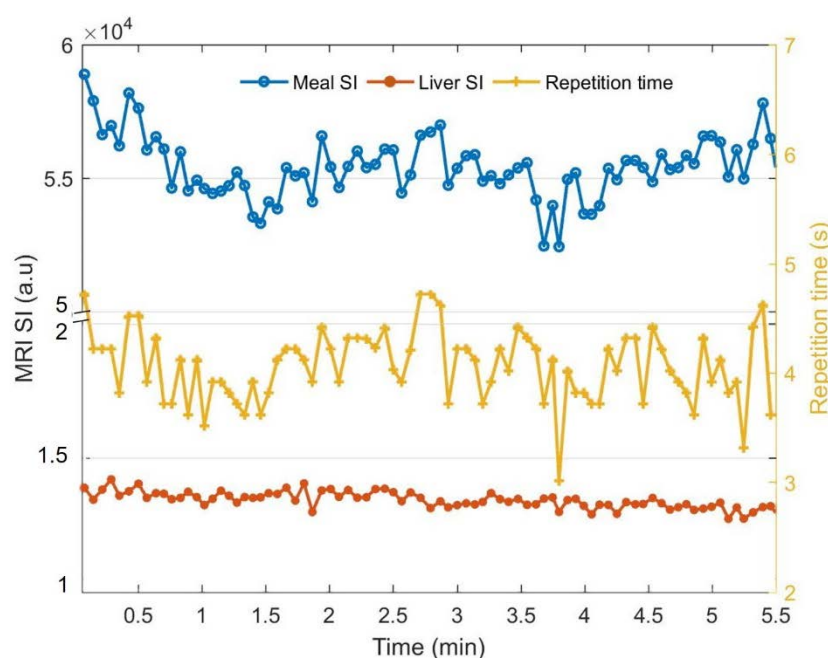


Figure 7.18 – Plots showing the signal intensity of the meal (alginate spheres without microbubbles) and the liver within the selected ROIs in each of the image frames, with their corresponding repetition time. The signal intensity changes with the change in the repetition time on each of the frames, especially in the meal.

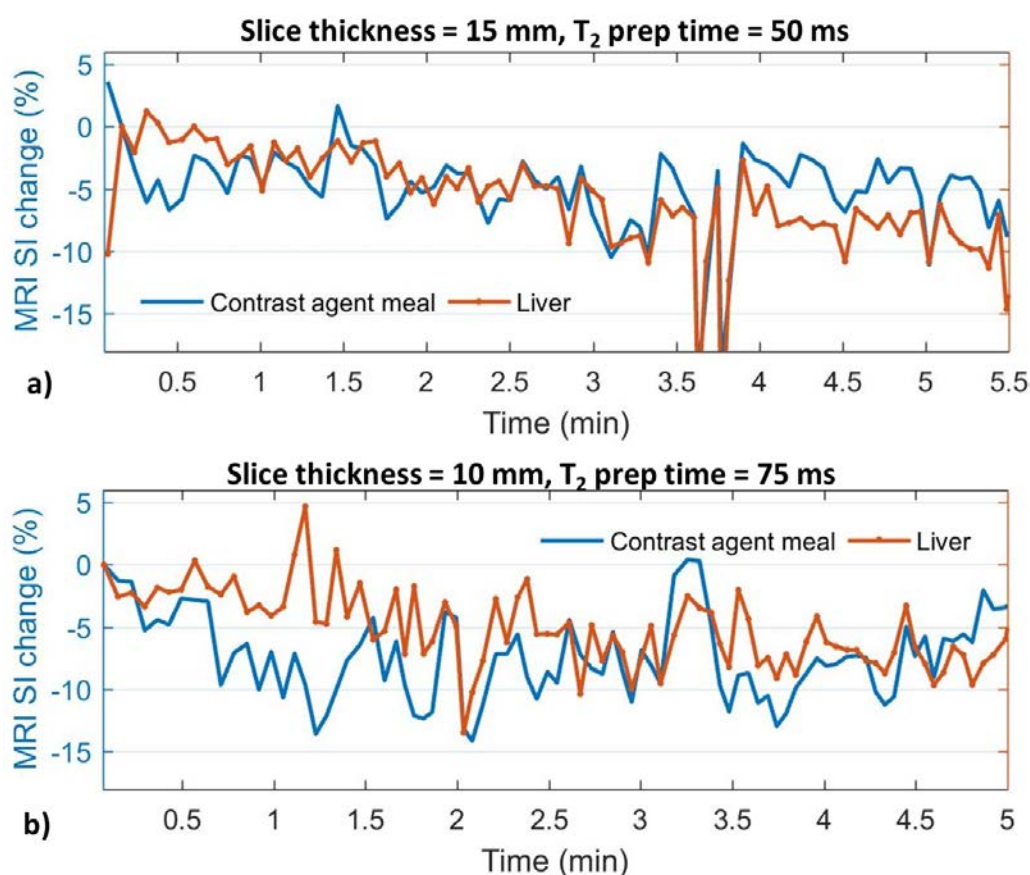


Figure 7.19 – Plots demonstrating the signal intensity change in the meal (alginate spheres without microbubbles) and the liver, when exploring the effect of changing MRI parameters. The parameters are changed in reference to the experiment in Figure 7.17; (a) slice thickness 15 mm, T₂ prep time 50 ms and (b) slice thickness 10 mm, T₂ prep time 75 ms. The imaging was performed with the use of the respiratory triggering. By comparing to the plot in Figure 7.17(b), there is no obvious sensitivity change observed with the change of these parameters.

7.7.2 In-Vivo Study on Alginate Spheres with Microbubbles

7.7.2.1 Method

The meal with a volume of 500 ml consisted of the alginate spheres with microbubbles in locust bean gum. In previous *in-vivo* studies, the microbubbles were prepared approximately 24 hours before the MRI acquisition, but this time, they were prepared in the morning of the day of the experiment, as we anticipated that the sensitivity of the contrast agent could be further enhanced if the microbubbles were prepared immediately before the examination. The total amount ingested by the volunteer was

about 250 ml, in two separate smaller meals. The same volunteer had participated in the previous study (section 7.7.1) with the same meal without microbubbles.

For this experiment, the volunteer was in a prone position in the MR scanner, with the hope that in this position the body or the stomach movement caused by the breathing would be minimised. The scanning was undertaken using the BTFE sequence (T_2 -prep time = 50 ms, slice thickness = 5 mm) with the respiratory triggering.

7.7.2.2 Results

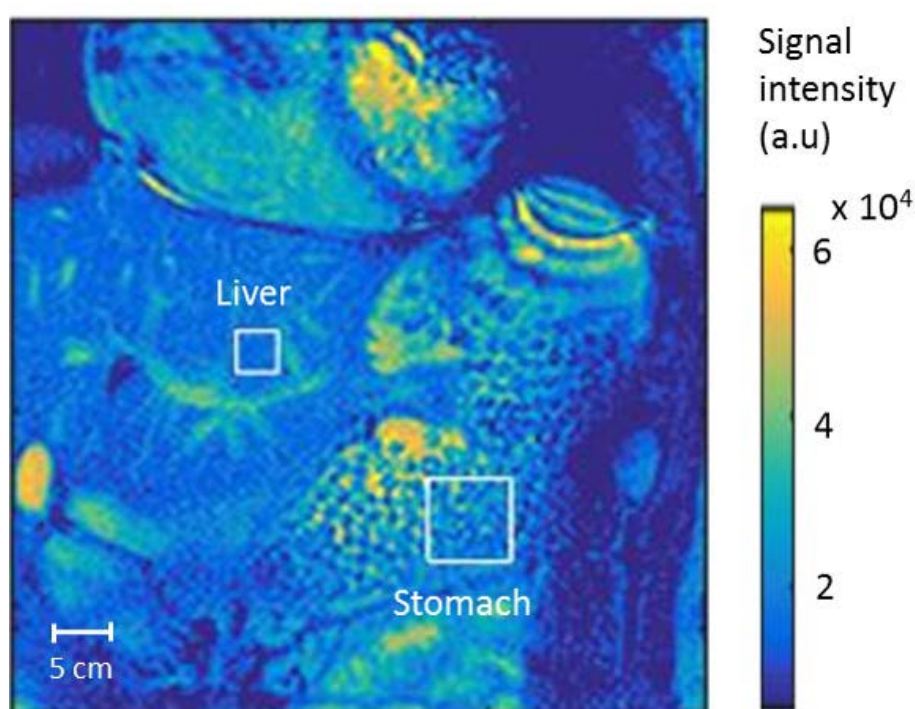


Figure 7.20 – a) MRI image showing the meal (alginate spheres with microbubbles) in the stomach, with the surrounding organs, acquired with the BTFE sequence with the respiratory gating. The white squares represent the ROI selections for signal intensity analysis in the meal and the liver.

The images were analysed by selecting two square-shaped ROIs (Figure 7.20), one from the meal, where pixel intensity changes due to the pressure are expected, and another one from a small section of the liver, where pixel intensity deviations are expected to be much lower. The main challenge of the signal intensity analysis is to find a suitable area where the meal spatial structure holds fairly constant, as there is a lot of movements

within the meal due to the natural peristaltic effect coming from the wall of the stomach. Hence, similar to the analysis undertaken in the previous study (7.7.1.2), an ROI tracking from frame to frame was performed on the interpolated images, with eight additional pixels in both dimensions, by using a cross-correlation analysis with the interpolated image of the first frame on both ROIs. The purpose is to try to have the selected ROIs to track the same tissue area in each of the acquired dynamic images. The meal tracking here is easier due to its severe heterogeneity. The tracking does not work very well in a homogeneous area, hence the successful tracking of the ROI in the liver required the selection of a second ROI with heterogeneous structure, taken from the blood vessels within the liver. Then, after tracking of the corresponding tissue was successful, the plots of the signal intensity coming from both of these areas are produced.

Initially, the signal intensity coming from the meal is seen to exhibit changes within 10 %. However, the signal coming from the liver, which should be constant, is also seen to fluctuate within 5 % (Figure 7.21). The similar effect has been previously exhibited (section 7.7.1), and we suggest that this could be due to the effect of the T_1 . This is further evidenced when we observed the fluctuation of the signal intensity where it is seen to follow closely the changes in the acquisition time length of each of the image frames (Figure 7.22). Although there was certain instance in the measurement shown in Figure 7.21 (from 1.1 to 2 min), where the signal intensity in the liver is fairly constant while in the stomach exhibited 5 %, the length of this occasion was too short to enable us to conclude that this was genuinely coming from pressure exerted by the stomach.

By assuming the signal coming from the liver as the baseline, a plot then produced by dividing the mean signal intensity of the meal over the liver (Figure 7.23). We were hoping that this plot is closer to disclosing the effect of the pressure changes within the antrum of the stomach, although unfortunately these signal changes are also resulting from the meal motion combined with the meal heterogeneity, the meal elasticity, the SNR and the T_1 differences of the meal and the liver. In comparison with the previous experiment where a meal without microbubbles was explored in section 7.7.1, the signal intensity changes here are definitely larger, but the meal heterogeneity is also much enhanced, and we cannot unfortunately conclude that the larger signal intensity changes here are solely due to the pressure changes.

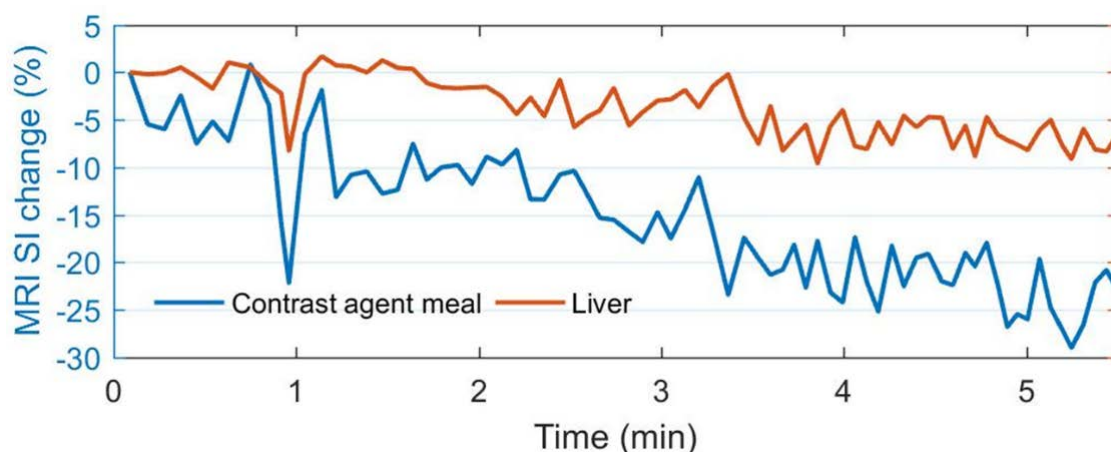


Figure 7.21 – MRI Signal intensity changes within the ROIs (shown in Figure 7.20) in the meal of alginate spheres with microbubbles (antrum area) and the liver, acquired with the BTFE sequence with the respiratory triggering. The signal intensity change in the meal is between 5 to 10 %, while it is less than 5 % in the liver.

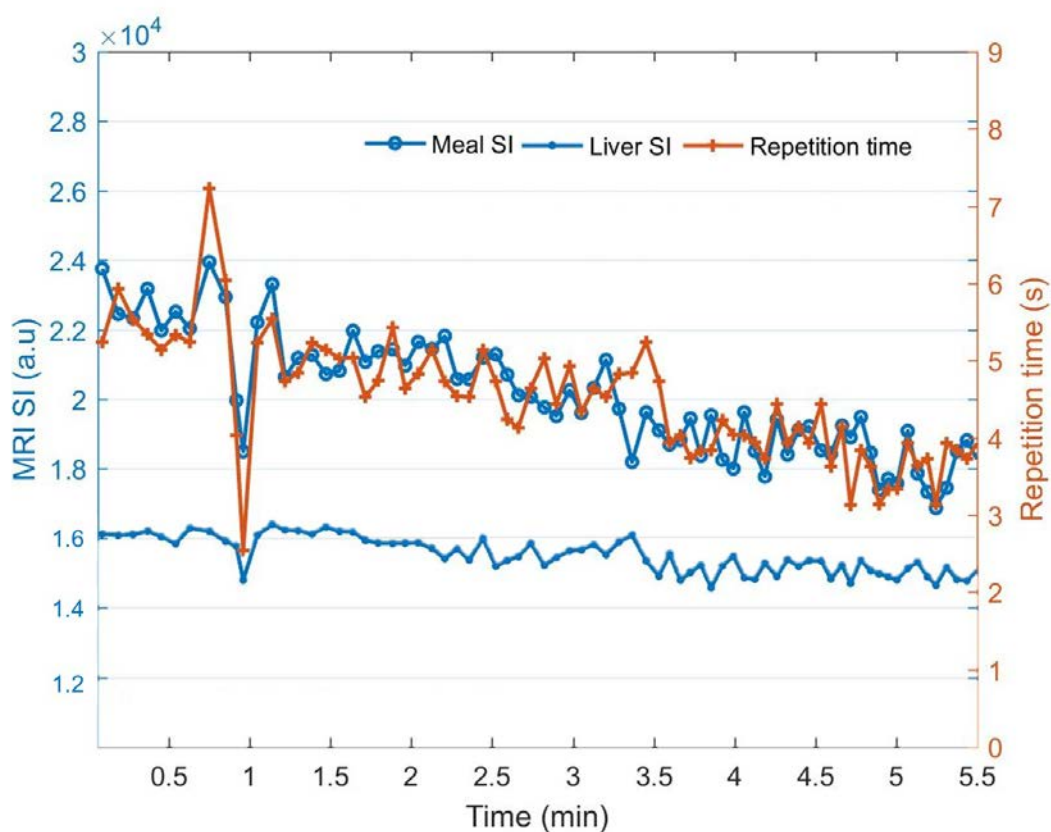


Figure 7.22 – Plots showing the signal intensity of the meal (alginate spheres with microbubbles) and the liver within the selected ROIs in each of the image frames, with their corresponding repetition time. The signal intensity changes with the change in the time acquisition in each the frames.

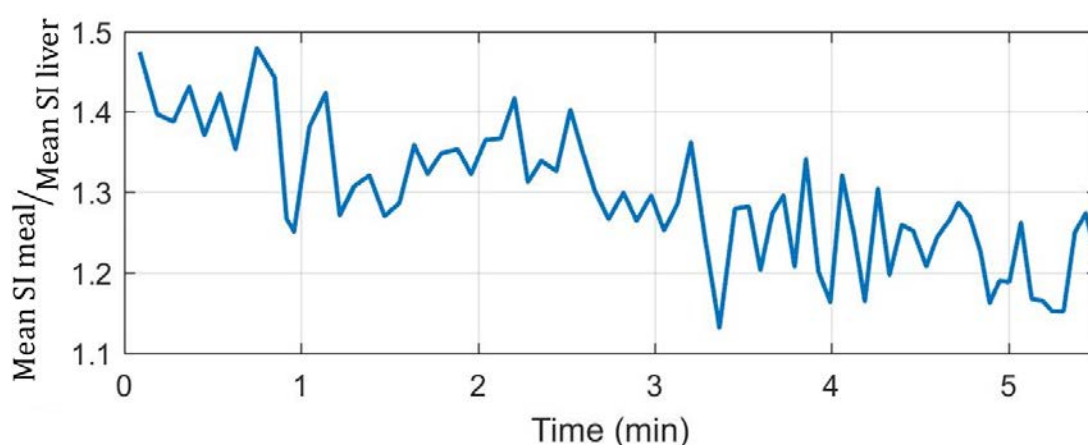


Figure 7.23 – Plot showing the division of the mean signal intensity in the meal over the liver. The fluctuation seen here could be due to the pressure changes, however, this could also be influenced by the T_1 differences between the liver and that of the meal.

In spite of the respiratory triggering, some relative tissue displacements taking place from frame to frame can be seen, the meal is being pro-actively moved by the stomach, and the meal itself exhibits elasticity which makes the tracking of a portion of the meal very difficult. The meal pixel intensity is very heterogeneous locally within the length scale of the alginate spheres, due to the T_2^* effect of microbubbles, and non-locally on the length scale of the stomach, which is the brightest towards the antrum, as would be expected as the pressure there is the highest. The meal exhibits little relative motion far away from the antrum, and large deviations from frame to frame in the antrum.

In addition, similarly to what can be seen in 7.7.1, it appears that the overall signal intensities coming from both the meal and the liver are decreasing over time, with a signal drift about 20 % and 8 %, respectively in the meal and in the liver, within this 5.5 minutes observation. The enhanced drift seen in the meal could be due to the effect of the acid on the meal.

7.8 Participants' Feedback

Every time after finishing each of the *in-vivo* experiments, the volunteers were asked for any feedback regarding their whole experience throughout the study, from ingesting the meal to the MRI measurements. In addition, a verbal follow-up regarding the volunteer

general conditions, especially related to any digestive issue, was also carried out a day after the investigation and none of them had any difficulties to report.

The main feedback we received from all of the participants was that the taste of the meal was too plain and could be further improved. This led to a difficulty in finishing ingesting the whole volume of the meal, and only one participant had managed to consume the whole meal. We did an initial investigation to try to add sweetener and flavouring (section 7.3), unfortunately this affected adversely the signal intensity of the meal, hence no taste enhancer was added. This should be further explored in the future to be able to provide a better experience for the volunteer (or patient). It was also mentioned that one of the challenges was not being allowed to chew the meal, instead we requested that the meal was swallowed whole, to keep the microbubbles functional by keeping the shape of the spheres. This perhaps could be tackled with the use of a liquid meal or reducing the size of the alginate sphere.

7.9 Conclusions

In this chapter, five MRI *in-vivo* studies involving human volunteers and three *in-vitro* experiments were undertaken to test the functionality of the lipid-based microbubbles suspended in alginate gel in the form of small spheres, to measure the dynamic pressure changes within the human stomach. Following the *in-vitro* experiments set-up, this contrast agent has been proven to be capable of sensing pressure changes with a typical sensitivity exhibited around 40 % signal changes per bar. In the initial *in-vivo* studies using the RARE sequence, the measurement was mainly flawed by the movement caused by breathing. Then, this effect was reduced by using a fast imaging sequence called the BTFE, incorporated with a spin echo pulse sequence. Then, we encountered a further issue where the signal variations due to the fact that each MRI image captures a slightly different area, but this was minimised by the use of the respiratory triggering.

Although the peristaltic movement within the stomach is seen to alter the overall signal intensity of the contrast agent meal, at this point of the study we could not conclude that these signal intensity changes are solely due to the pressure changes. The signal changes may result from (i) the T_1 effect because the MRI acquisition was triggered by respiratory gating, (ii) tissue elasticity (slight ingress of varying tissues in different frames

are seen in the analysed ROIs) (iii) the SNR. One alternative way perhaps can improve the condition caused by these factors is by replacing the meal with much smaller alginate spheres. Another option, using a homogeneous liquid meal would probably be one of the solutions, however, there is a high risk of the meal exhibiting an instantaneous pressure equilibration and possible faster effect of the stomach acid on the liquid meal.

For further application of this technique, instead of measuring the dynamic pressure change in the antrum, it could also be used to measure the tonic pressure change on feeding by the stretching and relaxation of the stomach wall muscles, which currently can only be measured invasively by a barostat.

References

1. BORTOLOTTI, ANNESE, COCCIA and BORTOLOTTI, M., 2000. Twenty-four hour ambulatory antroduodenal manometry in normal subjects (co-operative study). *Neurogastroenterology & Motility*, **12**(3), pp. 231-238.
2. FARRE, R., VANHEEL, H., VANUYTSEL, T., MASAOKA, T., TORNBLUM, H., SIMREN, M., VAN OUDENHOVE, L. and TACK, J.F., 2013. In functional dyspepsia, hypersensitivity to postprandial distention correlates with meal-related symptom severity. *Gastroenterology*, **145**(3), pp. 566-573.
3. HOAD, C.L., COX, E.F. and GOWLAND, P.A., 2010. Quantification of T2 in the abdomen at 3.0 T using a T2-prepared balanced turbo field echo sequence. *Magnetic Resonance in Medicine*, **63**(2), pp. 356-364.
4. HOAD, C., RAYMENT, P., COX, E., WRIGHT, P., BUTLER, M., SPILLER, R. and GOWLAND, P., 2009. Investigation of alginate beads for gastro-intestinal functionality, Part 2: In vivo characterisation. *Food Hydrocolloids*, **23**(3), pp. 833-839.
5. TACK, J., CAENEPEEL, P., FISCHLER, B., PIESSEVAUX, H. and JANSSENS, J., 2001. Symptoms associated with hypersensitivity to gastric distention in functional dyspepsia. *Gastroenterology*, **121**(3), pp. 526-535.

CHAPTER 8

DISCUSSION

8 DISCUSSION

This work is focusing on the development of microbubble-based contrast agents for ingestion, for humans, with applications in diagnostic Magnetic Resonance Imaging of the gastrointestinal system, by means of non-invasive meal pressure measurement. A pressure sensitive MR contrast agent has been manufactured and tested, through *in-vitro* and *in-vivo* investigations. The contrast agent comprised of gas-filled microbubbles suspended in soft-solid alginate spheres, which has been specifically tailored to sense the pressure changes in the human stomach. To our best knowledge, this method has never been explored before. The principle underlying the method is that of the compressibility of the microbubbles enabling size changes when the pressure is applied, causing a change of magnetic field perturbation on its surrounding, hence the change of the MR signal coming from water molecules diffusing in this environment.

The T_2^{eff} relaxation time of the alginate spheres has been assessed, in both the 2.35T small animal Bruker and the 3T whole body Philips MRI scanners, by comparing the preparations with and without the presence of microbubbles. A substantial decrease of the T_2^{eff} was observed in the presence of gas-filled microbubbles in the alginate spheres, by a factor of 2. Dynamic measurements have been further used to test the functionality of these contrast agents, through *in-vitro* investigations, in several conditions including in a solvent mimicking the human gastric solution at body temperature. The alginate spheres with microbubbles yielded a high level of sensitivity, up to 40 % MR signal change per bar, whilst the signal intensity remains constant in the alginate spheres without microbubbles. This further supports the fact that the signal intensity change coming from the contrast agent is solely due to the presence of microbubbles.

An interesting additional outcome of this study is the demonstration of a spatial gradient of T_2^{eff} value seen between the centre and the periphery of alginate spheres with microbubbles. We anticipated the microbubbles density and the curing process may both contribute to the mechanisms causing this radial spatial gradient. This effect was further explored by measuring the sensitivity of the two areas to pressure changes, where it was seen that the T_2^{eff} value in the centre of the alginate sphere was constantly higher compared to the periphery, suggesting microbubbles density is higher in the

periphery. Both of these regions contribute to the increase in the T_2^{eff} value of the whole alginate spheres when the pressure is increased, with the periphery exhibits a higher sensitivity, which is up to 58 % T_2^{eff} change per bar whilst the centre exhibits 24 % change per bar.

A gel solution made of the locust bean gum (2 % w/v) was used as a suspending medium and as an immobilisation tool, by restricting the alginate spheres from moving upwards due to the natural buoyancy of the entrapped microbubbles. At the same time, this gel was also found to be useful in slowing down the acidification effect, where it was seen to cause a decrease in the T_2^{eff} value of the spheres. With these in hand, the contrast agent was further tested *in-vivo* to demonstrate its capability to be used, in conjunction with an MRI scanner, as a novel technique in measuring the dynamic pressure change in the human stomach.

Five *in-vivo* studies were carried out on healthy human volunteers, and a 500-ml of the contrast agent was prepared as a meal for each volunteer. The initial result, when the RARE sequence was used, showed that the acquired signal change (up to 300 % change) was dominated by the motion artefact caused by breathing. This effect was successfully reduced by using an ultrafast BTFE (or TrueFIST) MRI sequence, with echo pulse preparation.

Later, a further issue was encountered where the signal variation being measured found to be largely due to the inhomogeneity of the meal with differing parts of the meal being captured on each separate consecutive MRI images. We attempted to minimise this by the use of the respiratory triggering and more advance post processing for image analysis, where the software was written on MATLAB to allow ROI tracking from frame to frame performed on interpolated images, by using a cross-correlation analysis with the interpolated image of the first frame on the selected ROIs. This was undertaken to try to have the selected ROIs within the exact same tissue area in each of the acquired dynamic images, in spite of small horizontal and vertical shifts taking place in the raw images.

However, the natural peristalsis of the stomach wall, especially in the antrum region, causing a partial volume effect which made it additionally challenging to capture the

same area of the meal in each of the dynamic images being acquired. By using the cross-correlation analysis, the signal intensity change exhibited in the meal is between 5 to 10 %. It has been shown previously by Bortolotti et al. (2000) that the pressure exerted in the stomach on its meal, within the antrum region, during the digestive period is ranging between 30 and 82 mmHg (40 to 109 mbar). This means, our result is slightly higher than expected, which is between 1.6 to 4.4 % signal change, when considering the sensitivity of the contrast agents at 40 % change per bar. Hence, at this point of the *in-vivo* study we could not conclude that these signal intensity changes are solely due to the pressure changes. The signal changes may result from (i) the T1 effect because the MRI acquisition was triggered by respiratory gating, (ii) tissue elasticity (slight ingress of varying tissues in different frames are seen in the analysed ROIs) (iii) the SNR.

For further work, possible solutions exist in the production of alginate spheres in a smaller form or in a liquid meal, however, there is a high risk of the meal exhibiting an instantaneous pressure equilibration and possible faster effect of the stomach acid on the liquid meal. This also means it is worth exploring different suspending medium which can slow down the deterioration of the sensitivity due to the acid. Another possible application is that the contrast agent can be used to measure the tonic pressure in the region of the body of the stomach, where less wall movement is seen, as compared to the dynamic changes in the antrum. In the future success of this technique, we may also be able to use this contrast agent to track down further to the intestines, not just for measuring the pressure but also for other investigations such observing the effect of acidic and alkaline environment in digestive system.

Besides, there has still many scopes can be further explored; the preparations and the sensitivity of the contrast agent meal, as well as the combination of the MRI technique such as the use of a different MRI sequence and differing in the external magnetic field strength.

When we increased the bubble to twice of the density, the sensitivity only increased approximately 29 %, which is much less than we expected, a 200 % increase as demonstrated by Bencsik et al. (2013). We suspect that at higher bubbles density, the gradient fields originating from individual bubbles start to overlap causing the sensitivity of the contrast agent with bubble density to leave linearity. Nonetheless, the sensitivity

of the microbubble still can be changed by exploiting the magnetic susceptibility of the microbubble shell by incorporating magnetic materials on the shell of the bubble, e.g. iron nanoparticles. Additionally, the sensitivity of the contrast agent can be further increased by exploring different size of microbubbles.


In terms of the contrast agent preparation, the curing effect can be further investigated in forming a stable alginate sphere by manipulating the concentration of the calcium lactate solution. Also, it is worth exploring a different method of manufacturing the alginate spheres that could result in the creation of homogeneous spheres, in particular, internal gelation mechanism which has been previously demonstrated as an alternative method with such a potential. Furthermore, we should be able to explore the physical condition of the meal, in terms of structure and nutrient content, which can be used to observe different behaviour of the stomach for example, the high fat containing materials could bring different effect on the stomach function compared to the low fat materials.

In conclusion, these microbubble-loaded alginate spheres have shown great potential as biocompatible MR contrast agents measuring localised pressure changes in the human stomach. With further improvement, this exciting work will open up an alternative and less invasive route for the clinicians to achieve a better understanding of the clinical condition related to functional dyspepsia. In comparison to the current existing techniques, manometry and bariatric, this method also provides a shorter examination time.


APPENDIX

Appendix A

Poster for the International Conference on Magnetic Resonance Microscopy (ICMRM) 2015



The University of
Nottingham



NOTTINGHAM
TRENT UNIVERSITY

Mapping Pressure Gradient Variation Using MRI and Microbubbles

Edwin Abdurakman¹, Martin Bencsik¹, David Fairhurst¹, Gareth Cave¹, Richard Bowtell²
¹ School of Science & Technology, Nottingham Trent University, UK
² Sir Peter Mansfield Magnetic Resonance Centre, University of Nottingham, UK

1. Introduction

Gas-filled microbubbles with lipid membranes have been used as a pressure sensitive probe in MRI [1] [2]. Due to the gas-liquid interface of the microbubble shell, it creates a magnetic susceptibility step change at the microbubble periphery. The compressibility of these bubbles enable them to undergo a radius change when an external pressure is applied, which consequently changes the external magnetic field perturbation and thus the T_2^* relaxation time [2]. The aim of this work is to use MRI to map spatial pressure gradient using a microbubble contrast agent which has never been demonstrated before.




Figure 1 – Gas-filled microbubbles create a magnetic disturbance on it's surrounding.

2. Methods

Monodisperse microbubbles with diameter in the range 2-3 μm were prepared with a 1,2-dihexadecanoyl-sn-glycero-phosphocholine (DPPC) lipid shell with 1,2-distearoyl-sn-glycero-3-phosphoethanolamine-N-[methoxy (polyethylene glycol) - 2000 (PEG2000 PE)] and filled with C_3F_8 gas.




Figure 2 – CapMixTM

Microbubble preparations:
 The lipid solution was transferred into a 2ml vial with a rubber septum cap and then 10ml of C_3F_8 gas was bubbled through the solution via a gas-tight syringe within 30s. The vial was then shaken for 45s using a capsule mixing device (CapMixTM, 3M, Bracknell, UK). Fairly monodisperse microbubbles are made by cavitation.

To prevent buoyant advection, the preparation was further immobilized in a polysaccharide gel [3], 1.5% Gellan gum suspending medium and loaded into a homemade sample holder. This comprised of two compartments, separated by a 3mm thick sintered glass disc with 5-15 μm pores to create a low permeability step between the two compartments. The pressure was applied to one compartment and the cell was further imaged using a Bruker Biospec 2.35T scanner with the RARE sequence.

MRI Measurement:

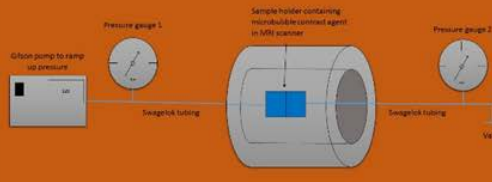


Figure 3 – An illustration showing the equipment set-up for the experiment. A sample holder containing a microbubble contrast agent was connected to a pump by Swagelok tubing. The pressure gauges were placed at both sides of the compartments to measure the pressure changes.

3. Results

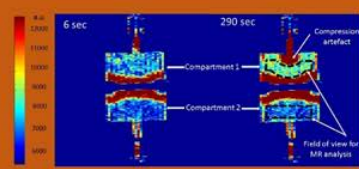


Figure 4 – MR images showing both compartments at time 6 seconds and 290 seconds respectively.

Figure 4 shows two images of both compartments taken at different times and also demonstrates the spatial pressure gradient. At 6 seconds after switching on the pump, the signal intensity in both compartments are almost identical, compared to the signal taken at 290 seconds, the signal intensity in compartment 1 is much higher. Figure 4 also shows the selected field of view for the MR signal analysis. The FOVs were selected in order to avoid 'compression' artefacts. These artefacts are the result of the Gellan gel (without microbubble) in the tubing entering the contrast agent solution in compartment 1 of the sample holder after the pressure pumped up.




Figure 5 – MR signal intensity change to pressure in both compartments

Figure 5 shows the change in MR signal intensity due to the variation of pressure across the two compartments. The signal intensity in compartment 1 starts to increase 150 seconds after the pump was turned on. This is followed by a later signal increase, 30 seconds later, in compartment 2. Moreover, the signal in compartment 1 increases more rapidly which indicates an increasing spatial pressure gradient between both compartments. As the pump stopped, the signal intensity in compartment 1 decreased whilst in compartment 2 it continued to rise, indicating the pressure is still equilibrating.

4. Conclusion

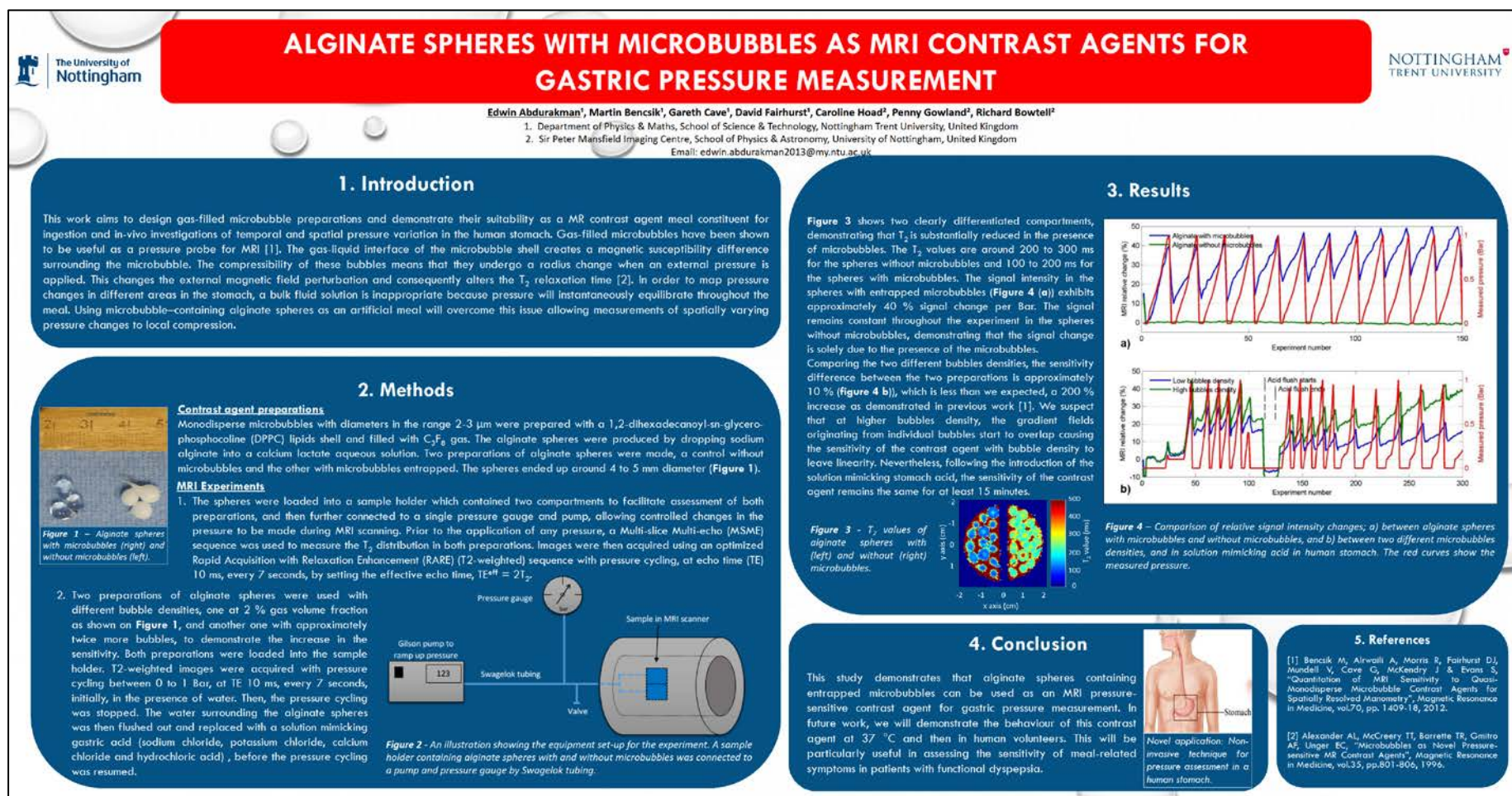
A spatial pressure gradient on microbubbles is demonstrated by MR imaging in this preliminary study which has never been done before with this contrast agent. We show that the MR signal and its time course are different in both compartments. For a future work, we will observe the time taken for the pressure to reach equilibrium for separating porous media with different permeabilities and match the MR signal intensity changes to pressure for a longer time of experiment. We will also quantitatively investigate the T_2 relaxation changes due to the change of microbubble radius. This work shows a great potential use of microbubbles contrast agents e.g. in medical application to measure intracardiac pressure changes and gradient pressure across a vascular stenosis using MRI.

5. References

1. Bencik M, Alwali A, Morris R, Fairhurst DJ, Mundell V, Cave G, McKendry J & Evans S, "Quantitation of MRI Sensitivity to Quasi-Monodisperse Microbubble Contrast Agents for Spatially Resolved Manometry", *Magnetic Resonance in Medicine*, vol.70, pp. 1409-18, 2012.
2. Alexander AL, McCrory TT, Barrette TR, Gmitro AF, Unger EC, "Microbubbles as Novel Pressure-sensitive MR Contrast Agents", *Magnetic Resonance in Medicine*, vol.35, pp.801-806, 1996.
3. Morris RH, Bencsik M, Wendle N, Gaborait J, Fairhurst D, Vargha A, Perrie S, Michele G, "Robust spatially resolved pressure measurements using MRI with novel buoyant advection-free preparations of stable microbubbles in polysaccharide gels", *Journal of Magnetic Resonance*, vol.193, pp.159-167, 2008.

Appendix B

Poster for the European Society for Magnetic Resonance in Medicine and Biology (ESMRMB) Conference 2016



Appendix C

Poster for the European Society for Magnetic Resonance in Medicine and Biology (ESMRMB) Conference 2017

